Aus dem
Lehrstuhl für Physiologische Genomik, Biomedizinisches Centrum (BMC)
Ludwig-Maximilians-Universität München

Characterising molecular mechanisms underlying muscle spindle function in wildtype and mutant mice: Insights into neuromuscular disease and pharmacological effects

Dissertation
zum Erwerb des Doctor of Philosophy (Ph.D.)
an der Medizinischen Fakultät der
Ludwig-Maximilians-Universität München

vorgelegt von
Bridgette Michelle Watkins

aus
Frankston (Australia)

Jahr
2024

Mit Genehmigung der Medizinischen Fakultät der
Ludwig-Maximilians-Universität München

Erstes Gutachten:	Prof. Dr. Stephan Kröger
Zweites Gutachten:	Prof. Dr. Anja Horn-Bochtler
Drittes Gutachten:	Prof. Dr. Claudia Veigel
Viertes Gutachten:	Prof. Dr. Angela Abicht

Dekan: Prof. Dr. med. Thomas Gudermann

Tag der mündlichen Prüfung: 28.05.2024

Affidavit

LMU LUDWIG-MAXIMILIANS-UNIVERSITÄT MÜNCHEN

Promotionsbüro Medizinische Fakultät

MMRS

Affidavit

Watkins, Bridgette

Surname, first name

Grosshaderner Strasse 9

Street

82152 Planegg-Martinsried

Zip code, town, country

I hereby declare, that the submitted thesis entitled:

Characterising molecular mechanisms underlying muscle spindle function in wildtype and mutant mice: Insights into neuromuscular disease and pharmacological effects

is my own work. I have only used the sources indicated and have not made unauthorised use of services of a third party. Where the work of others has been quoted or reproduced, the source is always given.

I further declare that the dissertation presented here has not been submitted in the same or similar form to any other institution for the purpose of obtaining an academic degree.

Munich, 10.06.2024 — Bridgette Watkins

place, date — Signature doctoral candidate

Confirmation of Congruency

LMU LUDWIG-MAXIMILIANS-UNIVERSITÄT MÜNCHEN

Promotionsbüro Medizinische Fakultät

MMRS

Confirmation of congruency between printed and electronic version of the doctoral thesis

Watkins, Bridgette

Surname, first name

Grosshaderner Strasse 9

Street

82152 Planegg-Martinsried

Zip code, town, country

I hereby declare, that the submitted thesis entitled:

Characterising molecular mechanisms underlying muscle spindle function in wildtype and mutant mice: Insights into neuromuscular disease and pharmacological effects

is congruent with the printed version both in content and format.

Munich, 10.06.2024 — Bridgette Watkins

place, date — Signature doctoral candidate

Table of Contents

Table of Figures

List of Abbreviations

$^{-/-}$	Knock-out
129/SvJ	129X1/SvJ; The Jackson Laboratories; strain #000691
Aa	Catwalk XT footfall pattern Alternate: RF - RH - LF - LH
Ab	Catwalk XT footfall pattern Alternate: LF - RH - RF - LH
ACh	Acetylcholine
AChE	Acetylcholinesterase
AChR	Acetylcholine Receptor
ACSF	Artificial Cerebrospinal Fluid
ANOVA	Analysis of Variance
ASIC	Acid-sensing ion channel
Asic2$^{-/-}$	Acid-sensing ion channel 2 knockout: B6.129-*Asic2*^{tm1Wsh}/J; The Jackson Laboratory; #013126
ATP	Adenosine triphosphate
ATPase	Adenosine triphosphatase
AU	Arbitrary Units
C57BL6	C57BL/6J
Ca	Catwalk XT footfall pattern Cruciate: RF - LF - RH - LH
Ca^{2+}	Calcium ions
Cb	Catwalk XT footfall pattern Cruciate: LF - RF - LH - RH
CNS	Central nervous system
Cont	Control
CT	Computer Tomography
DAPI	4′,6-diamidino-2-phenylindole
DEG/ENaC	Degenerins/ epithelial sodium channel
DI	Dynamic Index: firing rate of dynamic peak – initial static time
DNA	Deoxyribonucleic acid
DP	Dynamic Peak: highest firing rate during ramp
DRG	Dorsal root ganglion
EDL	Extensor digitorum longus muscle
ERT	Enzyme replacement therapy
FST	Final static time: firing rate 3.25–3.75 s into stretch
Gaa	(Alpha) α-acid glucosidase gene
Gaa$^{-/-}$	(Alpha) α-acid glucosidase gene knockout mice - B6;129- *Gaa*^{tm1Rabn}/J; The Jackson Laboratories, strain #004154
GAA	(Alpha) α-acid glucosidase (enzyme)
GABA	(Gamma) γ-aminobutyric acid
GFP	Green fluorescent protein
GLUT1	Glucose transporter 1
GTO	Golgi tendon organs
HGMD	Human gene mutation database (https://www.hgmd.cf.ac.uk/ac/index.php)
IC_{50}	Inhibitory concentration 50%
IST	Initial Static Time: firing rate 0.25–0.75 s into stretch
JAX	Jackson Laboratories

KO	Knock-out
L_0	Baseline muscle length defined as the minimal length at which maximal twitch contractile force is generated
LAMP1	Lysosomal associated protein 1
LC3A/B	Light chain 3 isoforms A and B
LF	Left front
LH	Left hind
Max tetanic	Maximal tetanic force
mRNA	messenger Ribonucleic Acid
MS	Muscle spindle
Na^+	Sodium ions
$Na_v1.4$	Voltage-gated sodium channel 1.4
NF-200	Neurofilament Heavy
NMJ	Neuromuscular junction
O.C.T	Optimal cutting temperature medium
PBS	Phosphate buffered saline
PCR	Polymerase chain reaction
PFA	Paraformaldehyde
PIEZO2	Piezo-Type Mechanosensitive Ion Channel Component 2
PNS	Peripheral nervous system
PvalbCre	B6.129P2-*Pvalb*$^{tm1(cre)Arbr}$/J ; The Jackson Laboratory; #017320
Ra	Catwalk XT footfall pattern Rotate: RF - LF - LH - RH
Rb	Catwalk XT footfall pattern Rotate: LF - RF - RH - LH
RF	Right front
RH	Right hind
RIMS	Refractive index matching solution
Rosa26	B6.Cg-*Gt(ROSA)26Sor*$^{tm9(CAG\text{-}tdTomato)Hze}$/J; The Jackson Laboratory, #007909
S46	Antibody against slow tonic myosin heavy chain
TA	Tibealis anterior
Thy1-YFP	B6.Cg-Tg(Thy1-YFP)16Jrs/J; The Jackson Laboratory; #003709
TrkC	Tropomyosin receptor kinase C
TRP	Transient receptor potential channels
VBA	Visual Basic for Applications
vGluT1	Vesicular glutamate transporter 1
WT	Wildtype mice
α-btx	α-bungarotoxin

List of Publications

Publications included in dissertation:

I. **Watkins, B**., Schuster, H. M., Gerwin, L., Schoser, B., & Kröger, S. (2022). The effect of methocarbamol and mexiletine on murine muscle spindle function. *Muscle Nerve*, *66*(1), 96-105. https://doi.org/10.1002/mus.27546

II. **Watkins, B**., Schultheiss, J., Rafuna, A., Hintze, S., Meinke, P., Schoser, B., & Kröger, S. (2023). Degeneration of muscle spindles in a murine model of Pompe disease. *Sci Rep*, *13*(1), 6555. https://doi.org/10.1038/s41598-023-33543-y

III. Bornstein, B., **Watkins, B**., Passini, F. S., Blecher, R., Assaraf, E., Sui, X. M., Brumfeld, V., Tsoory, M., Kröger, S., & Zelzer, E. (2023). The mechanosensitive ion channel ASIC2 mediates both proprioceptive sensing and spinal alignment. *Exp Physiol*, *Epub ahead of print*, 1-13. https://doi.org/10.1113/EP090776

Publications not included in dissertation:

IV. Kröger, S., & **Watkins, B.** (2021). Muscle spindle function in healthy and diseased muscle. *Skelet Muscle*, *11*(1), 3. https://doi.org/10.1186/s13395-020-00258-x

1. Contribution to the Publications

1.1 Contribution to Paper I

The effect of methocarbamol and mexiletine on murine muscle spindle function.

The effects of skeletal muscle relaxants, including peripherally acting neuromuscular blocking agents, have been well studied in extrafusal fibres (Boon et al., 2018; Hunter, 1995; Raghavendra, 2002). Acetylcholine receptors (AChRs) are one target of muscle relaxants because they are crucial in transmitting neuronal signals from α-motoneurons to extrafusal muscle fibres, and skeletal muscle relaxants therefore target these receptors to alleviate muscle tension and reduce muscle contraction (Boon et al., 2018). A previous doctoral student (Laura Gerwin) established that AChRs negatively modulate muscle spindle stretch responses (Gerwin et al., 2019), and this work led the lab to investigate further effects of skeletal muscle relaxants on muscle spindle function. In 2016, using *ex-vivo* electrophysiology, former lab members (Hedwig Schuster and Laura Gerwin) determined that the skeletal muscle relaxant methocarbamol has an inhibitory effect on muscle spindle afferent action potential generation in C57BL6/J mice. Hedwig Schuster generated preliminary data to construct methocarbamol dose-response curves (methocarbamol concentrations 0-2000µM), determined that methocarbamol inhibitory effects are reversible in muscle spindles, and performed the associated functional experiments (Figure 5, methocarbamol data only). The dose-response curves were incomplete, and in order to obtain a more detailed overview of the effect of methocarbamol on muscle spindle afferent action potential generation, I initially verified the previously obtained data, and then extended the work by analysing muscle spindle function at increasing concentrations of methocarbamol dosages (3000-4000µM). I next expanded the study by including a muscle relaxant that is chemically and structurally similar to methocarbamol – mexiletine. I initially established that mexiletine also inhibits muscle spindle afferent action potential generation, and subsequently designed all protocols and executed all *ex-vivo* electrophysiology functional experiments involving mexiletine. In collaboration with the Wilkinson lab in San Jose, California, USA, I optimised previously established data collection protocols in the lab by implementing new ramp and hold macros in LabChart. I then curated all data collected from methocarbamol and mexiletine experiments, and, using GraphPad Prism, performed precise statistical modelling required for the generation of dose-response curves and associated IC_{50} values, as well as maximum tetanic force and tension calculations. From these results, I was able to conclude that mexiletine and methocarbamol inhibit muscle spindle afferent action potential generation in a reversible manner,

without decreasing overall muscle tension at rest and during ramp and hold stretch protocols. Furthermore, I integrated the results from mexiletine and methocarbamol into a cohesive study, demonstrating that both drugs have a similar inhibitory effect on muscle spindle afferent action potential generation, with both drugs resulting in an all-or-nothing action potential generation, albeit at different concentrations (Watkins et al., 2022).

As methocarbamol had been recently shown to directly affect $Na_v1.4$ in extrafusal muscle fibres (Zhang et al., 2021), I also investigated whether $Na_v1.4$ is present in intrafusal fibres using immunohistochemistry. To this end, I optimised previously used staining protocols (Gerwin et al., 2019; Gerwin et al., 2020; Zhang et al., 2014) and performed high-resolution confocal microscopy to determine the precise subcellular distribution of $Na_v1.4$ in the contractile ends of intrafusal fibres. I designed and executed all associated quantitative immunohistochemistry experiments and provided the first evidence that the subcellular distribution of the T-tubule system in intrafusal fibres may potentially differ to that present in extrafusal fibres (Watkins et al., 2022). Additionally, I contributed to the drafting and subsequent reviewing of the manuscript, including the generation of all Figures used in the final manuscript accepted for publication.

1.2 Contribution to Paper II

Degeneration of muscle spindles in a murine model of Pompe disease.

Muscle spindle function is known to be either affected directly in the pathology of muscular and neuromuscular disorders (Aimonetti et al., 2005; Cazzato & Walton, 1968; Gerwin et al., 2020; Papaioannou & Dimitriou, 2020; Swash & Fox, 1976) or indirectly as a secondary effect of, for example the degeneration of extrafusal fibres (Abbruzzese & Berardelli, 2003; Cameron et al., 2008; Conte et al., 2013; Sangari et al., 2016; Swash & Fox, 1975; Vaughan et al., 2015). To investigate muscle spindle function in a degenerative neuromuscular disorder, we characterised muscle spindle structure and function in a murine model of Pompe disease (*Gaa*$^{-/-}$ mice (B6;129-Gaa^{tm1Rabn}/J mice; JAX stock #004154)). This project was conceptualised in collaboration with the group of Prof. Schoser (Benedikt Schoser, Peter Meinke and Stefan Hintze; Friedrich Baur Institut, LMU Klinikum). We hypothesised that an impaired muscle spindle function may contribute to the frequent falls and motor coordination deficits experienced by Pompe patients. I initially identified suitable time points (4 and 8 months) to assess whether *Gaa*$^{-/-}$ mice display motor coordination impairments in comparison to age-matched 129/SvJ control mice (129X1/SvJ; The Jackson Laboratories; strain #000691). I then conducted observer-independent behavioural experiments using the CatWalk XT system on *Gaa*$^{-/-}$ mice and aged-matched 129/SvJ mice. After acquiring all data, I implemented robust data analysis protocols, which allowed me to subsequently perform all statistical analyses using Microsoft Excel and GraphPad Prism. In order to determine if *Gaa*$^{-/-}$ mice displayed motor coordination impairments,

which could be a consequence of an impaired proprioceptive system, I grouped the parameters according to Pitzer et al, (2021). As the *Gaa*$^{-/-}$ mice displayed progressive inter-limb coordination deficits that were consistent with an altered motor coordination and, thus with an altered muscle spindle function in these mice, I next designed an experimental protocol using *ex-vivo* electrophysiology, to determine whether muscle spindles from *Gaa*$^{-/-}$ mice were functionally impaired. I performed all *ex-vivo* electrophysiology experiments, and performed the analyses of all data acquired from these experiments. I wrote VBA macros for Excel to specifically analyse the data recorded from muscle spindle afferents that were categorised as non-stretch responsive. I implemented new Python codes and verified existing components, which I then optimised for the analysis of all parameters on the recordings categorised as stretch responsive. I performed all statistical analyses associated with the functional *ex-vivo* electrophysiology experiments using Microsoft Excel, and GraphPad Prism. This allowed me to draw accurate conclusions that muscle spindle function progressively degenerates in *Gaa*$^{-/-}$ mice.

To investigate whether structural abnormalities accompanied the observed motor coordination impairments and functional deficits, I used immunohistochemistry to compare the morphology of age-matched 129/SvJ mice and *Gaa*$^{-/-}$ mice. I designed extended immunohistochemistry protocols (Gerwin et al., 2019; Gerwin et al., 2020; Watkins et al., 2022; Zhang et al., 2014) with multiple antigen retrievals to accurately visualise neuronal components (including fusimotor innervation), contractile apparatus, capsule integrity, lysosomal enlargement, and autophagosome presence in muscle spindles, and I produced all high-resolution confocal images shown in Figures 4 A, B, and Figures 5-8. I observed that the structural degeneration of muscle spindles was very heterogeneous within a given muscle. This, and additional data suggested that the structural degeneration process of muscle spindles in *Gaa*$^{-/-}$ mice is progressive. Jürgen Schultheiß consequently categorised muscle spindle structure into four groups, acquired the representative bright-field microscopy and confocal images and conducted the associated statistical analysis (Figure 4 C, D). Muscle spindle numbers in wildtype and *Gaa*$^{-/-}$ soleus muscles were determined by Andi Rafuna, a graduate student in the lab. I performed all experiments required for the quantitative analysis of LAMP1 and LC3A/B accumulation in *Gaa*$^{-/-}$ and 129/SvJ EDL, soleus and TA muscles. I conducted the associated statistical analyses of 'above threshold pixels' using Zen software and ImageJ. Collectively, my results demonstrated that muscle spindle structure progressively degenerates in *Gaa*$^{-/-}$ mice. Additionally, I contributed to the drafting and subsequent revising of the manuscript, and I generated Figures 1-4A, B, 5-8 of the published manuscript.

1.3 Contribution to Paper III (Appendix A)

The mechanosensitive ion channel ASIC2 mediates both proprioceptive sensing and spinal alignment

It has been suggested that whilst PIEZO2 is strictly required for the initiation of an action potential, other mechanosensitive channels contribute to the generation of the receptor potential and the propagation of the stretch response along the sensory neuron (Bewick & Banks, 2015; Wilkinson, 2022). I therefore was interested in identifying additional ion channels contributing to mechanotransduction. This project was conducted in collaboration with Bavat Bornstein and Elazar Zelzer (Weizmann Institute, Rehovot, Israel). We identified ASIC2 as one such potential candidate channel. I designed the data acquisition protocol for, and performed all *ex-vivo* electrophysiology experiments, including preparation of the findings to be included in the manuscript, and produced all elements of Figure 5 for the final manuscript.

2. Introductory Summary

2.1 Chapter 2.1: Introduction

Proprioception allows for coordinated movements by perceiving the body's position in space (Gandevia et al., 1993; Tuthill & Azim, 2018). While proprioception is an integrative system achieved through a combination of peripheral sensory inputs describing muscle length and tension, joint angle, and skin stretch (Macefield & Knellwolf, 2018), a key component of this intricate system is the muscle spindle (Matthews, 2015; Proske & Gandevia, 2012). Embedded in skeletal muscles, these primary proprioceptive sensors relay constant information about muscle length and tone to the central nervous system (CNS; Kröger, 2018; Proske & Gandevia, 2012). From this information, the CNS computes the spatial position and motion of the body in space. This process is crucial for motor control, sustaining posture and ensuring a stable gait (Kröger & Watkins, 2021).

The general functional properties of muscle spindles have been established, however many fundamental aspects of muscle spindle function remain unknown. In particular, the molecular basis of muscle spindle function and the pathological changes particularly in neuromuscular diseases are mostly uncharacterised. The recent introduction of transgenic mouse models, and electrophysiological techniques that enable the isolation and functional analysis of individual muscle spindles (Franco et al., 2014; Gerwin et al., 2019) allow the analysis of muscle spindle function on a molecular level. Moreover, the advances in observer-independent behavioural assays (Brooks & Dunnett, 2009; Garrick et al., 2021; Mock et al., 2018), now allow for the detailed effect of individual molecules on a systemic level. These new assay systems have introduced the possibility for further and more comprehensive investigations into specific structural and functional aspects of muscle spindles.

The objective of the following combined works is to provide a better understanding of muscle spindle structure and function on a molecular basis under healthy and pathological conditions.

2.1.1 Chapter 2.1.1: Muscle spindle history and recent implications

The concept of proprioception was first described as 'a sense of locomotion' by Julius Caesar Scaliger in 1557 (Cohen, 1958; Kaya et al., 2018), and in 1833 this idea was expanded by Charles Bell (Bell, 1833b). Bell described the 'muscle sense', where muscles themselves report back to the brain after receiving motor input (Bell, 1833a). Muscle spindles themselves were first described in 1862 by Kölliker (Kölliker, 1862) and in 1863 by Kühne (Kühne, 1863). However, it wasn't until 1894 when Sir Charles Sherrington initially characterised 'sensory organs' in feline subjects (Sherrington, 1894) and their

sensory contribution was described by Ruffini in 1898 (Ruffini, 1898). In 1907, Sherrington coined the term 'Proprioception' (Sherrington, 1907), and experiments two decades later demonstrated that these structures are sensitive to stretch (Adrian & Zotterman, 1926; Matthews, 1933).

More recently, the proprioceptive system and especially muscle spindles, have been implicated in the regulation of many additional roles. These include skeletal function and development (Bornstein et al., 2021), particularly spinal alignment (Blecher et al., 2017b; Bornstein et al., 2021), bone fracture healing (Blecher et al., 2017a), joint morphogenesis (Assaraf et al., 2020; Bornstein et al., 2021) and recovery of basic locomotor skills after injury to the spinal cord, including neuronal circuit recovery and reorganisation (Takeoka & Arber, 2019; Takeoka et al., 2014). Furthermore, muscle spindles have been demonstrated to be affected in muscular and neuromuscular diseases (Cazzato & Walton, 1968), for example Muscular Dystrophies (Aimonetti et al., 2005; Gerwin et al., 2020; Swash & Fox, 1976), and additionally affected as a secondary consequence in other neuromuscular diseases including Parkinson's disease (Conte et al., 2013), Multiple Sclerosis (Cameron et al., 2008), Huntington's disease (Abbruzzese & Berardelli, 2003), Amyotrophic Lateral Sclerosis (ALS; Sangari et al., 2016; Vaughan et al., 2015), and Myasthenia Gravis (Swash & Fox, 1975). Therefore, it is of considerable clinical relevance to characterise muscle spindle structure and function on the molecular level, in order to enhance our understanding of their role under healthy and diseased conditions.

2.1.2 Chapter 2.1.2: Structure and Function of the Muscle Spindle

Muscle spindles are found in almost every muscle of the body, yet their abundance is relatively low. Rough estimations suggest that there are approximately 50,000 muscle spindles in the human body (Banks & Barker, 2004). Muscle spindle abundance within a given muscle does not appear to be correlated with muscle size, but rather the precision of the movement required by the muscle, with muscles requiring more precise proprioception exhibiting a higher density of muscle spindles (Macefield & Knellwolf, 2018). Additionally, muscle spindle abundance within a given muscle is highly correlated with muscle fascicle length, absolute fascicle length change and velocity of fibre lengthening (Kissane et al., 2022).

Muscle spindles of adult mice are approximately 200 µm – 400 µm in length and consist of 3-5 encapsulated and independently innervated intrafusal muscle fibres (Banks, 1994b; Bewick & Banks, 2015; Lionikas et al., 2013).

These intrafusal fibres can be distinguished into two distinct groups – nuclear bag or nuclear chain fibres. Nuclear bag fibres have a high density of nuclei clustering in the central region (Ovalle & Smith, 1972), and depending on the myosin ATPase isoform specificity, can be further categorised into nuclear bag I and nuclear bag II type fibres (Banks et al.,

1977; Barker, 1974; Kissane et al., 2022). All types of intrafusal fibres are highly organised on the subcellular level, and consist of non-contractile equatorial regions, and contractile polar ends (Bewick & Banks, 2015).

Additionally, the muscle spindle is enclosed by a connective tissue capsule (Banks, 1994a; Boyd, 1962). Formed from collagenous fibres, this capsule is critical in maintaining the functional integrity of the muscle spindle. This is achieved by providing support and serving as a protective barrier, separating the intrafusal fibres from the surrounding extrafusal fibres and thus maintaining the niche environment (Ovalle & Dow, 1985), allowing for the mechanical forces generated by the surrounding extrafusal fibres to be transmitted to the intrafusal fibres (Bewick & Banks, 2015; Kröger & Watkins, 2021; Ovalle & Dow, 1985).

2.1.3 Chapter 2.1.3: Muscle Spindle Innervation

Intrafusal fibres are innervated by both afferent and efferent neurons. The central or equatorial region is associated with two different types of myelinated, proprioceptive sensory neurons, group Ia and group II afferent endings (Banks, 2015; Hunt, 1990). Group Ia afferents coil around the equatorial region forming the annulospiral endings, and innervate bag I, bag II and chain fibres (Banks, 1986; Hulliger, 1984). Group Ia afferents have a higher conduction velocity (50-80 ms^{-1}) in contrast to the 'flower-spray' Group II endings (30-70 ms^{-1}). First described by Ruffini (Ruffini, 1898), group II endings selectively innervate bag II and chain fibres (Banks et al., 1982; Sonner et al., 2017). Additionally, bag II fibres predominantly control the resting discharge of primary endings (Proske et al., 1991).

The firing frequency of both group Ia and group II endings are proportional to the magnitude of muscle stretch (De-Doncker et al., 2003; Matthews, 1972). Group Ia afferents respond primarily to the dynamic component of stretch (i.e. the speed of length change), whilst group II endings respond primarily to static stretch (i.e. the amount of length change; Boyd et al., 1977). The cell bodies of both group Ia and group II afferents are located in the dorsal root ganglion (DRG), where they make up approximately 5-10% of the total neurons in the DRG (Oliver et al., 2021). Their projections extend into the spinal cord, where they divide into two distinct branches. One branch consists of a centrally orientated neurite that transmits proprioceptive information to the brain, while the other remains within the specific spinal cord segment, establishing direct monosynaptic connections with α-motoneurons (Marasco & de Nooij, 2023). These sensory neurons serve as afferents, while the α-motoneurons act as an efferent component of the monosynaptic stretch reflex circuit.

Intrafusal fibres receive additional efferent innervation from γ-motoneurons, referred to as the fusimotor innervation (Banks, 1994b; Proske, 1997). Along with the afferent neurites,

γ-motoneuron axons enter the spindle in the equatorial region, but within the spindle capsule project to the polar ends of the intrafusal fibres, where they form cholinergic synapses that are functionally similar to the neuromuscular junction (NMJ; Banks, 1994b; Hunt & Kuffler, 1951a). Their cell bodies account for approximately 30% of all motoneurons in the ventral horn (Nyberg-Hansen, 1965). By inducing contraction in the polar regions of intrafusal fibres, and consequently exerting tension on the equatorial region of the intrafusal fibres, the γ-motoneurons are able to continuously control the mechanical sensitivity of the muscle spindle over varying muscle lengths and stretch velocities (Banks, 1994b; Proske, 1997). When both intrafusal and extrafusal fibres are simultaneously stretched through α- and γ-coactivation, the sensitivity of muscle spindles is controlled by γ-motoneurons, which modulate the length of intrafusal fibres (Colon et al., 2017; Manuel & Zytnicki, 2019). This mechanism allows for muscle spindle sensitivity under both relaxation and contraction conditions (Bewick & Banks, 2015; Hunt & Kuffler, 1951b; Kröger & Watkins, 2021).

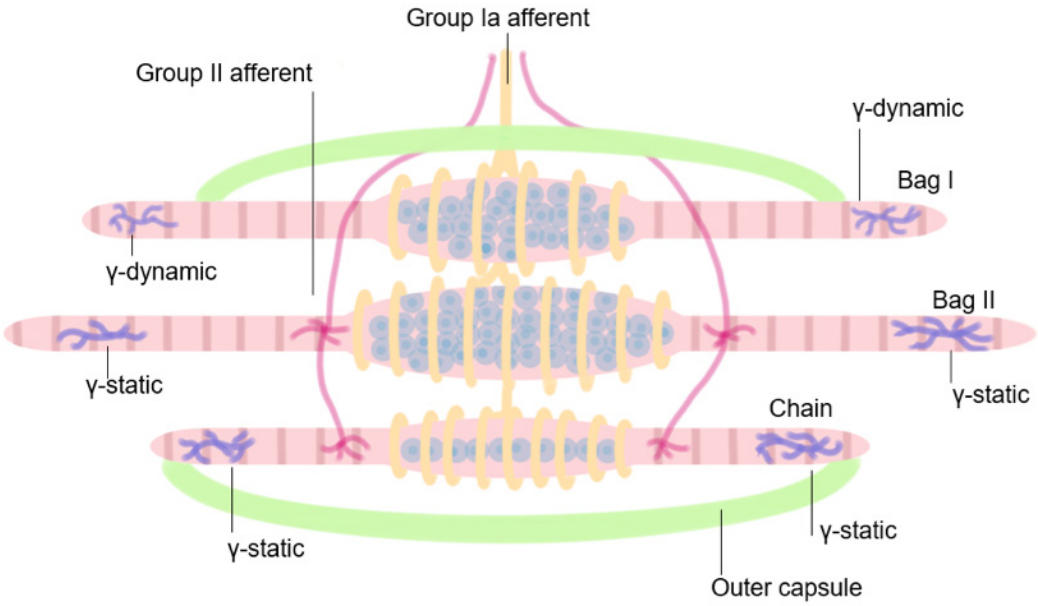

Figure 1: Schematic representation of a muscle spindle. The intrafusal muscle fibres (pink) are encased within a protective connective tissue capsule (green). All intrafusal muscle fibres receive innervation from group Ia afferents (yellow) and form the annulospiral endings in the equatorial region. Bag II and chain fibres are additionally innervated by flanking group II afferents. In the polar regions, bag II and chain fibres are innervated by static γ-motoneurons (purple), while bag I fibres are innervated by dynamic γ-motoneurons (purple). Adapted from Kröger & Watkins, 2021.

2.2 Chapter 2.2: Muscle Relaxants

2.2.1 Chapter 2.2.1: Introduction to muscle relaxants

Skeletal muscle relaxants represent a large and diverse group of chemical compounds that can lead to a reduction in skeletal muscle tone. This can prevent and effectively relieve painful muscle symptoms and increase muscle mobility (Chou et al., 2004; See & Ginzburg, 2008b). As a large class of pharmaceuticals with differing mechanisms of action, muscle relaxants have varying efficiencies and adverse side effects (Abdel Shaheed et al., 2017; Witenko et al., 2014).

There are two main classes of muscle relaxant – antispasticity and antispasmodic (See & Ginzburg, 2008a). Spasticity is described as disordered sensorimotor coordination resulting from damage to upper motoneurons, and presents as sporadic or continuous involuntary muscle activation (Kheder & Nair, 2012; Pandyan et al., 2005; See & Ginzburg, 2008b). Antispasticity muscle relaxants are clinically used to relieve symptoms of hypertonicity, clonus, exaggerated deep tendon reflexes and muscle spasms (Niemi, 2019; Pau, 2023). These drugs are usually prescribed to treat symptoms associated with chronic conditions such as multiple sclerosis, cerebral palsy, post-stroke syndrome and traumatic brain injuries, and are indicated for long term use (Pau, 2023; See & Ginzburg, 2008b).

The term ‘muscle spasm’ is used to describe involuntary and long-lasting muscle contractions (Mense & Masi, 2010; Simons & Mense, 1998). Muscle relaxants used to relieve the symptoms of muscle spasms are known as antispasmodic. Antispasmodics are indicated for short-term use (2-3 weeks) and are used to treat muscle spasms that are most commonly associated with muscle injury (Niemi, 2019; Pau, 2023).

Furthermore, skeletal muscle relaxants can be categorised as either centrally acting or peripherally acting, depending on whether they act upon the CNS or the peripheral nervous system (PNS), respectively (See & Ginzburg, 2008a).

Centrally acting antispasticity and antispasmodic muscle relaxants act on spinal neurons and reflex arcs (Davidoff, 1985), where they either enhance γ-aminobutyric acid (GABA) inhibitory neurotransmitter effects in the brain (e.g. baclofen, benzodiazepines), or modulate spinal reflexes by targeting GABA receptors located in the spinal cord, thus, effectively reducing the excitability of motoneurons (e.g. cyclobenzaprine, chlorzoxazone; McCarthy & Baum, 2017; Pau, 2023).

Peripherally acting antispasticity and antispasmodic muscle relaxants either directly affect excitation-contraction coupling (dantrolene; Davidoff, 1985) or act via the NMJ (a specialised synapse between an α-motoneuron and an extrafusal fibre) by affecting cholinergic synaptic transmission (Boon et al., 2018; Hunter, 1995; Raghavendra, 2002).

The release of acetylcholine (ACh) is triggered by calcium ions (Ca^{2+}) entering the presynaptic terminal, leading to the binding of ACh to receptors (AChRs) on the postsynaptic motor end plate (Rodriguez Cruz et al., 2020; Tintignac et al., 2015). This binding activates ligand-gated sodium channels, resulting in an influx of sodium ions (Na^{+}), which depolarises the membrane potential (Tanabe et al., 1990). If depolarisation reaches the threshold, voltage-gated sodium channels ($Na_V1.4$ – encoded by the *SCN4a* gene) open, allowing the action potential to propagate along muscle fibres via transverse tubules (T-tubules; Calderon et al., 2014; Sandow, 1952). This triggers the release of Ca^{2+} from the sarcoplasmic reticulum (SR), enabling actin and myosin to form cross-bridges and initiate muscle contraction (Calderon et al., 2014; Tanabe et al., 1990). To prevent continuous contraction, ACh in the synaptic cleft is rapidly hydrolysed by acetylcholinesterase (AChE; Soreq & Seidman, 2001). Muscle sarcomeres return to their resting length, and Ca^{2+} is pumped back into the SR via active ATP transport mechanisms (Ebashi & Lipmann, 1962).

Peripherally acting antispasmodic muscle relaxants can be further divided into two distinct subcategories dependent on their mechanism of action – depolarising muscle relaxants and non-depolarising muscle relaxants (Meleger, 2006). Depolarising muscle relaxants such as succinylcholine and tubocurarine bind competitively to AChRs (Foldes et al., 1957); however, these drugs are resistant to AChE and result in continuous stimulation of the AChRs. Consequently, there is a sustained influx of Na^{+}, prolonging depolarisation in the sarcolemma. The prolonged depolarisation results in desensitisation of the AChRs, which are left unresponsive to further stimulation, ultimately preventing action potential generation and subsequent muscle contraction (Foldes et al., 1957; Martyn et al., 2009). Similarly, non-depolarising muscle relaxants such as atracurium, pancuronium and gallamine also bind competitively to AChRs, however, in contrast to depolarising muscle relaxants, non-depolarising muscle relaxants prevent the activation of AChRs by ACh. Consequently, muscle contraction is prevented as the threshold for membrane potential is not reached, and thus action potential generation is blocked (Ellis & Carpenter, 1972; Krause et al., 2004; Kruidering-Hall & Campbell, 2017; Martyn et al., 2009).

2.2.2 Chapter 2.2.2: Skeletal muscle relaxants and muscle spindles

The effects of these pharmaceuticals, particularly peripherally acting muscle relaxants, have been well studied in extrafusal fibres; however, only limited studies have been conducted to investigate their effect on muscle spindle function (Gerwin et al., 2019; Watkins et al., 2022). Early studies noted that skeletal muscle relaxants have the potential to affect the function of all neuronal structures involved in reflex arcs – including the fusimotor innervation of muscle spindles (Davidoff, 1985). Further studies demonstrated an excitatory effect of cholinergic agents and anti-cholinesterases (including nicotine and succinyl-

choline) on intrafusal neuromuscular transmission, and an inhibitory effect of anti-cholinergic blocking agents (including tubocurarine and gallamine; Brown & Butler, 1973; Carr et al., 1996; Carr & Proske, 1996; Durbaba et al., 2006; Dutia, 1980; Gerwin et al., 2019; Gregory & Proske, 1987; Hunt, 1952; Smith, 1963; Taylor et al., 1992; Yamamoto et al., 1994). This could be of important clinical relevance as the afferent nerves from muscle spindles directly stimulate the synergistic muscles' α-motoneurons via the monosynaptic stretch reflex. Therefore, a compound that relaxes intrafusal muscle fibres will consequently decrease excitatory input received by α-motoneurons (Gerwin et al., 2019; Watkins et al., 2022), and could result in muscle damage, because the muscle does not contract as forcefully and efficiently as is required to prevent overstretching of the muscle (Chen et al., 2003; Pierrot-Deseilligny & Mazevet, 2000). Accordingly, it has been reported that patients prescribed with peripherally acting muscle relaxants are more likely to be hospitalised due to frequent falls and the resulting complications (Billups et al., 2011), however the effect of more recently developed skeletal muscle relaxants particularly on individual muscle spindles have not been studied.

2.2.3 Chapter 2.2.3: Skeletal muscle relaxant: methocarbamol

Methocarbamol is one such drug that has so far not been studied in the context of muscle spindles. It is an antispasmodic, non-benzodiazepine medication that is clinically used as a short-term muscle relaxant (Aljuhani et al., 2017; Park, 1958; Weiss & Weiss, 1962). Methocarbamol is one of the most highly prescribed skeletal muscle relaxants used in the treatment of acute musculoskeletal pain, and more recently has been used at practitioner's discretion to treat acute and chronic non-specific lower back pain, fibromyalgia, myofascial pain and in perioperative care in orthopaedic surgeries (Beebe et al., 2005; Looke & Kluth, 2013; Richards et al., 2012). Methocarbamol was traditionally thought to act only centrally (Roszkowski, 1960; Truitt & Little, 1958; Witenko et al., 2014), however, it has been recently demonstrated that methocarbamol elicits additional effects peripherally, where it specifically blocks the muscular voltage-gated sodium channel 1.4 ($Na_v1.4$; Zhang et al., 2021). As action potential initiation and propagation in skeletal muscle fibres is instigated by $Na_v1.4$, methocarbamol administration has been accordingly reported to result in a prolonged refractory period and suppression of polysynaptic reflex contractions, without spinal interneuron involvement (Crankshaw & Raper, 1968; Crankshaw & Raper, 1970).

2.2.4 Chapter 2.2.4: Skeletal muscle relaxant: mexiletine

Mexiletine is a class IB antiarrhythmic medication that is structurally similar to methocarbamol. Mexiletine is an antispasmodic, non-benzodiazepine, which is used clinically to treat cardiac arrhythmia, and at healthcare professionals' discretion, muscle cramps, neuropathy, brain ischemia and skeletal muscle channelopathies (D'Mello & Shum, 2016;

Ginanneschi et al., 2017; Logigian et al., 2010; Monk & Brogden, 1990; Oskarsson et al., 2018; Statland et al., 2012; Stunnenberg et al., 2018; Suetterlin et al., 2015). Mexiletine has been reported to have local anaesthetic, anticonvulsant and antiarrhythmic properties (Campbell, 1987; Monk & Brogden, 1990; Suetterlin et al., 2015). Similar to methocarbamol, mexiletine effectively, but non-selectively blocks fast voltage-gated sodium channels, including $Na_v1.4$ (Monk & Brogden, 1990; Nakagawa et al., 2019). Similar to methocarbamol, mexiletine prolongs the refractory period of voltage-gated sodium channels, which delays recovery from the inactivated state and thus, prevents further continuous muscle contraction (De Bellis et al., 2017; Watkins et al., 2022).

2.2.5 Chapter 2.2.5: Study aims

Although muscle spindle function is reasonably well characterised, the molecules that mediate their role, along with the potential mechanisms that influence their specific functions are not well understood. As neither methocarbamol nor mexiletine have been studied in the context of muscle spindles, the aim of this project was to determine whether these medications may also affect muscle spindle function.

2.2.6 Chapter 2.2.6: Summary

In order to determine the impact of mexiletine and methocarbamol on muscle spindle function, I initially conducted functional experiments. Administering these two common skeletal muscle relaxants to an *ex-vivo* electrophysiological assay demonstrated a dose-dependent effect on muscle spindle function. Notably, I discovered that in response to the administration of both mexiletine and methocarbamol, there was no gradual decline of action potential frequency under resting conditions or during stretched states, but muscle spindles instead only responded with an ‘all-or-nothing’ response, i.e. action potentials were either generated, or they were not. Thus, there was no apparent dose-dependent change in the frequency or amplitude of the action potentials. As both mexiletine and methocarbamol affect muscle spindle afferent function via similar molecular mechanisms, there is a strong possibility that both of these drugs target the same voltage-gated sodium channel in muscle spindle afferents (Watkins et al., 2022).

To investigate whether the voltage-gated sodium channel $Na_v1.4$ - a potential target of both drugs - is present in intrafusal fibres, I analysed 20-30µm cryo-sections that were fluorescently labelled with anti-$Na_v1.4$ and anti-vGluT1 antibodies. $Na_v1.4$ is concentrated in the membrane of the T-tubule system of extrafusal fibres (Caldwell, 1986; Caldwell et al., 1986), and, accordingly, can be used as a marker to investigate the structure of the T-tubule system. High-resolution confocal microscopy analyses of the polar ends revealed the exact subcellular distribution of $Na_v1.4$ in intrafusal fibres. I demonstrated that

similar to extrafusal fibres, phalloidin and anti-Na_v1.4 colocalise. Interestingly, the subcellular distribution of Na_v1.4 is different in intrafusal fibres compared to extrafusal fibres. In the immunohistochemical analysis, the signal observed in intrafusal fibres stained with anti-Na_v1.4 antibodies, was present as a single band, rather than a double band as in the T-tubule system of extrafusal fibres (Watkins et al., 2022). Previous studies have shown that a T-tubule system is present in intrafusal fibres on the electron-microscopic level (Ovalle, 1971), however, this result suggests that the T-tubule system present in intrafusal fibres may have a different structure to that of the T-tubule system in extrafusal fibres. These results demonstrate that Na_v 1.4 – one potential target for mexiletine and methocarbamol – are present in intrafusal fibres.

This is the first study to look at mexiletine and methocarbamol and their dose-dependent effects on muscle spindle function. Additionally, dose-response curves revealed that the applied dosages of mexiletine may be of clinical relevance, and that therefore the administration of these drugs might contribute to the frequent falls and unstable gait seen in patients that have received this muscle relaxant (Watkins et al., 2022).

2.3 Chapter 2.3: Pompe Disease

2.3.1 Chapter 2.3.1: Introduction to Pompe Disease

Pompe disease, also known as Glycogen storage disease II or acid maltase deficiency, is a rare, progressive neuromuscular degenerative disease (Kohler et al., 2018; Lim et al., 2014; Peruzzo et al., 2019; van der Ploeg & Reuser, 2008). It has an autosomal recessive mode of inheritance, with incident rates approximated at 1 in 40,000 (Ausems et al., 1999). This disorder was first described in 1932 by Drs J.C Pompe (Pompe, 1932), and G. Bischoff and W. Putschar (Bischoff, 1932; Putschar, 1932). These physicians independently described it as a generalised muscle weakness that presented with idiopathic cardiac hypertrophy along with generalised glycogen accumulation throughout bodily tissues (Reuser & Schoser, 2022). However, it was not until 1963 when H. Hers first characterised the crucial enzyme, α-acid glucosidase (GAA), noting “a clear correlation between the absence of acid maltase (α-acid glucosidase) in the liver, heart and skeletal muscles, and the large deposition of glycogen that characterises Pompe disease.” (Hers, 1963; Reuser & Schoser, 2022). In 1970, Andrew Engel first described a late onset form of the disease, which he noted as mimicking muscular dystrophies or other myopathies (Engel, 1970).

2.3.2 Chapter 2.3.2: Pompe Disease Aetiology

Pompe disease is a result of a mutation in the *GAA* gene. This gene encodes the enzyme α-acid glucosidase (GAA), which catalyses the degradation of glycogen in lysosomes by breaking the internal α-1,4- and α-1,6-glucosidic linkages (Hirschhorn & Reuser, 2001; Martiniuk et al., 1991). Mutations in the gene result in reduced or completely absent GAA enzyme activity, with an estimate that 25% or less of remaining enzyme activity will result in disease symptoms (Niño et al., 2021). More than 550 different mutations have so far been described and listed at the human gene mutation database – HGMD - https://www.hgmd.cf.ac.uk/ac/ (Peruzzo et al., 2019). Some of these mutations arise through abnormal splicing sites and result in incorrectly spliced mRNA products, which lead to the abortion of enzyme synthesis, whilst other mutations cause incorrect protein folding, rendering a non-functional protein (de Faria et al., 2021; Niño et al., 2021; Reuser et al., 2019). However, the outcome in all cases is that lysosomal glycogen cannot be effectively broken down, resulting in large glycogen deposits in lysosomes, which then continuously enlarge, and lead to the destruction of the entire cell, and eventually entire organs (De Filippi et al., 2014). All tissues have been shown to be affected by the accumulation of these glycogen deposits, however skeletal and cardiac muscle appear to be the most severely affected by the disease (Griffin, 1984; Lim et al., 2014).

2.3.3 Chapter 2.3.3: Pompe Disease Classification

The severity of disease is typically correlated inversely to remaining enzyme function (De Filippi et al., 2014), and although considered as a continuation spectrum, in accordance with the official Pompe variant database, Pompe disease is classified as either Infantile Onset-Pompe disease, childhood or Adult Onset Pompe disease - https://www.pompevariantdatabase.nl (Angelini & Engel, 1972; de Faria et al., 2021; Niño et al., 2021; Reuser & Schoser, 2022).

Classic Infantile Onset Pompe disease patients present with rapidly progressing symptoms within the first few weeks of life and death by cardio-respiratory failure usually occurs within 12 months (Angelini & Engel, 1972; Kishnani et al., 2006). This severe form of the disease is characterised by either completely absent or less than 1% of remaining enzyme activity, leading to cardiomegaly, hepatomegaly, hypotonia, and muscle weakness (Cabello & Marsden, 2016; Kishnani & Howell, 2004).

Non-classic Infantile Onset Pompe disease, also more recently referred to as childhood Pompe disease, presents within the first 18 years of life. As there is more GAA enzymatic activity remaining, disease progression is slower and cardiomyopathy symptoms are less severe in these patients (Holzwarth et al., 2022; van Capelle et al., 2016).

Depending on the remaining GAA enzyme activity, Adult Onset Pompe disease can present from early adulthood, up until the sixth decade of life (Chan et al., 2017; Van der

Beek et al., 2009). With up to 25% of detectable GAA enzyme activity remaining, Adult Onset Pompe disease is usually characterised by a slowly progressing myopathy that predominantly affects skeletal muscle but does not typically include severe cardiomyopathy (Kroos et al., 2012; Schoser & Laforet, 2022; Schüller et al., 2012; Soliman et al., 2008; Toscano et al., 2019; Umapathysivam et al., 2005).

Currently, the standard treatment for Pompe disease is Enzyme Replacement Therapy (ERT; Angelini & Semplicini, 2012; Kishnani & Beckemeyer, 2014; Reuser & Schoser, 2022; Toscano & Schoser, 2013); where recombinant GAA enzyme is introduced intravenously to aid in glycogen degradation. However, ERT has little effect on the motor coordination deficits, and skeletal muscle exhibits a very limited response to this treatment (Koeberl et al., 2011; Ravaglia et al., 2010; Strothotte et al., 2010; van Capelle et al., 2010). Moreover, this treatment is extremely costly, limiting its application to a minority of patients.

Non-classic Infantile and Adult Onset Pompe disease patients often experience areflexia, poor stability and balance as well as an abnormal gait (McIntosh et al., 2015; Schneider et al., 2020; Valle et al., 2016). As a result, these patients have an increased tendency to fall, which may lead to hospitalisation and prolonged immobilisation, which exacerbates symptoms (Horlings et al., 2008; Puthucheary et al., 2010). Possible contributing factors towards these symptoms could include muscle spindle function deficits or altered proprioceptive information in the brain.

2.3.4 Chapter 2.3.4: Pompe Disease Mouse Models

There are several mouse lines that recapitulate different aspects of Pompe disease (Geel et al., 2007). The most widely used preclinical murine model for Pompe disease was generated by Nina Raben (Raben et al., 1998). Created by inserting a neomycin cassette at exon 6, and completely stopping GAA enzyme production, these mice effectively model aspects of both Infantile and Adult Onset Pompe disease. These mice are commercially available (B6;129-Gaa^{tm1Rabn}/J mice; JAX stock #004154; *Gaa*$^{-/-}$), and homozygotes are phenotypically normal at birth (Raben et al., 1998; Raben et al., 2000). By 3 weeks of age, progressively increasing glycogen deposits can be detected in diaphragmatic, cardiac and skeletal muscle lysosomes. Between 3-4 weeks of age, these mice exhibit reduced strength and mobility, and glycogen accumulates can be detected in intrafusal fibres. By 15-16 weeks of age, *Gaa*$^{-/-}$ mice exhibit progressive muscle weakness, failing in vertical and inverted hanging tests; and by 8-9 months of age, animals exhibit extreme muscle wasting, and a weak, unstable gait (Raben et al., 1998; Schaaf et al., 2015). In previous studies, these mice have performed poorly in coordination tests demonstrating muscle weakness, an abnormal gait and reduced activity in open field tests (Raben et al., 2000). The cause for the motor coordination symptoms is unknown.

2.3.5 Chapter 2.3.5: Study aims

It has been reported that muscle spindle function is affected in neuromuscular diseases and that these patients have symptoms caused by an impaired proprioceptive system (Cazzato & Walton, 1968). Understanding the underlying mechanisms that lead to an impaired motor control system could allow for earlier interventions in proprioceptive symptoms.

As Pompe patients often exhibit an unstable gait and frequent falls, particularly in the absence of visual input (McIntosh et al., 2015; Schneider et al., 2020), and *Gaa*$^{-/-}$ mice perform poorly on coordination tests (Raben et al., 2000), I hypothesised that an impaired muscle spindle function contributes to motor control deficits in Pompe patients (Watkins et al., 2023).

2.3.6 Chapter 2.3.6: Summary

In order to investigate whether an impaired muscle spindle function contributes to the motor deficits experienced by Pompe patients, I analysed *Gaa*$^{-/-}$ mice at four and eight months of age and compared them to age-matched 129/SvJ control mice. To this end, I conducted an observer-independent behavioural analysis using the Catwalk XT system (Chen et al., 2014) to identify and quantify motor coordination deficits, where I specifically looked at temporal parameters, spatial parameters, interlimb coordination parameters, run characteristics and kinetic parameters (Pitzer et al., 2021). My analysis revealed several altered parameters in 4- and 8-month-old *Gaa*$^{-/-}$ mice in comparison to age-matched 129/SvJ control mice. Whilst many of the results can be attributed to muscle weakness (e.g. steps per run and print area), the interlimb coordination parameter analysis strongly depends on proprioceptive information. *Gaa*$^{-/-}$ mice exhibited an increased base of support, an increased ipsilateral paw displacement, and a decrease of recognised walking patterns. These results are consistent with an impaired motor control in *Gaa*$^{-/-}$ mice (Watkins et al., 2023).

To examine if the motor control deficits are accompanied by an altered function of muscle spindles, I recorded the neural activity of single-unit proprioceptive afferents in response to ramp and hold protocols, using *ex-vivo* electrophysiology in 4- and 8-month-old *Gaa*$^{-/-}$ mice. The ramp and hold protocol consisted of 2.5, 5 and 7.5% L_0 length changes (with 40% L_0 per second ramp speed), where I analysed four parameters during the stretch response – dynamic peak (DP), dynamic index (DI), initial static time (IST) and final static time (FST). These parameters are illustrated in Figure 2 F.

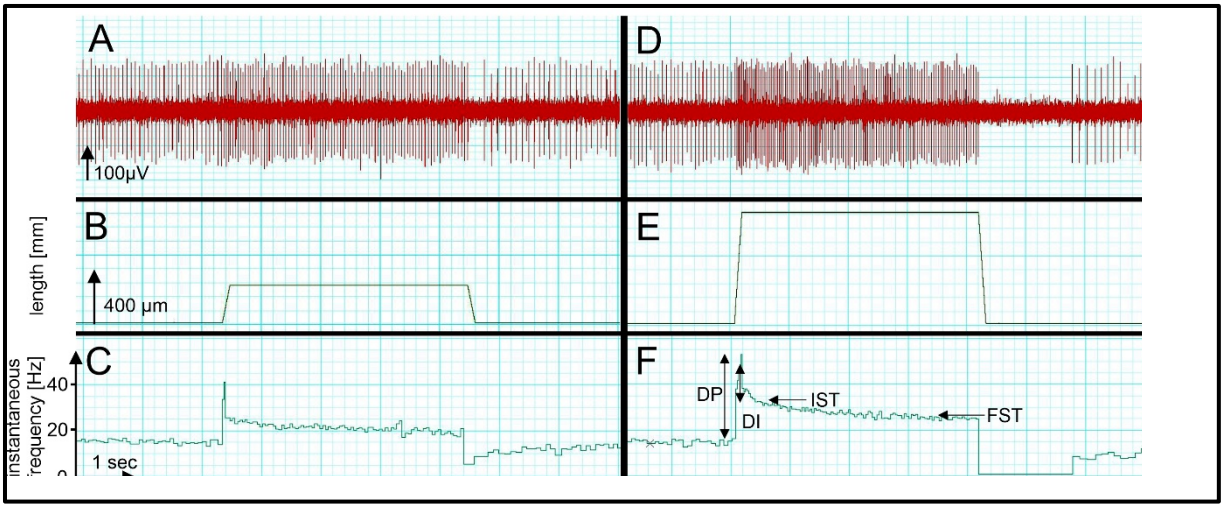

Figure 2: **Typical response from a muscle spindle in response to stretch stimuli.** Single unit action potentials are shown in response to (a) 2.5% of baseline length (L_0) and (d) 7.5% of L_0 over 4s stretch protocols. The length change corresponds to (b) 260 µm and (e) 780 µm. The instantaneous frequency plotted against time is shown in panels (c) and (f). In panel f, the different parameters that are analysed are displayed. The dynamic peak (DP) is the highest firing rate during the ramp, the initial static time (IST) is the rate of firing over the first 0.5 secs of static hold, the dynamic index (DI) is the difference in firing rate between the DP and IST, and the final static time (FST) is the average firing rate over the last 0.5 secs of static stretch. Adapted from Kröger & Watkins, 2021.

All proprioceptive afferents from 4-month-old *Gaa*$^{-/-}$ mice, and ~70% from 8-month-old *Gaa*$^{-/-}$ mice were responsive to stretch (i.e. the instantaneous action potential frequency increased in response to the stretch stimulus). However, in comparison to age matched 129/SvJ controls, both 4- and 8-month-old *Gaa*$^{-/-}$ mice exhibited a significantly decreased instantaneous action potential frequency during all four stretch parameters analysed. This demonstrates a reduced dynamic and static sensitivity to stretch in *Gaa*$^{-/-}$ mice (Watkins et al., 2023). Approximately 30% of recordings from 8-month-old *Gaa*$^{-/-}$ mice exhibited action potential bursts, where bursts of action potentials followed by short rest periods (no action potentials) were observed. Whilst the bursts within a given muscle spindle were

invariant, bursts between different muscle spindles were very heterogeneous. Importantly, all muscle spindle afferents that exhibited action potential bursting behaviour, were not responsive to stretch (i.e. the instantaneous action potential frequency did not increase in response to the stretch stimulus), and they instead maintained the action potential bursting behaviour throughout the ramp and hold protocols. These results are consistent with functionally impaired muscle spindle afferent responses in 4- and 8-month-old *Gaa*$^{-/-}$ mice in comparison to age-matched 129/SvJ mice, and are indicative of a severely diminished muscle spindle sensitivity to stretch that develops into a complete absence of stretch sensitivity with disease progression in *Gaa*$^{-/-}$ mice (Watkins et al., 2023).

In order to determine whether structural abnormalities accompanied the behavioural and functional impairments, I used immunohistochemistry to compare the morphology of age matched 129/SvJ mice and 4- and 8-month-old *Gaa*$^{-/-}$ mice. I analysed 20-30µm thick cryo-sections of EDL and soleus muscles that were fluorescently labelled with different antibodies in order to visualise neuronal components including sensory and motor innervation (anti-vGluT1, anti-neurofilament 200, α-bungarotoxin), contractile apparatus (anti-S46, anti-Na_v1.4), capsule integrity (anti-versican), lysosomal enlargement (anti-LAMP1) and autophagosome presence (anti-LC3AB) in muscle spindles. Although the structural degradation of muscle spindles was heterogeneous within a given muscle, high-resolution confocal microscopy suggested that the degeneration process of muscle spindles in *Gaa*$^{-/-}$ mice was progressive. As the disease advances, increased numbers of autophagosomes and lysosomes can be detected. Furthermore, the sensory nerve terminals degenerate and withdraw from the annulospiral structure around the intrafusal fibres, to form large neuronal varicosities, typical of the axonal dying back mechanism (Yong et al., 2021). Additionally, the contractile apparatus is no longer restricted to the polar ends of intrafusal fibres and is instead observed throughout the central region. This is accompanied by an increased and non-restricted distribution of capsule associated proteins throughout the muscle spindle. These findings demonstrate severe, progressive structural degradation of the sensory innervation, connective tissue capsule and intrafusal fibres in the muscle spindles of *Gaa*$^{-/-}$ mice (Watkins et al., 2023).

This study represents the first analysis of muscle spindle structure and function in *Gaa*$^{-/-}$ mice. Taken together, the results are indicative that degenerating muscle spindles in *Gaa*$^{-/-}$ mice could contribute to the poor motor coordination, unstable gait, and consequent frequent falls of Pompe patients (Watkins et al., 2023). Pompe patients may therefore benefit from having proprioceptive training (Aman et al., 2014; Yong & Lee, 2017) incorporated into their treatment regime (Lamartine & Remiche, 2019; Valle et al., 2016).

2.4 Chapter 2.4: Mechanosensitive ion channels

2.4.1 Chapter 2.4.1: Introduction to mechanosensitive ion channels

The molecular basis underlying the transformation of the rate and speed of stretching in the equatorial region of intrafusal fibres into a receptor potential and subsequently into action potentials remains largely unknown (Bewick & Banks, 2015). The calcium permeable ion channel PIEZO2 has been identified as the key mechanotransduction channel (Florez-Paz et al., 2016; Woo et al., 2015). The discovery of the family of mechano-gated channels of the Piezo family was awarded the Nobel Prize in Physiology or Medicine in 2021 (Martinac, 2022). In humans and mice, loss of function mutations in the *Piezo2* gene result in the loss of mechanotransduction in proprioceptive neurons, and additionally, in scoliosis and hip dysplasia (Assaraf et al., 2020; Blecher et al., 2018; Blecher et al., 2017a; Chesler et al., 2016; Delle Vedove et al., 2016). However, evidence suggests that whilst PIEZO2 is strictly required for the initiation of an action potential, other mechanosensitive channels contribute to the generation, modulation and propagation of the stretch response along the sensory neuron (Wilkinson, 2022).

More recently, single nuclei transcriptomics and muscle spindle proteomics of muscle spindles (Bornstein et al., 2023a; Kim et al., 2020) and proprioceptive sensory neurons (Oliver et al., 2021; Wu et al., 2021) were performed. These transcriptomic analyses revealed that other mechanosensitive ion channels are expressed by proprioceptive sensory neurons – including members of the DEG/ENaC (Simon et al., 2010; Wu et al., 2021), TRP families (Simon et al., 2010; Wu et al., 2021), as well as glutamate receptors (Bewick et al., 2005; Than et al., 2021; Wu et al., 2004), acetylcholine receptors (Gerwin et al., 2019) and acid sensing ion channels (ASICs; Lin et al., 2016; Wilkinson, 2022; Wu et al., 2021). However, their roles in mechanotransduction are not well understood. It is therefore possible that these additional ion channels have a modulatory effect on muscle spindle excitability (Bewick & Banks, 2015; Bewick & Banks, 2021; Wilkinson, 2022).

2.4.2 Chapter 2.4.2: Acid sensing ion channels (ASICs)

Asic2 and *Asic3* transcripts have been identified in transcriptomic analyses of proprioceptive neuron terminals (Lin et al., 2016; Simon et al., 2010), and in the absence of *Asic3*, the dynamic stretch sensitivity was increased in response to ramp stimuli, but all other aspects of mechanotransduction and muscle spindle function appeared unaffected (Lin et al., 2016). This suggests that ASIC3 modulates muscle spindle sensitivity to stretch. In contrast, the epithelial sodium channel antagonist, amiloride (which non-specifically blocks DEG/ENaC channels) was demonstrated to completely inhibit muscle spindle afferent firing (Simon et al., 2010). Furthermore, ruthenium red (used to block TRPA1 and

Piezo channels, but not ASICs or ENaC channels), has been demonstrated to significantly reduce, but not completely inhibit, stretch-induced firing of rat muscle spindle afferents, via TRP channel inhibition (Suslak et al., 2015). Thus, there is a discrepancy between the specific genetic deletion, and the broader pharmacological inhibition, suggesting the possibility that other ASIC channels might also contribute to mechanotransduction in proprioceptive afferents.

2.4.3 Chapter 2.4.3: Study aims

In a complete transcriptomic analysis of proprioceptive endings, *Asic2* was found to be more differentially expressed in several different proprioceptors (Bornstein et al., 2023a), and we therefore hypothesised that the ASIC2 channel may specifically contribute to proprioceptive mechanotransduction in the proprioceptive sensory afferent terminal (Bornstein et al., 2023b).

2.4.4 Chapter 2.4.4: Summary

Through the electrophysiological characterisation, using an *ex-vivo* preparation of the EDL muscle from *Asic2*$^{-/-}$ mice (B6.129-*Asic2*^{tm1Wsh}/J; The Jackson Laboratory; #013126), I provide evidence that in comparison to littermate controls, *Asic2*$^{-/-}$ mice exhibit altered muscle spindle afferent responses to ramp and hold stretching protocols. Muscle spindles from *Asic2*$^{-/-}$ mice displayed heterogeneous stretch responses to the ramp and hold protocol consisting of 2.5, 5 and 7.5% L_0 length changes (with 40% L_0 per second ramp speed). I analysed four parameters during the stretch response – dynamic peak (DP), dynamic index (DI), initial static time (IST) and final static time (FST); see Figure 5 in Bornstein et al., 2023b for a more detailed explanation of parameters analysed. The stretch responses were qualitatively categorised as either sustained stretch (i.e. the muscle spindle responded with a sustained, increased action potential firing frequency for the duration of the stretch protocol) or non-sustained stretch (i.e. the muscle spindle was responsive to the stretch stimulus, however could not sustain action potential firing for the duration of the stretch, and ceased firing momentarily through the stretch protocol). Of the muscle spindle afferents that responded with a sustained stretch response to the ramp stimuli, I found that these muscle spindles had a significantly increased dynamic, but not static, sensitivity to stretch in comparison to the littermate controls (*Asic2*$^{+/+}$ or *Asic2*$^{+/-}$). In contrast, muscle spindle afferents that responded with a non-sustained stretch response to the stretch stimulus had a significantly increased dynamic and static sensitivity to stretch in comparison to littermate controls. These results provide further evidence that ASIC2 is required for normal muscle spindle function. Its function may be to moderate, stabilise and sustain muscle spindle afferent responses to stretch (Bornstein et al., 2023b).

2.5 Chapter 2.5: Research Impact Statement

Muscle spindle functions are poorly understood on the molecular level. In order to enhance our understanding of muscle spindles on the molecular level, I utilised an *ex-vivo* electrophysiology assay to characterise muscle spindle function, immunohistochemistry and high-resolution confocal microscopy to investigate muscle spindle morphology, and observer-independent behaviour analysis (Catwalk XT system) to identify potential motor-coordination deficits in healthy and diseased mouse models.

I have provided evidence that the two common skeletal muscle relaxants, methocarbamol and mexiletine, in a dose-response manner, significantly reduce muscle spindle afferent sensitivity to stretch, in particular sensitivity to static stretch. Additionally, I provided the first evidence that the subcellular distribution of the T-tubule system in intrafusal fibres may differ from extrafusal fibres (Watkins et al., 2022).

Furthermore, I accumulated evidence that muscle spindle morphology and function are affected in a neuromuscular disorder model. In a murine model of Pompe disease, I have provided evidence that muscle spindles undergo a severe and progressive degeneration process, which eventually results in completely non-functional muscle spindles. *Gaa*$^{-/-}$ mice exhibit poor motor and inter-paw coordination. In agreement with this, muscle spindle afferents exhibit a significantly reduced response to both dynamic and static stretch, and as the degeneration process advances, that muscle spindle afferents become unresponsive to stretch. I also demonstrate that morphological degradation of the muscle spindle neuronal components, contractile apparatus and connective tissue capsule occurs (Watkins et al., 2023).

Additionally, I have characterised muscle spindle afferent responses from *Asic2*$^{-/-}$ mice and have provided evidence that ASIC2 functionally modulates muscle spindle afferent responses to stretch (Bornstein et al., 2023b).

These combined works enhance our understanding of muscle spindle structure and function under healthy and pathological conditions, and consequently provides an explanation how proprioceptive information from muscle spindles may be significantly diminished under these conditions in human patients. Health care practitioners should consider the effects that common muscle relaxants can elicit on proprioception when prescribing muscle relaxants (Watkins et al., 2022), and additionally consider integrating proprioceptive physiotherapy in the treatment regimens of patients diagnosed with neuromuscular disorders (Watkins et al., 2023).

3. Paper I

Watkins, B., Schuster, H. M., Gerwin, L., Schoser, B., & Kröger, S. (2022). The effect of methocarbamol and mexiletine on murine muscle spindle function. *Muscle Nerve*. *66*(1), 96-105. https://doi.org/10.1002/mus.27546

Received: 23 March 2021 | Revised: 23 February 2022 | Accepted: 25 February 2022
DOI: 10.1002/mus.27546

BASIC SCIENCE RESEARCH ARTICLE

MUSCLE

The effect of methocarbamol and mexiletine on murine muscle spindle function

Bridgette Watkins MBiotech[1] | Hedwig M. Schuster MD[1] | Laura Gerwin PhD[1] | Benedikt Schoser MD[2] | Stephan Kröger PhD[1]

[1]Department of Physiological Genomics, Biomedical Center, Ludwig-Maximilians-University, Planegg-Martinsried, Germany

[2]Department of Neurology, LMU Klinikum, Friedrich-Baur-Institute, Ludwig-Maximilians-University, Munich, Germany

Correspondence
Stephan Kröger, Biomedical Center, Ludwig-Maximilians-University, Grosshaderner Strasse 9, D-82152 Planegg-Martinsried, Germany.
Email: skroeger@lmu.de

Funding information
Deutsche Forschungsgemeinschaft, Grant/Award Number: KR1039/16-1; Deutsche Gesellschaft für Muskelkranke; Munich Center for Neurosciences - Brain and Mind; Recordati Pharma GmbH

Abstract

Introduction/Aims: The muscle relaxant methocarbamol and the antimyotonic drug mexiletine are widely used for the treatment of muscle spasms, myotonia, and pain syndromes. To determine whether these drugs affect muscle spindle function, we studied their effect on the resting discharge and on stretch-induced action potential frequencies of proprioceptive afferent neurons.

Methods: Single unit action potential frequencies of proprioceptive afferents from muscle spindles in the murine extensor digitorum longus muscle of adult C57BL/6J mice were recorded under resting conditions and during ramp-and-hold stretches. Maximal tetanic force of the same muscle after direct stimulation was determined. High-resolution confocal microscopy analysis was performed to determine the distribution of $Na_v1.4$ channels, a potential target for both drugs.

Results: Methocarbamol and mexiletine inhibited the muscle spindle resting discharge in a dose-dependent manner with IC_{50} values around 300 μM and 6 μM, respectively. With increasing concentrations of both drugs, the response to stretch was also affected, with the static sensitivity first followed by the dynamic sensitivity. At high concentrations, both drugs completely blocked muscle spindle afferent output. Both drugs also reversibly reduced the specific force of the extensor digitorum longus muscle after tetanic stimulation. Finally, we present evidence for the presence and specific localization of the voltage-gated sodium channel $Na_v1.4$ in intrafusal fibers.

Discussion: In this study we demonstrate that both muscle relaxants affect muscle spindle function, suggesting impaired proprioception as a potential side effect of both drugs. Moreover, our results provide additional evidence of a peripheral activity of methocarbamol and mexiletine.

Abbreviations: AU, arbitrary units; CNS, central nervous system; EDL, extensor digitorum longus; Na_v, voltage-gated sodium channel; Lo, baseline length; ACSF, artificial cerebrospinal fluid; DP, dynamic peak; SR, static response.

Bridgette Watkins and Hedwig M. Schuster have contributed equally to this work

KEYWORDS
intrafusal fiber, mechanosensation, muscle relaxant, proprioception, stretch response, voltage-gated sodium channel

1 | INTRODUCTION

Skeletal muscle relaxants can be classified as antispasticity or antispasmodic agents and they act in the central nervous system (CNS) or peripherally.[1-4] For many of these drugs, it is not known whether tissues other than skeletal muscle are also affected.

Muscle spindles are encapsulated sensory structures located within almost every skeletal muscle.[5] They provide the CNS with proprioceptive information, the processing of which is required for all coordinated movements.[5-7] Muscle spindles consist of specialized muscle fibers (intrafusal fibers) that are innervated by two types of neurons: in the central (equatorial) region, the terminals of group Ia and group II proprioceptive sensory neurons encircle intrafusal muscle fibers with annulospiral endings. These sensory nerve terminals are mechanosensitive structures and detect how much and how fast a muscle is lengthened. In addition, efferent gamma-motoneurons innervate the peripheral (polar) regions of intrafusal fibers (fusimotor innervation), where they form cholinergic synapses that are functionally and developmentally similar to the neuromuscular junctions formed by alpha-motoneurons on extrafusal fibers.[8,9]

Although the effects of peripherally acting muscle relaxants on extrafusal muscle fibers have been rather well characterized, their effect on muscle spindles is less well understood. Patients experience an increased risk of falls and bone fractures after the initiation of a skeletal muscle relaxant,[10] suggesting that these drugs in addition to skeletal muscle fibers may also affect proprioception. Therefore, data on the action of muscle relaxants on muscle spindles are essential to understand the mode of action of the drugs in patients.

In our study, we investigated the effect of a muscle relaxant (methocarbamol) and the antimyotonic drug mexiletine on proprioceptive sensory output of adult murine muscle spindles. Methocarbamol, mexiletine, and their derivatives belong to the most widely prescribed antispasmodic, non-benzodiazepine group of muscle relaxants.[3,11] Methocarbamol is used for the treatment of lower back pain, as an adjunct to physical therapy for the relief of acute musculoskeletal pain, such as after acute traumatic injury,[4,12-15] treatment of stiff-man syndrome,[16] and painful muscle spasm.[12,13,17-20] For many years, methocarbamol was considered a centrally acting relaxant[4,21,22]; however, recently the specific inhibition of the voltage-gated sodium channel 1.4 ($Na_v1.4$), but not of $Na_v1.7$, was reported.[23] Because $Na_v1.4$ is the primary voltage-gated sodium channel responsible for the initiation of action potentials in skeletal muscle fibers, a peripheral action of methocarbamol is likely to contribute to its muscle-relaxing activity. Accordingly, Crankshaw and Raper reported that methocarbamol caused a prolongation of the refractory period of cat tibialis muscle and a suppression of polysynaptic reflex contractions without an effect on spinal interneurons.[24,25]

Mexiletine is an orally active class IB antiarrhythmic, which is clinically used to treat cardiac arrhythmia, muscle cramps, and skeletal muscle channelopathies, including dystrophic and nondystrophic myotonias and myotonic syndromes.[26-34] Similar to methocarbamol, mexiletine's primary mechanism of action is blocking fast sodium channels, including $Na_v1.4$.[26,35] Like methocarbamol, mexiletine prolongs the refractory period of sodium channels by delaying their recovery from the inactivated state.[36]

In this study we tested the hypothesis that methocarbamol and mexiletine, in addition to their effect on extrafusal fibers, also influence muscle spindle function. Toward this end, we determined single unit sensory neuron afferent resting discharges and changes in the frequency of firing in responses to ramp-and-hold stretches. Moreover, because both drugs bind to the $Na_v1.4$ channel, we investigated its distribution in intrafusal fibers using high-resolution confocal microscopy.

2 | METHODS

2.1 | Animals and muscle preparation

Experiments were performed on muscles from 43 C57BL/6J mice of both sexes aged 10 to 15 weeks and weighing 22 to 28 grams. Fourteen animals were used for the electrophysiological analysis of methocarbamol, 16 for mexiletine, 9 were used to analyze vehicle (dimethysulfoxide or artificial cerebrospinal fluid), and 4 were used for immunocytochemistry. Animal procedures were performed according to guidelines from Directive 2010/63/EU of the European Parliament on the protection of animals used for scientific purposes. All experiments were approved by the local authorities of the State of Bavaria, Germany (ROB-55.2-2532.Vet 02-17-82).

2.2 | Electrophysiology

Afferent sensory neuron responses to stretch were assayed using an isolated muscle-nerve preparation, as described elsewhere.[37-40] In brief, the extensor digitorum longus (EDL) muscle from adult C57BL/6J mice was dissected and the sensory activity was determined using extracellular recording.[37] A detailed description of the electrophysiological analysis can be found in the Supplementary Information online.

The effect of the drugs on the resting discharge was quantified by determining the number of action potentials over a 30-second period at 15-minute intervals after addition of the drug. The results are shown as percent of the action potentials of the same muscle spindle before addition of drug. The effect of the drugs selectively on the dynamic and static response to ramp-and-hold stretches was analyzed by determining the dynamic peak

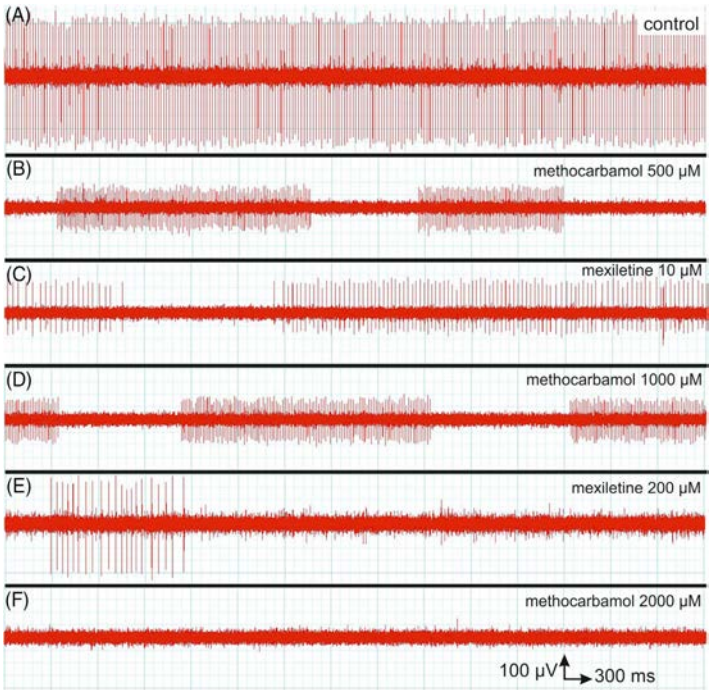

FIGURE 1 Mexiletine and methocarbamol reduce muscle spindle afferent firing in resting muscle spindles. Representative recordings of the resting discharge are shown in the absence (A) and presence (B-F) of various concentrations of mexiletine or methocarbamol. Each panel represents approximately 15 seconds of recording taken 60 minutes after addition of drug. Without any drug, muscle spindle afferents show a constant resting discharge frequency (A). In contrast, with increasing concentrations of either drug, the time in which the muscle spindle afferent did not fire action potentials ("silent periods") also increased. At concentrations of 2000 μM (methocarbamol) or 500 μM (mexiletine), the muscle spindle afferents were completely silenced (F, and data not shown). Different action potential amplitudes in the various recordings are the result of different resistance levels between suction electrode and nerve during the extracellular recordings and do not represent an effect of the drug. Scale bars for time and membrane potential are shown in F

(highest instantaneous frequency during ramp − baseline firing rate) and the static response (firing rate 3.25 to 3.75 seconds into stretch − baseline firing rate[39,40]) using LabChart version 8.1.5 (ADInstruments, Sydney, Australia). Dose-response curves were calculated using:

$$y = \frac{100}{1 = 10^{((logIC50 - x) \times hillslope)}}$$

where x = concentration (μM) ($\log_{10}$). The mean passive mechanical tension generated at maximum length (Lo) under resting conditions as well as 2 seconds after the start of the ramp-and-hold stretch were determined in triplicate and the values of the same muscle spindle were compared before and after addition of drug. The values are expressed as mean ± standard error of the mean (SEM), and the statistical significance of differences before and after addition of drug was determined using the unpaired t test.

2.3 | Maximal tetanic force

At the end of each recording, the maximal contractile force during a direct tetanic stimulation of the muscle via paddle electrodes in the tissue bath (500-millisecond train at 120 Hz and approximately 1-millisecond square pulse length, supramaximal voltage [Grass SD9 stimulator; Natus, Pleasanton, California]) was determined, as described elsewhere.[37,39,40] The specific force (force / physiological cross-sectional area: a measure of the general health status of the muscle) of the EDL muscle at Lo was determined in the presence and absence of

the drug as well as after a 1-hour washout. Toward this end, the EDL muscle was weighted at the end of the experiment (average weight was between 8 and 11 mg) and the maximal tetanic force was calculated using the equation:

$$\text{maximal tetanic force}\left[\mathrm{N/cm^2}\right] = \frac{Tension\,[N]/1000}{\frac{muscle\ weight\,[g]}{Lo\,[cm]\times 1.06\,[g/cm^3]}}.$$

The values were then compared with the previously reported peak force of the healthy EDL of 23.466 ± 6 N/cm^2.[37,41,42]

2.4 | Statistical analysis

The number of action potentials in a 30-second period before addition of the drug was counted and set as 100%. After addition of drug, the number of action potentials was counted again and expressed as percentage of the initial frequency before addition of drug. The means of the overall changes in firing rate of all groups were compared statistically vs the no-drug control group using one-way analysis of variance with Dunnett post hoc test. The Wilcoxon test was used to calculate the significance of effects of drug application on dynamic peak and static response during ramp-and-hold stimulations. The IC_{50} values were determined by plotting the log of the drug concentration against the normalized response (expressed as percent of control, which was set to 100%). All statistical analyses were performed using GraphPad Prism (GraphPad, Inc, La Jolla, California). The levels of significance (*P* values) for the statistical tests were set at $^*P < 0.05$, $^{**}P < 0.01$, and $^{***}P < 0.001$.

2.5 | Immunocytochemistry

Immunofluorescence labeling was performed as described elsewhere.[39,40,43] Refer to the Supporting Information online for a more detailed description of the staining protocol.

Sensory nerve terminals were identified using antibodies from guinea pig against vGluT1 (AB5905; Millipore, Darmstadt, Germany [1:1000]).[9,39] The $Na_v1.4$ distribution was determined by staining with a polyclonal rabbit antibody (SCN4A; #ASC-020; Alomone Labs, Jerusalem, Israel [1:500]). This antibody is specific for the alpha-subunit of the $Na_v1.4$ channel and shows no cross-reactivity with other voltage-gated sodium channels. The S46 monoclonal antibody against the slow tonic myosin heavy chain 6, developed by Miller et al[44] (diluted 1:50), was obtained from the Developmental Studies Hybridoma Bank, created by the National Institute of Child Health of the National Institutes of Health and maintained at the University of Iowa (Department of Biology, Iowa City, Iowa).[45-47]

Primary antibodies were detected using the appropriate Alexa 488-, Alexa 594-, and Alexa 647-conjugated goat anti-rabbit (A11034; Thermo Fisher Scientific-Invitrogen, Waltham, Massachusetts [1:1000]), goat anti-guinea pig (A11076; Thermo Fisher-Invitrogen [1:1000]), or goat anti-mouse (A32723; Thermo Fisher-Invitrogen [1:1000]) secondary antibody. Actin filaments were labeled using Alexa 488-conjugated phalloidin (A123379; Thermo Fisher-Invitrogen [1:500]).

After immunofluorescence labeling, the sections were embedded in Mowiol mounting medium (Carl Roth, Karlsruhe, Germany) and analyzed using a laser scanning confocal microscope (LSM 710; Carl Zeiss AG, Oberkochen, Germany), as described elsewhere.[39,40] We observed no difference in the structure of muscle spindles from male and female mice.[48]

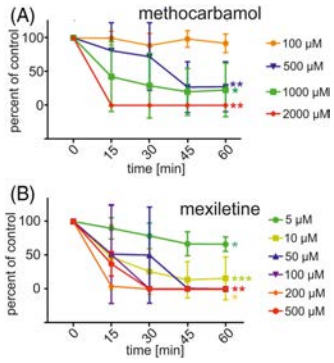

FIGURE 2 Dose- and time-dependent inhibition of muscle spindle resting discharge by mexiletine and methocarbamol. Different concentrations of methocarbamol (A) and mexiletine (B) were added to the bathing solution and the effect on the resting discharge over time was monitored every 15 minutes. The inhibitory effect of both muscle relaxants on the action potential frequency is expressed as percent of control, that is, the resting discharge before addition of drug. There was no significant difference between the 45-minute values and the 60-minute values for any drug or concentration, demonstrating that an equilibrium concentration was reached after 45 minutes. The values represent the mean ± standard error of the mean (SEM) of triplicate recordings of a single muscle spindle per extensor digitorum longus muscle from each of the 30 mice. For clarity, significant differences vs control (before addition of drug) are indicated by asterisks only for the 60-minute values. See Table S1 for values of the mean and SEM and the statistical significance of the other data points

3 | RESULTS

3.1 | Effect of methocarbamol and mexiletine on resting discharge of muscle spindle afferents

We first determined the action potential frequency in resting muscle spindles in the presence and absence of either relaxant. We did not observe an effect of either drug on the kinetics of individual action potentials or a gradual decline of the frequency of the resting

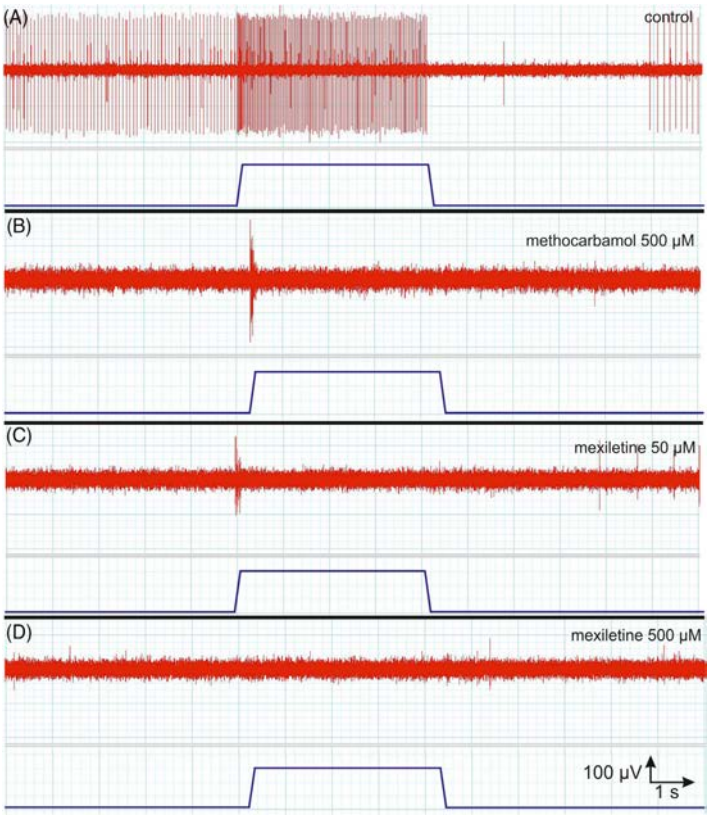

FIGURE 3 Mexiletine and methocarbamol progressively abolish firing of muscle spindle afferents in response to ramp-and-hold stretches. Representative muscle spindle afferent responses to ramp-and-hold stretches were recorded in the absence (A) and presence (B-D) of different concentrations of methocarbamol (B) or mexiletine (C,D). Although under control conditions muscle spindle afferents fire action potentials with frequencies that are determined by the length change and to the speed of stretching (A), this response is impaired by increasing concentrations of either muscle relaxant. In the presence of 500 μM methocarbamol (B) or 50 μM mexiletine (C), only a dynamic response during the ramp phase could be recorded. Higher concentrations of either muscle relaxant completely inhibited any response to ramp-and-hold stretches (D, and data not shown). The length changes (as indicated by the blue line below the action potential recordings) and the speed of stretching are identical in A-D. Scale bars for the extracellular recordings and the time are shown in D

discharge. Instead, while under control conditions (before addition of drug), the resting discharge frequency was constant over time (Figure 1A), and increasing concentrations of either muscle relaxant resulted in prolonged periods in which the muscle spindle afferent was silent (Figure 1B-F). The frequency of the resting discharge outside the silent periods was not altered by either drug (with the exception of the last action potentials before a silent period, which sometimes appeared after a small delay; Figure 1C,E) and was similar to the instantaneous frequency before addition of drug. The silent periods were first observed at a concentration of 100 μM methocarbamol or 5 μM mexiletine, respectively (Figure 1). At concentrations of 2000 μM (methocarbamol) and 500 μM (mexiletine), resting muscle spindles completely ceased action potential firing (Figure 1F).

We next determined the number of action potentials over a period of 30 seconds at different time-points after addition of drug and expressed this value as a percent of control (action potentials in 30 seconds before addition of drug; Figure 2). We observed no statistically significant difference between results after 45 and after 60 minutes, demonstrating that an incubation time of 60 minutes is sufficient for maximal effect of methocarbamol and mexiletine activity. All data points in Figure 2, including SEM and statistical significance, are summarized in Table S1. The IC_{50} value for the blockade of the resting discharge was calculated as 298 μM (mean with 95% confidence interval between 208.3 and 428.5 μM; n = 14) for methocarbamol and 5.86 μM (mean with 95% confidence interval between 4.6 and 7.4 μM; n = 16) for mexiletine. These results demonstrate that methocarbamol and mexiletine influence muscle spindle discharge frequencies at rest, albeit at different concentrations.

3.2 | Effect of methocarbamol and mexiletine on response of muscle spindle afferents to ramp-and-hold stretches

We observed a progressively reduced response to ramp-and-hold stretches in the presence of increasing concentrations of mexiletine

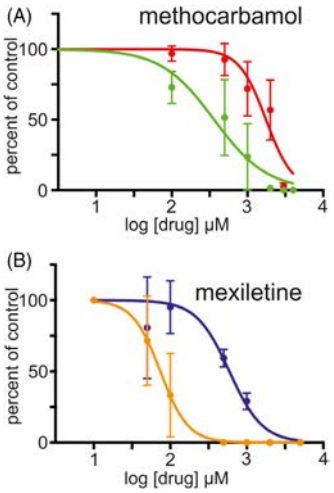

FIGURE 4 Dose-dependent inhibition of the dynamic and static response to stretch. The effects of methocarbamol (A) and mexiletine (B) on the dynamic (red line in A, blue line in B) and static (green line in A, orange line in B) responses to stretch 60 minutes after addition of drug are indicated. Results are expressed as percent of control, that is, the dynamic peak and the static response before addition of drug. Data points represent the mean of triplicate recordings ± standard error of the mean (n = 30). Note that both muscle relaxants inhibit the static response at lower concentrations compared with the dynamic response

or methocarbamol compared with control conditions (Figure 3A). At low concentrations of either drug, the resting discharge and static response were absent and the muscle spindle fired only during the ramp phase (Figure 3B,C). The response to ramp-and-hold stretches was completely abolished in the presence of 4 mM methocarbamol or 500 µM mexiletine (Figure 3D, and data not shown).

We next determined the dynamic peak and the static response in the presence of increasing concentrations of either drug (Figure 4). From these dose-response curves, the IC_{50} values for methocarbamol were calculated as 1756 (mean with 95% confidence intervals of 1265 to 2331; hillslope coefficient: −2.44; n = 11) for the dynamic response and 362 (mean with 95% confidence intervals of 160.4 to 676.2; hillslope coefficient: −1.24, n = 16) for the static response. Likewise, the IC_{50} values for mexiletine were 59.2 µM (mean with 95% confidence intervals of 32.42 to 88.11 µM; hillslope coefficient: −2.01) and 7.42 µM (mean with 95% confidence intervals of 5.27 to 10.86 µM; hillslope coefficient: −2.40) for static and dynamic responses, respectively. These results demonstrate that the response of muscle spindles to ramp-and-hold stretches is impaired by methocarbamol and mexiletine in a dose-dependent manner and that the dynamic response is less sensitive to either drug compared with the static response.

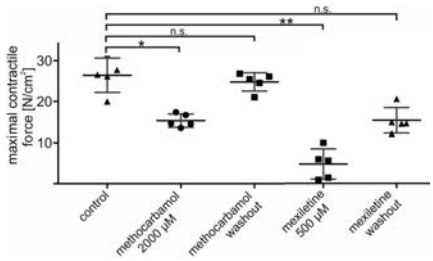

FIGURE 5 Reversible inhibition of the specific contractile force after tetanic stimulation by methocarbamol and mexiletine. Dot plot shows the maximal specific contractile force (in N/cm^2) after tetanic stimulation of muscle spindles in the presence or absence and after washout of methocarbamol (2 mM) or mexiletine (0.5 mM). Both drugs reduced the specific force to approximately 50% (methocarbamol) or 20% (mexiletine). After a 60-minute washout of the drug, the specific contractile force returned to almost control values. Each dot represents an independent experiment. Error bars represent the mean ± standard error of the mean (n = 5)

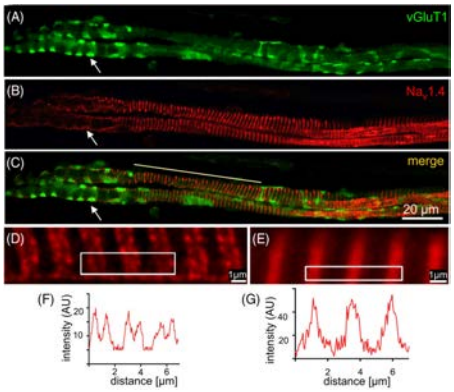

FIGURE 6 Distribution of the $Na_v1.4$ alpha-subunit in muscle spindles. Single confocal longitudinal cryostat sections of adult soleus (A-D) muscles were stained with antibodies against vGluT1 (A) to label the sensory nerve endings and against $Na_v1.4$ (B). The merged picture is shown in C. Note that $Na_v1.4$ immunoreactivity is distributed in a striated pattern localized primarily in the polar regions of intrafusal fibers (indicated by a yellow line in C). Considerably less immunoreactivity was observed in the equatorial region of intrafusal fibers. There appears to be no specific accumulation of $Na_v1.4$ immunoreactivity at the contact site between the sensory nerve ending and the intrafusal fiber in the equatorial region (arrows). High magnifications of the distribution of the $Na_v1.4$ immunoreactivity in extrafusal (D) and intrafusal (E) muscle fibers, respectively. Note the double stripes in extrafusal and the single stripes in intrafusal fibers. Optical intensity measurements of the $Na_v1.4$ immunoreactivity distribution in the areas marked by the rectangles in D and E are shown in F and G, respectively. Scale bars: C, 20 µm; D and E, 1 µm

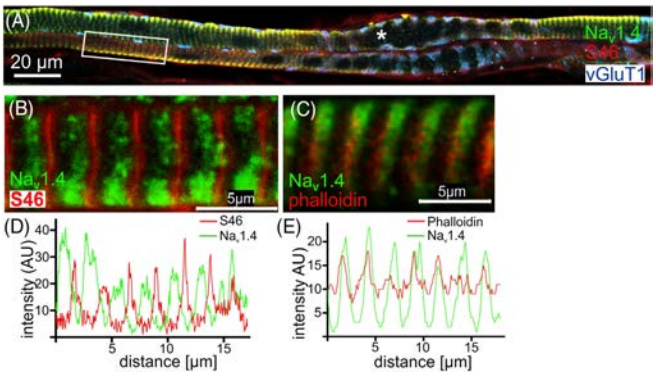

FIGURE 7 $Na_v1.4$ codistributes with actin but not with myosin filaments. Intrafusal fibers from adult extensor digitorum longus (EDL) muscles labeled with antibodies against vGluT1, $Na_v1.4$ and against slow tonic myosin heavy chain (MYH6; antibody S46) are shown (A). Note the similarly striped distribution of $Na_v1.4$ in the predominantly fast-twitch EDL muscle (A-C) and in the slow-twitch soleus muscle (see Figure 6B). The area marked by a rectangle (A) is also shown at higher magnification (B) to compare the distribution of both proteins. C, Comparable area in the polar region of an intrafusal fiber stained for actin filaments with fluorescently labeled phalloidin (red channel) and antibodies against $Na_v1.4$ (green channel). The stripes labeled by anti-$Na_v1.4$ antibodies were strictly non-overlapping with the distribution of the slow myosin heavy chain labeled by the S46 antibody (B), as indicated by the corresponding optical intensity measurement (D). In contrast, $Na_v1.4$ immunofluorescence codistributed with the distribution of actin filaments labeled by fluorescent phalloidin (C), as indicated by the corresponding optical intensity measurement (E). Scale bar: A, 20 µm; B and C, 5 µm

We did not observe a statistically significant difference in the tension displayed at Lo before (set to 100%) compared with after the addition of either drug (data not shown; 500 µM mexiletine: 85.1 ± 7.9% [mean ± SEM], n = 3, P = .09; 4 mM methocarbamol: 93.1 ± 8.4%, with n = 3, P = .28). Likewise, the passive tension during a stretch was similar before (set to 100%) compared with after the addition of either drug (500 µM mexiletine: 75.7 ± 12.6%, with n = 3, P = .10; 4 mM methocarbamol: 100.3 ± 10.2%, with n = 3, P = .99). This indicates that both drugs had no apparent effect on the passive viscoelastic properties of the EDL muscle under resting conditions and in response to stretch.

3.3 | Methocarbamol and mexiletine reduce maximal tetanic force

The physiological specific force (in N/cm^2) during high-frequency tetanic stimulation was reduced by approximately 40% at a methocarbamol concentration of 2 mM and by about 80% at a concentration of 500 µM mexiletine (Figure 5A). After a 1-hour washout, however, the specific maximal force returned to almost normal values, demonstrating that the interaction of both drugs with their target protein is reversible and that both drugs do not apparently induce long-lasting effects in extrafusal muscle fibers.

3.4 | $Na_v1.4$ expression in intrafusal fibers

Particularly in the polar region of intrafusal fibers, antibodies against the alpha-subunit of $Na_v1.4$ specifically labeled transverse oriented structures, which appeared as individual stripes oriented perpendicular to the longitudinal axis of intrafusal fibers (Figures 6A-C and 7A). In the equatorial region of intrafusal fibers, $Na_v1.4$ immunoreactivity was mostly absent, consistent with the small number of sarcomeres in this region. Likewise, anti-$Na_v1.4$ immunoreactivity was not particularly concentrated at the contact sites between the sensory nerve terminal (labeled by antibodies against vGluT1; see arrows in Figure 6A-C) and the intrafusal fiber. In extrafusal fibers, anti-$Na_v1.4$ antibodies labeled a double band (Figure 6D). Optical intensity measurements showed that the distance between the single bands was ~1 µm and the distance between the double bands was ~2 µm, consistent with them being T tubules. In contrast, the same antibodies labeled single bands in the polar region of intrafusal fibers (Figures 6E and 7A). These bands exhibited a spacing of ~2.3 µm, as determined by optical intensity measurements (Figure 6G). The distribution of $Na_v1.4$ bands in intrafusal fibers did not overlap with the slow myosin heavy chain (labeled by the S46 antibody; Figure 7B,D). In contrast, actin filaments (detected with fluorescently labeled phalloidin) and $Na_v1.4$ immunoreactivity were codistributed (Figure 7C,E). These results demonstrate that $Na_v1.4$ is present in intrafusal fibers, particularly in their polar

regions, albeit with a different distribution compared with extrafusal fibers. In addition, these results are consistent with the possibility that both drugs may carry out their effects on muscle spindle function by affecting this channel.

4 | DISCUSSION

In this study we have shown that methocarbamol and mexiletine inhibit generation of action potentials in muscle spindle afferents at rest as well as in response to stretch, but they do not affect muscle tension. Mexiletine and methocarbamol both bind to several voltage-gated sodium channels, including $Na_v1.4$, and both drugs preferentially affect the inactivated state.[23,33] Several sodium channels have been localized in muscle spindles by immunocytochemistry.[49] $Na_v1.6$ immunoreactivity is concentrated in the first heminodes, as well as in the sensory terminals of group Ia afferents. Likewise, $Na_v1.1$ is concentrated in sensory terminals together with $Na_v1.6$, whereas $Na_v1.7$ is mainly expressed in the axons of the sensory neuron. Consistently, single nucleus transcriptome analyses revealed that proprioceptive sensory neurons express $Na_v1.1$, $Na_v1.2$, $Na_v1.6$, and $Na_v1.7$, but little if any $Na_v1.3$, $Na_v1.4$, $Na_v1.5$, $Na_v1.8$, or $Na_v1.9$.[50] It remains to be solved, however, which of these sodium channels is the target of mexiletine and/or methocarbamol in muscle spindles. Both drugs are promiscuous with respect to the sodium channels they interact with, but the strong similarity of the effect of both drugs on the muscle spindle resting discharge and the stretch-induced action potentials suggest that both drugs affect muscle spindles via the same sodium channel.

We have provided evidence that $Na_v1.4$ is present in intrafusal fibers, particularly in their polar regions, which is consistent with the accumulation of sarcomeres in this region. We did not observe any $Na_v1.4$ immunoreactivity associated with the sensory neuron and there was no concentration of $Na_v1.4$ in the contact region between the sensory nerve terminal and intrafusal fiber. Interestingly, the subcellular distribution of $Na_v1.4$ was different in extrafusal fibers (double band) when compared with intrafusal fibers (single bands). The double bands in extrafusal fibers have been shown to correspond to the T-tubule system.[51,52] It will therefore be of considerable interest to determine whether the single bands observed in intrafusal fibers similarly correspond to T tubules, which would suggest a different three-dimensional distribution of the T-tubule system in intrafusal fibers. In principle, T tubules have been detected in intrafusal fibers by electron microscopy,[53,54] but their exact spatial distribution has not been analyzed by light microscopy. Therefore, the subcellular structure with which $Na_v1.4$ is associated in intrafusal fibers remains to be determined.

We did not observe a gradual decline of the muscle spindle resting discharge frequency in response to increasing concentrations of either drug. In contrast, the periods in which the muscle spindle was silent became longer, suggesting an "all-or-none" effect of the drugs on action potentials. Therefore, we consider an effect of both drugs on the initial generation of action potentials or on their conduction along the proprioceptive afferents more likely than an effect on the generation or modulation of the mechanically gated change of the membrane potential. It remains to be determined whether both drugs affect proprioceptive sensory neuron activity by inhibiting intrafusal fiber–associated $Na_v1.4$. The absence of an effect of both drugs on the passive muscle tension at rest and during ramp-and-hold stretches would suggest a different target. Moreover, the preferential effect of both drugs on the static compared with dynamic sensitivity also supports our idea that action potential generation is affected and not a mechanosensation.

The US Food and Drug Administration recommendation for the treatment of muscle spasms with methocarbamol is an initial dose of 1500 mg orally four times per day for the first 48 to 72 hours, up to a maximum dose of 8 g/day for severe symptoms. Peak levels of the plasma concentration are 20 μg/mL (corresponding to ~83 μM) about 1 hour after oral application of 1500 mg methocarbamol.[55] The concentration of methocarbamol used in our study (IC_{50} at ~300 μM for the resting discharge) is approximately fourfold higher than the concentration achieved in the plasma of patients with commonly accepted dosing levels, suggesting that the concentration of methocarbamol needed to affect muscle spindles may not be reached in patients. On the other hand, intramuscular injections could cause much higher local concentrations.

Mexiletine is used at a typical dose of between 100 and 200 mg three times per day, but the frequency of muscle cramps in amyotrophic lateral sclerosis patients can be reduced with doses as low as 150 mg twice daily.[32] The mean mexiletine serum level at the end of a 4-week treatment period at 600 mg/day was approximately 1 μg/mL (corresponding to ~5.6 μM).[33] The concentration of mexiletine used in our study is approximately equivalent to the concentration reached in vivo (IC_{50} = 5.8 μM for resting discharge), suggesting that an effect of this drug on proprioception is clinically relevant.

The consequences of the inhibitory activity of methocarbamol and mexiletine on muscle spindle proprioceptive afferents in humans would include coordination difficulties, unstable gait, and frequent falls. An increased risk of injury after administration of skeletal muscle relaxants, including methocarbamol, has been consistently reported, particularly in the elderly.[10,56,57] Our results suggest that the effects of mexiletine and methocarbamol on muscle spindles may contribute to these symptoms. Accordingly, the Beers Criteria for Potentially Inappropriate Medication Use in Older Adults, a collection of recommendations for health-care providers on medications with potential adverse side effects, includes methocarbamol, due to the increased risk for falls and fractures.[58] Moreover, because muscle relaxants are often used in general anesthesia, the recovery of proprioceptive function in the postanesthetic period should be monitored. In general, cautionary use of these medications, particularly in elderly patients, continues to be advisable.

ACKNOWLEDGMENTS

The authors thank Jürgen Schultheisse and Martina Bürkle for expert technical assistance and Nikola Klier for invaluable help with the Python code. We also gratefully acknowledge the critical reading and

improvement of the manuscript by Katherine Wilkinson, Bob Banks, and Guy Bewick. Open Access funding enabled and organized by Projekt DEAL.

CONFLICT OF INTEREST

The lab of S.K. has received financial support from Recordati Pharma GmbH, Ulm, Germany. The funder had no role in the design and conduct of the study, collection, management, analysis, and interpretation of the data or in the preparation, review, approval of the manuscript, or decision to submit the manuscript for publication. The remaining authors declare no conflicts of interest.

ETHICAL PUBLICATION STATEMENT

We confirm that we have read the Journal's position on issues involved in ethical publication and affirm that this report is consistent with those guidelines.

DATA AVAILABILITY STATEMENT

Data openly available in a public repository that issues datasets with DOIs

ORCID

Stephan Kröger https://orcid.org/0000-0002-4626-1690

REFERENCES

1. Chou R, Peterson K, Helfand M. Comparative efficacy and safety of skeletal muscle relaxants for spasticity and musculoskeletal conditions: a systematic review. *J Pain Symptom Manage*. 2004;28:140-175.
2. See S, Ginzburg R. Skeletal muscle relaxants. *Pharmacotherapy*. 2008;28:207-213.
3. Abdel Shaheed C, Maher CG, Williams KA, McLachlan AJ. Efficacy and tolerability of muscle relaxants for low back pain: systematic review and meta-analysis. *Eur J Pain*. 2017;21:228-237.
4. Witenko C, Moorman-Li R, Motycka C, et al. Considerations for the appropriate use of skeletal muscle relaxants for the management of acute low back pain. *Pharm Ther*. 2014;39:427-435.
5. Kröger S, Watkins B. Muscle spindle function in healthy and diseased muscle. *Skeletal Muscle*. 2021;11:3.
6. Proske U, Gandevia SC. The proprioceptive senses: their roles in signaling body shape, body position and movement, and muscle force. *Physiol Rev*. 2012;92:1651-1697.
7. Kröger S. Proprioception 2.0: novel functions for muscle spindles. *Curr Opin Neurol*. 2018;31:592-598.
8. Banks RW. The motor innervation of mammalian muscle-spindles. *Progr Neurobiol*. 1994;43:323-362.
9. Zhang Y, Lin S, Karakatsani A, Rüegg MA, Kröger S. Differential regulation of AChR clustering in the polar and equatorial region of murine muscle spindles. *Eur J Neurosci*. 2015;41:69-78.
10. Billups SJ, Delate T, Hoover B. Injury in an elderly population before and after initiating a skeletal muscle relaxant. *Ann Pharmacother*. 2011;45:485-491.
11. Richards BL, Whittle SL, Buchbinder R. Muscle relaxants for pain management in rheumatoid arthritis. *Cochrane Database Syst Rev*. 2012;1:CD008922.
12. Aljuhani O, Kopp BJ, Patanwala AE. Effect of methocarbamol on acute pain after traumatic injury. *Am J Ther*. 2017;24:e202-e206.
13. Überall MA, Emrich OMD, Müller-Schwefe GHH. Real-life efficacy and tolerability of methocarbamol in patients suffering from refractory muscle-related low/back pain---results of a health care research project based on data from the German pain practice registry. *MMW Fortschr Med*. 2017;159:6-17.
14. Dent RW, Ervin DK. Relief of acute musculoskeletal symptoms with intravenous methocarbamol (robaxin injectable): a placebo-controlled study. *Curr Ther Res Clin Exp*. 1976;20:661-665.
15. Brand RA. 50 years ago in CORR: a clinical study of 46 males with low-back disorders treated with methocarbamol. Andres Grisolia MD and J.E.M. Thomson CORR 1959;13:299-304. *Clin Orthopaed Rel Res*. 2009;467:2752-2754.
16. Voci JM, Al-Hakim M, Dokko Y, Katirji MB. Intravenous methocarbamol in the treatment of stiff-man syndrome. *Muscle Nerve*. 1993;16:434-435.
17. Valtonen EJ. A double-blind trial of methocarbamol versus placebo in painful muscle spasm. *Curr Med Res Opin*. 1975;3:382-385.
18. Park HW. Clinical results with methocarbamol, a new interneuronal blocking agent. *JAMA*. 1958;167:168-172.
19. Weiss M, Weiss S. Methocarbamol in low-back pain: clinical study. *J Am Osteopath Assoc*. 1962;62:142-144.
20. Emrich OM, Milachowski KA, Strohmeier M. Methocarbamol in acute low back pain. A randomized double-blind controlled study. *MMW Fortschr Med*. 2015;157(Suppl 5):9-16.
21. Truitt EB Jr, Little JM. A pharmacologic comparison of methocarbamol (AHR-85), the monocarbamate of 3-(o-methoxyphenoxy)-1,2-propanediol with chemically related interneuronal depressant drugs. *J Pharmacol Exp Ther*. 1958;122:239-246.
22. Roszkowski AP. A pharmacological comparison of therapeutically useful centrally acting skeletal muscle relaxants. *J Pharmacol Exp Ther*. 1960;129:75-81.
23. Zhang Y, Otto P, Qin L, et al. Methocarbamol blocks muscular Nav 1.4 channels and decreases isometric force of mouse muscles. *Muscle Nerve*. 2021;63:141-150.
24. Crankshaw DP, Raper C. Some studies on peripheral actions of mephenesin, methocarbamol and diazepam. *Br J Pharmacol*. 1968;34:579-590.
25. Crankshaw DP, Raper C. Mephenesin, methocarbamol, chlordiazepoxide and diazepam: actions on spinal reflexes and ventral root potentials. *Br J Pharmacol*. 1970;38:148-156.
26. Monk JP, Brogden RN. Mexiletine. Review of its pharmacodynamic and pharmacokinetic properties, and therapeutic use in the treatment of arrhythmias. *Drugs*. 1990;40:374-411.
27. Logigian EL, Martens WB, Moxley RT IV, et al. Mexiletine is an effective antimyotonia treatment in myotonic dystrophy type 1. *Neurology*. 2010;74:1441-1448.
28. Statland JM, Bundy BN, Wang Y, et al. Mexiletine for symptoms and signs of myotonia in nondystrophic myotonia: a randomized controlled trial. *JAMA*. 2012;308:1357-1365.
29. Suetterlin KJ, Bugiardini E, Kaski JP, et al. Long-term safety and efficacy of mexiletine for patients with skeletal muscle channelopathies. *JAMA Neurol*. 2015;72:1531-1533.
30. D'Mello S, Shum L. A review of the use of mexiletine in patients with myotonic dystrophy and non-dystrophic myotonia. *Eur J Hosp Pharm*. 2016;23:359-363.
31. Ginanneschi F, Mignarri A, Lucchiari S, et al. Neuromuscular excitability changes produced by sustained voluntary contraction and response to mexiletine in myotonia congenita. *Neurophysiol Clin*. 2017;47:247-252.
32. Oskarsson B, Moore D, Mozaffar T, et al. Mexiletine for muscle cramps in amyotrophic lateral sclerosis: a randomized, double-blind crossover trial. *Muscle Nerve*. 2018;58:42-48.
33. Stunnenberg BC, Raaphorst J, Groenewoud HM, et al. Effect of mexiletine on muscle stiffness in patients with nondystrophic myotonia evaluated using aggregated N-of-1 trials. *JAMA*. 2018;320:2344-2353.
34. Podrid PJ, Lown B. Mexiletine for ventricular arrhythmias. *Am J Cardiol*. 1981;47:895-902.

35. Nakagawa H, Munakata T, Sunami A. Mexiletine block of voltage-gated sodium channels: isoform- and state-dependent drug-pore interactions. *Mol Pharmacol.* 2019;95:236-244.
36. De Bellis M, Sanarica F, Carocci A, et al. Dual action of mexiletine and its pyrroline derivatives as skeletal muscle sodium channel blockers and anti-oxidant compounds: toward novel therapeutic potential. *Front Pharmacol.* 2017;8:907.
37. Wilkinson KA, Kloefkorn HE, Hochman S. Characterization of muscle spindle afferents in the adult mouse using an in vitro muscle-nerve preparation. *PLoS One.* 2012;7:e39140.
38. Franco JA, Kloefkorn HE, Hochman S, Wilkinson KA. An in vitro adult mouse muscle-nerve preparation for studying the firing properties of muscle afferents. *JoVE.* 2014;91:51948.
39. Gerwin L, Haupt C, Wilkinson KA, Kröger S. Acetylcholine receptors in the equatorial region of intrafusal muscle fibres modulate mouse muscle spindle sensitivity. *J Physiol.* 2019;597:1993-2006.
40. Gerwin L, Rossmanith S, Haupt C, et al. Impaired muscle spindle function in murine models of muscular dystrophy. *J Physiol.* 2020;598:1591-1609.
41. Larsson L, Edstrom L. Effects of age on enzyme-histochemical fibre spectra and contractile properties of fast- and slow-twitch skeletal muscles in the rat. *J Neurol Sci.* 1986;76:69-89.
42. Brooks SV, Faulkner JA. Contractile properties of skeletal muscles from young, adult and aged mice. *J Physiol.* 1988;404:71-82.
43. Zhang Y, Wesolowski M, Karakatsani A, Witzemann V, Kröger S. Formation of cholinergic synapse-like specializations at developing murine muscle spindles. *Dev Biol.* 2014;393:227-235.
44. Miller JB, Crow MT, Stockdale FE. Slow and fast myosin heavy chain content defines three types of myotubes in early muscle cell cultures. *J Cell Biol.* 1985;101:1643-1650.
45. Pedrosa F, Soukup T, Thornell LE. Expression of an alpha cardiac-like myosin heavy chain in muscle spindle fibres. *Histochemistry.* 1990;95:105-113.
46. Kucera J, Walro JM, Gorza L. Expression of type-specific MHC isoforms in rat intrafusal muscle fibers. *J Histochem Cytochem.* 1992;40:293-307.
47. Walro JM, Kucera J. Why adult mammalian intrafusal and extrafusal fibers contain different myosin heavy-chain isoforms. *Trends Neurosci.* 1999;22:180-184.
48. Gartych M, Jackowiak H, Bukowska D, Celichowski J. Evaluating sexual dimorphism of the muscle spindles and intrafusal muscle fibers in the medial gastrocnemius of male and female rats. *Front Neuroanat.* 2021;15:734555.
49. Carrasco DI, Vincent JA, Cope TC. Distribution of TTX-sensitive voltage-gated sodium channels in primary sensory endings of mammalian muscle spindles. *J Neurophysiol.* 2017;117:1690-1701.
50. Oliver KM, Florez-Paz DM, Badea TC, Mentis GZ, Menon V, de Nooij JC. Molecular correlates of muscle spindle and Golgi tendon organ afferents. *Nature Comm.* 2021;12:1451.
51. Jayasinghe ID et al. Revealing T-tubules in striated muscle with new optical super-resolution microscopy techniques. *Eur J Transl Myol.* 2015;25:4747.
52. Wetzel P, Scheibe RJ, Hellmann B, et al. Carbonic anhydrase XIV in skeletal muscle: subcellular localization and function from wild-type and knockout mice. *Am J Physiol.* 2007;293:C358-C366.
53. Ovalle WK Jr. Fine structure of rat intrafusal muscle fibers. The polar region. *J Cell Biol.* 1971;51:83-103.
54. Adal MN. The transverse tubular system of cat intrafusal muscle fibres. *Cell Tissue Res.* 1986;244:197-202.
55. Schlegelmilch R, Eydeler AU, Barkworth M, Radeke A. Bioequivalence study with two different oral formulations of methocarbamol in healthy subjects. A mono-centre, comparative, randomized, open-label, single-dose, 2-way crossover study. *Arzneimittelforschung.* 2009;59:238-242.
56. Spence MM, Shin PJ, Lee EA, Gibbs NE. Risk of injury associated with skeletal muscle relaxant use in older adults. *Ann Pharmacother.* 2013;47:993-998.
57. Derner MM, Linhart CA, Pederson LAM, et al. Injuries in adults 65 years of age and older prescribed muscle relaxants. *Consult Pharm.* 2016;31:511-517.
58. By the American Geriatrics Society Beers Criteria Update Expert, P. American Geriatrics Society 2019 Updated AGS Beers Criteria® for potentially inappropriate medication use in older adults. *J Am Geriat Soc.* 2019;67:674-694.

SUPPORTING INFORMATION

Additional supporting information may be found in the online version of the article at the publisher's website.

How to cite this article: Watkins B, Schuster HM, Gerwin L, Schoser B, Kröger S. The effect of methocarbamol and mexiletine on murine muscle spindle function. *Muscle & Nerve.* 2022;66(1):96-105. doi:10.1002/mus.27546

4. Paper II

Watkins, B., Schultheiss, J., Rafuna, A., Hintze, S., Meinke, P., Schoser, B., & Kröger, S. (2023). Degeneration of muscle spindles in a murine model of Pompe disease. *Sci Rep*, *13*(1), 6555. https://doi.org/10.1038/s41598-023-33543-y

www.nature.com/scientificreports

scientific reports

Check for updates

OPEN

Degeneration of muscle spindles in a murine model of Pompe disease

Bridgette Watkins[1], Jürgen Schultheiß[1], Andi Rafuna[1], Stefan Hintze[2], Peter Meinke[2], Benedikt Schoser[2] & Stephan Kröger[1]✉

Pompe disease is a debilitating medical condition caused by a functional deficiency of lysosomal acid alpha-glucosidase (GAA). In addition to muscle weakness, people living with Pompe disease experience motor coordination deficits including an instable gait and posture. We reasoned that an impaired muscle spindle function might contribute to these deficiencies and therefore analyzed proprioception as well as muscle spindle structure and function in 4- and 8-month-old *Gaa*$^{-/-}$ mice. Gait analyses showed a reduced inter-limb and inter-paw coordination in *Gaa*$^{-/-}$ mice. Electrophysiological analyses of single-unit muscle spindle proprioceptive afferents revealed an impaired sensitivity of the dynamic and static component of the stretch response. Finally, a progressive degeneration of the sensory neuron and of the intrafusal fibers was detectable in *Gaa*$^{-/-}$ mice. We observed an increased abundance and size of lysosomes, a fragmentation of the inner and outer connective tissue capsule and a buildup of autophagic vacuoles in muscle spindles from 8-month-old *Gaa*$^{-/-}$ mice, indicating lysosomal defects and an impaired autophagocytosis. These results demonstrate a structural and functional degeneration of muscle spindles and an altered motor coordination in *Gaa*$^{-/-}$ mice. Similar changes could contribute to the impaired motor coordination in patients living with Pompe disease.

Pompe disease (OMIM #232300; glycogen storage disease II) is a rare, autosomal recessive, progressive, debilitating, and, in the case of the infantile onset form, lethal lysosomal storage disease[1–4]. The cause for Pompe disease are mutations in the *GAA* gene (MIM#606800), which codes for the lysosomal enzyme acid maltase (α-1,4-glucosidase; GAA; EC 3.2.1.20)[5]. The GAA enzyme catalyzes the degradation of glycogen and, accordingly, mutations, which affect the enzymatic activity of this enzyme, lead to an accumulation of glycogen in lysosomes[6]. This impairs lysosome function and leads to the degeneration of cells and entire organs[1]. The severity of the phenotype is proportional to the loss of enzyme activity[6].

Although pathological lysosomal glycogen accumulation occurs in many tissues, skeletal and cardiac muscle are most prominently affected. Accordingly, patients living with Pompe disease show extensive fiber- and contractile apparatus degeneration, leading to progressive muscle weakness and atrophy, as well as varying degrees of respiratory complications due to dysfunction of the diaphragm and of the intercostal muscles. In addition to the muscular weakness, patients with Pompe disease experience impairments in executing motor abilities, including postural instability and an unstable gait, in particular when visual input is missing[7–9]. The cause of the impaired motor control is unknown. However, since there is almost no correlation between muscle weakness and postural parameters[9], the motor control deficits are unlikely to be caused solely by degeneration and loss of skeletal muscle tissue.

Proprioceptive information informs the brain about the contractile status of our skeletal muscles and their force[10–12]. This information is required for the localization of our extremities in space and for the acquisition and execution of any coordinated movement, including walking and standing. Muscle spindles are the main proprioceptive sensors and are present in almost every muscle[12]. They consist of specialized muscle fibers (intrafusal fibers), which are grouped into nuclear bag and nuclear chain fibers, based on the number and arrangement of nuclei in their central (equatorial) region. Both types of intrafusal fibers are innervated in the equatorial region by group I and group II sensory afferents that generate action potentials, which are proportional to the length change as well as to the speed of stretching[13]. In addition, both ends of the intrafusal fibers (polar regions) are innervated by γ-motoneurons, which maintain the proprioceptive sensitivity of muscle spindles at all lengths and during all contraction phases of the skeletal muscle[14].

[1]Department of Physiological Genomics, Biomedical Center, Ludwig-Maximilians-University, Grosshaderner Strasse 9, 82152 Planegg-Martinsried, Germany. [2]Department of Neurology, Friedrich-Baur-Institute, LMU Klinikum, Ludwig-Maximilians-University, Munich, Germany. ✉email: skroeger@lmu.de

In this study, we tested the hypothesis that an impaired muscle spindle function contributes to the motor control deficits, the instable gait and the frequent falls of Pompe disease patients. To this end, we structurally and functionally analyzed muscle spindles and locomotor behavior in 4- and 8-month-old *Gaa*$^{-/-}$ mice[15], which completely lack GAA enzymatic activity and have been used repeatedly as murine models for Pompe disease[16–20]. Our results show a reduced inter-limb and inter-paw coordination, a compromised response of muscle spindles to stretch and a severe degeneration of the sensory innervation, of the intrafusal fibers and of the muscle spindle outer capsule in 8-month-old *Gaa*$^{-/-}$ mice. A considerably weaker phenotype was observed in 4-month-old *Gaa*$^{-/-}$ mice. Collectively, these results demonstrate a progressively impaired muscle spindle structure and function as well as a reduced motor coordination in *Gaa*$^{-/-}$ mice.

Results

Gaa$^{-/-}$ mice have motor coordination deficits. To investigate gait deficits in *Gaa*$^{-/-}$ mice, we analyzed their motor behavior using the CatWalk XT system. This gait analysis system allows the automatic, quantitative and observer-independent investigation of a large number of dynamic and static movement parameters, which can be categorized into 4 major groups[21]: (a) run characteristics and kinetic parameters, (b) temporal parameters, (c) spatial parameters, and (d) interlimb coordination parameters (for a list of which parameter was categorized into which group see Supplementary Table 1). Many run characteristics and kinetic parameters assessing general gait and locomotor functions did not differ significantly between *Gaa*$^{-/-}$ mice and age-matched control mice. These included velocity (measured as distance over time; Fig. 1A), body speed (calculated by dividing the distance that the animal's body traveled from one initial contact of that paw to the next by the time to travel that distance; Supplementary Table 1) or stride length (distance between paw placement in two consecutive steps of the same paw; Supplementary Table 1). In contrast, from the ~ 200 parameters analyzed by the CatWalk XT system, 115 (4-month-old) and 83 (8-month-old) were significantly different between the *Gaa*$^{-/-}$ mice and age-matched 129/SvJ control mice (Supplementary Table 1). Some of these differences are likely to be the result of the reduced muscle strength and different weight of the *Gaa*$^{-/-}$ mice[16,20,21]. These include the number of steps per run in 4-month-old *Gaa*$^{-/-}$ mice (Fig. 1B), stand time (duration of contact of a paw with the glass plate; Supplementary Table 1), maximum intensity of the paw pressure to the ground (Fig. 1C) or the print area (surface of the complete print; Supplementary Table 1). On the other hand, several differences in the interlimb coordination parameters[21] between wildtype and *Gaa*$^{-/-}$ mice are consistent with an impaired motor control. These parameters include the lateral displacement (distance between the position of the hind paw and the position of the previously placed front paw on the same side of the body (ipsilateral) and in the same step cycle; Fig. 1D) and the wider base of support particular of the hind limbs (distance between two hind paws, Fig. 1E). Likewise, the regularity index, defined as the exclusive use of normal step sequence patterns during uninterrupted locomotion (number of normal step sequence patterns relative to the total number of paw placements) was significantly lower in 8-month-old animals compared age-matched control mice (Fig. 1F), demonstrating that *Gaa*$^{-/-}$ mice have more footprints outside of a recognized pattern.

The print position (distance between the position of the hind paw and the position of the previously placed front paw on the same side of the body (ipsilateral) and in the same step cycle) was increased on both sides of the body and at both ages in *Gaa*$^{-/-}$ mice (Fig. 1G). The relative duration of the simultaneous contact with the glass plate of all combinations of paws is another parameter, which differed significantly between *Gaa*$^{-/-}$ and control mice at both ages analyzed (Fig. 1H). None of the control or mutant mice had no paw on the glass plate at any time point during the run, and we observed no difference between *Gaa*$^{-/-}$ and wildtype control mice in the percent of time where only a single paw had contact with the glass plate (Supplementary Table 1). In contrast, the time each animal was supported by simultaneous contact of the diagonal pair of paws (right front paw and left hind paw or left front paw and right hind paw) were significantly lower in *Gaa*$^{-/-}$ mice compared to wildtype mice (Fig. 1H). The time of support for the girdle paws (right front paw and left front paw or right hind paw and left hind paw) was lower in 4-month-old and higher in 8-month-old *Gaa*$^{-/-}$ mice (Fig. 1H). Moreover, the relative amount of time the animal simultaneously spent on three or four paws was higher in *Gaa*$^{-/-}$ mice compared to age-matched control mice (Fig. 1H). The quantification of all approximately 200 parameters determined by the CatWalk system is summarized in Supplementary Table 1. Collectively, our results demonstrate an abnormal gait performance, locomotor function and particularly a compromised inter-limb- and inter-paw coordination in *Gaa*$^{-/-}$ mice.

Electrophysiological analysis of muscle spindles in Gaa$^{-/-}$ mice. To investigate changes in muscle spindle function in *Gaa*$^{-/-}$ mice, we recorded single-unit proprioceptive afferent responses to different stretch protocols in an ex vivo preparation of the extensor digitorum longus (EDL) muscle from 4- and 8-month-old *Gaa*$^{-/-}$ mice and compared them to age-matched 129/SvJ control mice. Responses to ramp protocols with length changes of 2.5, 5 and 7.5% L_0 (with ramp speeds of 40% L_0 per sec) were obtained and during each stretch response, four parameters were quantified: dynamic peak (DP), dynamic index (DI), initial static time (IST) and final static time (FST; for details on these parameters see "Methods" section). A representative recording from a control mouse-derived muscle spindle is shown in Fig. 2A. All 4- and 8-month-old wildtype as well as all 4-month-old and ~ 70% of the 8-month-old *Gaa*$^{-/-}$ mice responded to stretch with an increase of the instantaneous action potential frequency (Fig. 2A,C). However, the frequencies of the response to the different stretches were significantly lower in *Gaa*$^{-/-}$ mice of both ages (Fig. 2C). The quantification of the individual parameters at different hold lengths (2.5, 5 and 7.5% of L_0) of *Gaa*$^{-/-}$ mice compared to age-matched control mice is summarized in Fig. 3 (blue dots: 129/SvJ control mice; orange dots: *Gaa*$^{-/-}$ mice). On average, the instantaneous frequencies at all four time points during all stretch protocols were lower in *Gaa*$^{-/-}$ mice compared to 129/SvJ control mice, demonstrating a reduced static and dynamic sensitivity to stretch in *Gaa*$^{-/-}$ mice.

www.nature.com/scientificreports/

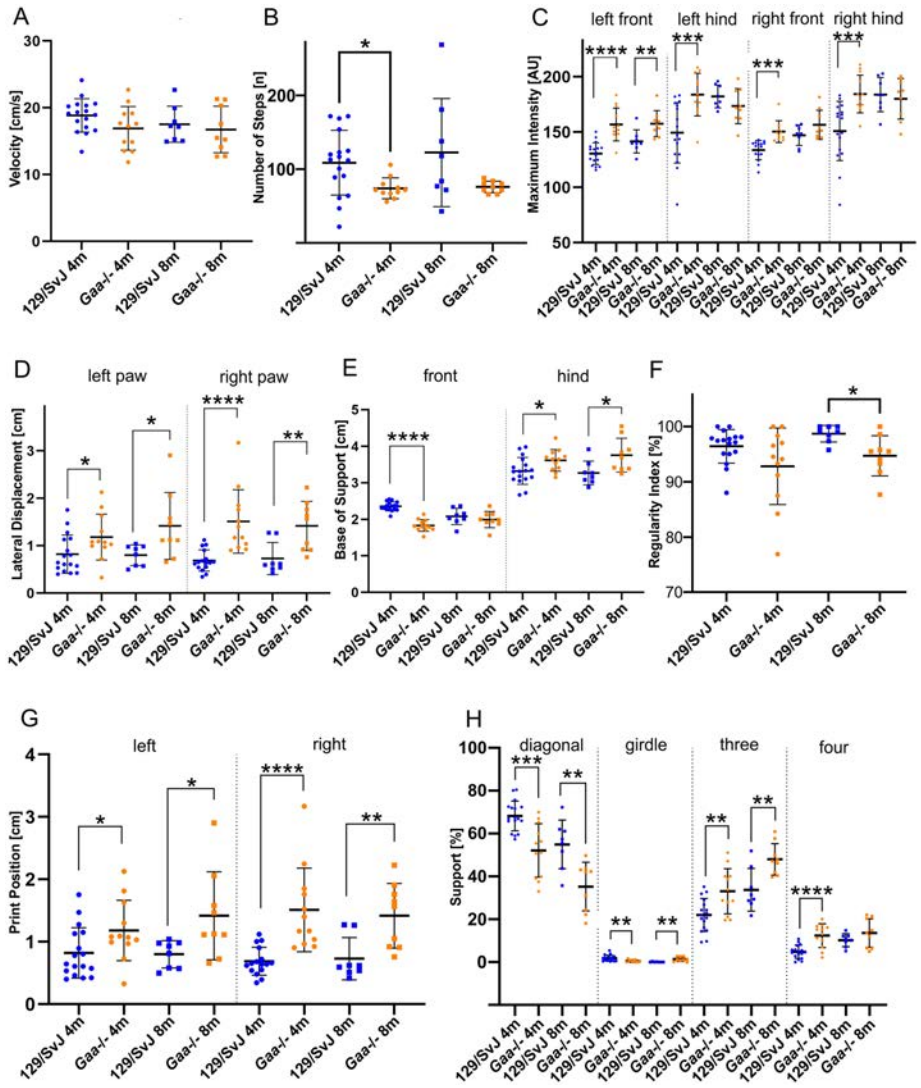

Figure 1. *Gaa*$^{-/-}$ mice have an abnormal motor coordination. Automatic gait analysis revealed that many general locomotor parameters were similar in wildtype 129/SvJ mice (blue dots) and *Gaa*$^{-/-}$ mice (orange dots), including velocity of movement (**A**) and number of steps ((**B**); the slightly reduced number of in 4-month-old mice is most likely due to the weight difference). Other parameters are different between *Gaa*$^{-/-}$ mice and age-matched control mice due to their different muscle force, including the maximum intensity of the footprints (**C**). On the other hand, both mouse lines behaved differently with respect to locomotion coordination parameters, including the lateral displacement (**D**), the base of support for the front- and hind limbs (**E**), as well as the regularity index (**F**). The distance between the position of the hind paw and the position of the previously placed front paw on the same side of the body and in the same step cycle (print position) was increased on the left as well as on the right side in *Gaa*$^{-/-}$ mice (**G**) at both ages examined. Moreover, the time the mice were supported by contacting the ground with the diagonal and girdle sides limbs as well as the time the animal was supported by three or four limbs was longer in *Gaa*$^{-/-}$ mice compared to 129/SvJ control mice (**H**). For a complete list of gait parameters analyzed see Supplementary Table 1. The bars show the mean ± SD with N = 17 (4-month-old 129SvJ) and N = 12 (4-month-old *Gaa*$^{-/-}$), N = 8 (8-month-old 129SvJ), N = 9 (8-month old *Gaa*$^{-/-}$) mice. Statistical significance was calculated using the unpaired student's t-test.

Scientific Reports | (2023) 13:6555 | https://doi.org/10.1038/s41598-023-33543-y nature portfolio 3

www.nature.com/scientificreports/

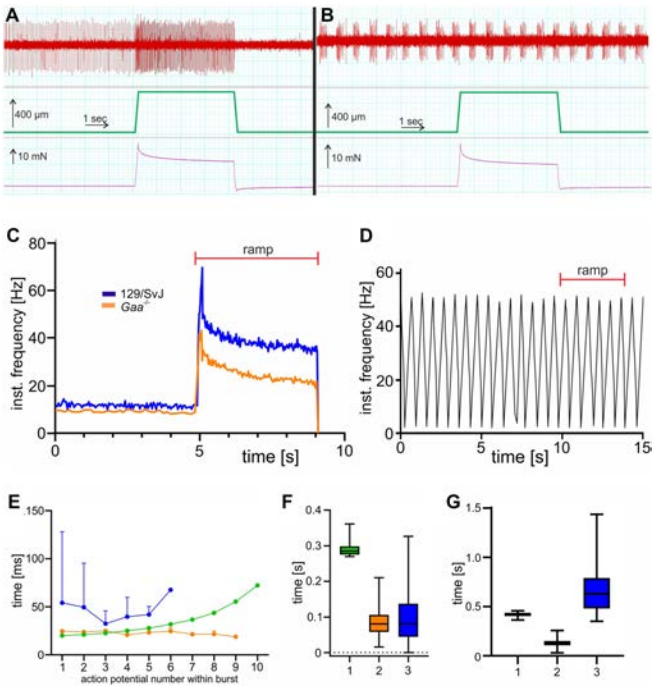

Figure 2. The response to stretch in muscle spindles from *Gaa*$^{-/-}$ mice is impaired. A representative example for the response of muscle spindle afferents to a ramp-and-hold stretch from 129/SvJ wildtype mice is shown in panel (**A**). Muscle spindles from wildtype mice had a constant resting discharge of approximately 10 Hz and responded to stretch with an increase in their instantaneous frequency (**A**). In contrast, 70% of the muscle spindles from 8-month-old *Gaa*$^{-/-}$ mice (orange line in panel (**C**)) responded to stretch, but had a lower frequency at all time points during a stretch compared to age-matched 129/SvJ wildtype mice. Approximately 30% of the 8-month-old *Gaa*$^{-/-}$ mice fired bursts at rest and did not respond to stretch (**B**). In some spindles, the bursts were rather regular even during a ramp-and-hold stretch (**D**). In other muscle spindles from 8-month-old *Gaa*$^{-/-}$ mice, which showed the bursting behavior at rest, the bursts varied with respect to the action potential frequency during the bursts (**E**), the duration of the bursts (**F**) and the interburst interval (duration of the silent period; (**G**)). Three representative spindles from three different 8-month-old *Gaa*$^{-/-}$ mice are shown to illustrate the spectrum of the busts. The red bars in panels (**C,D**) indicate the duration of the ramp-and-hold stretch. The middle parts of panels (**A,B**) show the length change (5% of L_0) and the lower parts show the passive tension generated by the muscle in response to the stretch. No difference between wildtype and *Gaa*$^{-/-}$ mice was observed with respect to the passive tension generated in response to the length change.

In approximately 30% of the recordings from 8-month-old *Gaa*$^{-/-}$ mouse muscle spindles at rest, we observed bursts of action potentials followed by short periods of silence without action potentials (Fig. 2B). In individual spindles, the bursts were rather regular (Fig. 2D and orange line in Fig. 2E). However, a more detailed analysis of the bursting behavior of three representative muscle spindles from three different mice demonstrated the variability of the bursts between different spindles with respect to the instantaneous frequency during the bursts (Fig. 2E), the duration of the bursts (Fig. 2F) and the length of the interburst interval (Fig. 2G), demonstrating a heterogeneity of the bursts in different muscle spindles. Most importantly, muscle spindle afferents with a bursting behavior did not respond to stretch with an increase of the instantaneous frequency but instead maintained the burst behavior throughout the stretch stimulus (Fig. 2B,D). These bursts were never observed in any of the control mice or in 4-month-old *Gaa*$^{-/-}$ mice. In summary, these results demonstrate a severely compromised sensitivity to stretch of muscle spindles from 4- and 8-month-old *Gaa*$^{-/-}$ mice and a complete insensitivity to stretch in ~ 30% of the recordings from 8-month-old *Gaa*$^{-/-}$ mice.

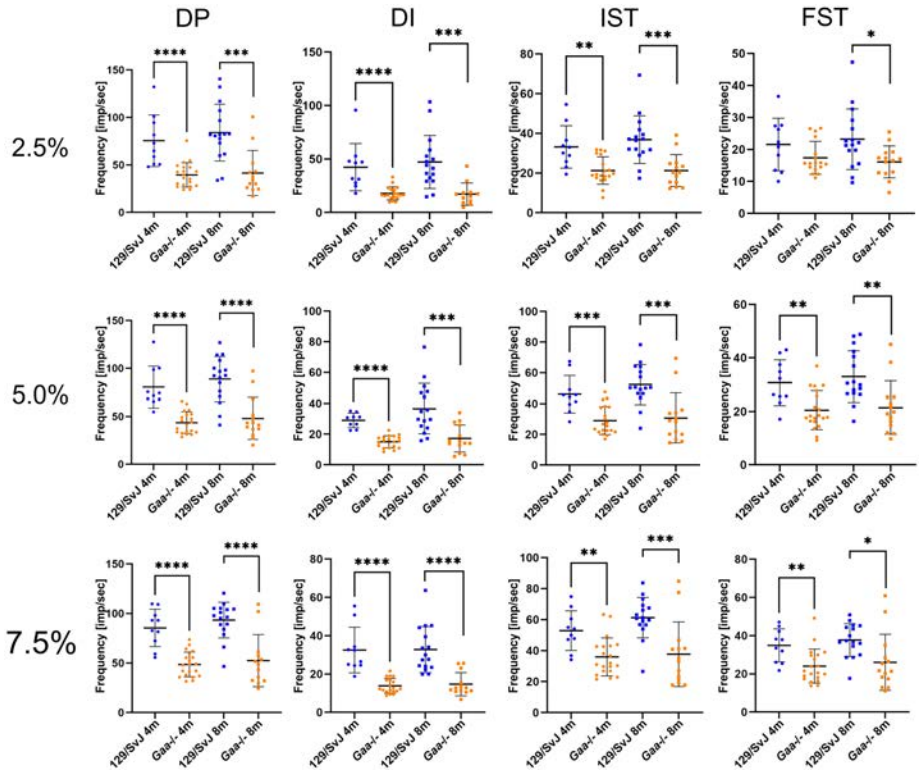

Figure 3. Stretch-responsive muscle spindles from *Gaa*$^{-/-}$ mice have lower instantaneous frequencies compared to control mice at all time points during ramp-and-hold stretches. The frequency at four time points during a ramp-and-hold stretch (dynamic peak (DP), dynamic index (DI), initial static time (IST) and final static time (FST); for details of these time points see "Methods" section) were lower in *Gaa*$^{-/-}$ mice (orange dots) compared to age-matched wildtype 129/SvJ control mice (blue dots). This was independent of the length change (2.5, 5.0 and 7.5% of L_0) and of the age of the mice (4- and 8-month-old mice, respectively). Each dot represents the recording of a single muscle spindle. Bars show the mean ± SD with N = 4 (4-month-old 129SvJ), N = 8 (4-month-old *Gaa*$^{-/-}$), N = 6 (8-month-old 129SvJ) and N = 16 (8-month-old *Gaa*$^{-/-}$). Statistical significance was calculated using the unpaired student t-test.

Structural degeneration of muscle spindles in *Gaa*$^{-/-}$ muscle spindles. To investigate, if the muscle spindle functional deficits and the impaired movement coordination in *Gaa*$^{-/-}$ mice were accompanied by structural changes, we compared the morphology of their muscle spindles with age-matched 129/SvJ mice using antibodies against several marker proteins. In adult muscle spindles, the vesicular glutamate transporter 1 (vGluT1) labels the sensory nerve terminal, which in mice revolves around the intrafusal muscle fibers in the form of an annulospiral ending[12]. This typical structure is visible in muscle spindles from 4- and 8-month-old wildtype animals (green channel in Fig. 4A and data not shown). Alpha-bungarotoxin labels nicotinic acetylcholine receptors (AChRs) predominantly at endplates of γ-motoneurons in the polar regions of the intrafusal fibers (red channel in Fig. 4A). The distribution of both, α-bungarotoxin and vGluT1, were severely altered in muscle spindles from 8-month-old *Gaa*$^{-/-}$ mice (Fig. 4B). The sensory nerve terminal had retracted from the intrafusal fiber, had lost its annulospiral morphology and had formed large varicosities (green arrow in Fig. 4B). The intrafusal fibers had also degenerated and often formed a round, myoball-like structure with patchy AChR clusters on its surface (red arrow in Fig. 4B).

Since the extent of degeneration of muscle spindles was rather heterogeneous even within the same muscle, we quantified the structural changes by defining four categories of progressively severe structural damage of muscle spindles (see "Methods" section for more details; Fig. 4C). Quantification showed that 4- and 8-month-old

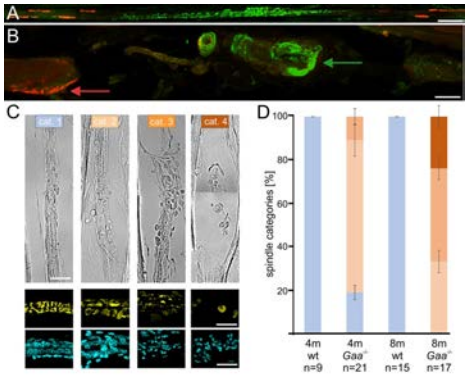

Figure 4. Quantification of the degenerative changes in muscle spindles from *Gaa*$^{-/-}$ mice. Intrafusal fibers are innervated by sensory nerve terminals in the central (equatorial) region (stained with antibodies against vGluT1; green channel in (**A,B**)) and by γ-motoneurons in the polar regions, which form a cholinergic synapse (indicated by α-bungarotoxin labeling of the AChRs; red channel in (**A,B**)). Note the normal structure of the intrafusal fiber innervation in muscle spindles from 8-month-old 129/SvJ mice (**A**) and the severely degenerated innervation in the 8-month-old *Gaa*$^{-/-}$ mice ((**B**); corresponding to a category 4 muscle spindle, see below). The sensory nerve terminal has retracted from the intrafusal fiber and has formed a large varicosity (green arrow). AChRs have disaggregated (red arrow) and the intrafusal fiber has lost its elongated shape and formed a spherical myoball-like structure. Panel (**C**) shows representative examples of the four different categories used to characterize the different levels of degeneration. For a more detailed description of the categories, see "Methods" section. The lower two rows of panel (**C**) show representative examples corresponding to the different categories of the morphology of the sensory ending (green channel) and the distribution of the nuclei (blue channel), respectively. Morphological analysis of 4- and 8-month-old muscle spindles from wildtype (wt) and *Gaa*$^{-/-}$ mice revealed a progressive increase of the number of damaged muscle spindles demonstrating the progressive degenerative changes (panel (**D**)). Bars show the mean ± SD with N = 3; n represents the number of muscle spindles analyzed. Color-coding of the different categories is identical in panels (**C,D**). Scale bar: (**A**) 50 µm, (**B**) 20 µm, (**C**) 20 µm.

129/SvJ control mice had muscle spindles without any detectable damage (category 1; Fig. 4D). In contrast, in 4-month-old *Gaa*$^{-/-}$ mice, only ~ 20% of the muscle spindles had a normal structure, whereas ~ 70% were mildly (category 2) and ~ 10% severely affected by degenerative processes (Fig. 4D). We observed no normal muscle spindle in 8-month-old *Gaa*$^{-/-}$ mice and about 65% of all spindles were either severely damaged (category 3) or had completely deteriorated (corresponding to category 4; Fig. 4D). Consistently, we observed a reduction of the total number of muscle spindles in the soleus muscle from 8.3 ± 0.96 in wildtype to 4.7 ± 0.58 (mean ± SD with N = 3) in 8-month-old *Gaa*$^{-/-}$ mice, respectively. These results demonstrate a progressive structural degeneration and a reduction of muscle spindle number in *Gaa*$^{-/-}$ mice.

In extrafusal muscle fibers from Pompe disease patients and from *Gaa*$^{-/-}$ mice, lysosomes are enlarged and their number is increased[2,22]. To investigate if intrafusal fibers show a similar change in lysosome size and number, we stained muscle spindles with antibodies against the lysosomal membrane protein LAMP1. We observed very few lysosomes in 4- and 8-month-old wildtype muscle spindles (red arrows in Fig. 5A,C). In contrast, small LAMP1-positive puncta and a few enlarged lysosomes were detectable in 4-month-old *Gaa*$^{-/-}$ muscle spindles (red and blue arrows in Fig. 5B, respectively). In 8-month-old *Gaa*$^{-/-}$ mice, anti-LAMP1 antibodies strongly stained aggregated lysosomes (red arrows in Fig. 5D), often associated with the varicosities formed by the sensory nerve terminal (white arrows in Fig. 5D). To quantify these changes, we determined the total number of pixels above threshold per area as well as the size of the lysosomal aggregates. This quantification revealed a non-significant increase of 38% ($p = 0.2304$) in the total number of pixels above threshold in 4-month-old *Gaa*$^{-/-}$ mice compared to age-matched 129/SvJ mice. In contrast, the total number of pixels above threshold was significantly increased ($p = 0.000002$) in 8-month-old *Gaa*$^{-/-}$ mice by 320%. Likewise, the size of the pixel aggregates was non-significantly increased by 22.8% ($p = 0.4920$) in 4-month-old *Gaa*$^{-/-}$ mice. In 8-month-old animals, the size of the pixel aggregates was significantly higher ($p = 0.0078$) in *Gaa*$^{-/-}$ mice by 86.58% compared to age-matched 129/SvJ control mice. Consistent with previously published results[23], an increase in the LAMP1 staining was also observed in extrafusal fibers from 4- and 8-month-old *Gaa*$^{-/-}$ mice, suggesting a parallel increase in lysosomes in extra- and intrafusal fibers. These results demonstrate an increase in the number and in the size of LAMP1-positive lysosomes in muscle spindles from 8-month-old *Gaa*$^{-/-}$ mice.

Degenerating axons in the central and peripheral nervous system (for example after spinal cord injury or peripheral nerve damage) form varicosities at their distal ends, which are filled with cellular debris such as disorganized cytoskeletal elements[24]. To investigate if the varicosities observed in muscle spindles from 8-month-old

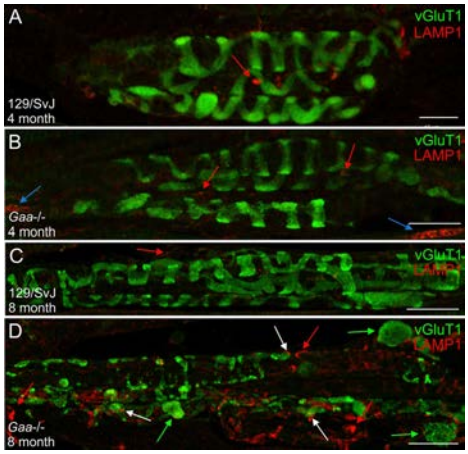

Figure 5. Accumulation and aggregation of lysosomes in muscle spindles from *Gaa*$^{-/-}$ mice. The structure and distribution of lysosomes was investigated using anti-LAMP1 antibodies in 4-month-old (**A,B**) and 8-month-old (**C,D**) 129/SvJ control mice (**A,C**) and *Gaa*$^{-/-}$ mice (**B,D**). The structure of the sensory nerve terminal (stained by antibodies against vGluT1; green channel) was indistinguishable in 4- and 8-month-old muscle spindles from wildtype mice and in 4-month-old *Gaa*$^{-/-}$ mice. In contrast, in 8-month-old *Gaa*$^{-/-}$ mice (category 2), the sensory nerve terminal had formed several varicosities within the spindle matrix (green arrows in panel (**D**)), had retraced from the intrafusal fibers and had lost the typical annulospiral morphology. Lysosomes were barely detectable in sections from 129/SvJ mice at 4- and 8 months of age (red arrows in panels (**A,C**)). In contrast, lysosomes were significantly enlarged and had formed aggregates in 4-month-old *Gaa*$^{-/-}$ mice (red and blue arrows in panel (**B**), respectively). By 8 months (panel (**D**)), lysosomes were abundant, highly aggregated (red arrows) and often associated with the varicosities formed by the sensory nerve terminals of *Gaa*$^{-/-}$ mice (white arrows). Scale bars: 20 µm.

Gaa$^{-/-}$ mice contain cytoskeletal elements (and might therefore indicate degeneration of the sensory nerve terminal), we stained muscle spindles with antibodies against neurofilament 200. In 8-month-old wildtype animals, neurofilament immunoreactivity was observed in the sensory nerve ending, overlapping with the vGluT1 staining of the annulospiral endings of the sensory terminal (Fig. 6A). In contrast, in age-matched *Gaa*$^{-/-}$ mice, neurofilament was disorganized and concentrated in the large vGluT1-positive varicosities (green arrows in Fig. 6B), suggesting that the sensory nerve terminals had degenerated and withdrawn from the intrafusal fiber and had aggregated neurofilament protein inside the varicosities.

Staining with antibodies against the myosin heavy chain 6 (S46 antibody; light blue channel in Fig. 6A,B) revealed few contractile filaments in the central region of intrafusal fibers in 8-month-old wildtype animals, in agreement with the almost complete absence of sarcomeres in this region (Fig. 6A[25]). In contrast, S46 staining was readily observed throughout the central region of intrafusal fibers in category 3-like muscle spindles from age-matched *Gaa*$^{-/-}$ mice (Figs. 6B, 8D), demonstrating a redistribution of this myosin heavy chain in the central region of intrafusal fibers.

To confirm the redistribution of proteins in the central region of intrafusal fibers, we compared the distribution of the voltage-gated sodium channel $Na_v1.4$ in 8-month-old wildtype and *Gaa*$^{-/-}$ mice. The immunoreactivity for this channel is coextensive with the phalloidin-labeled actin filaments in intrafusal muscle fibers from wildtype mice[25], and therefore an indicator of the contractile apparatus. Similar to the myosin heavy chain, we observed a concentration of $Na_v1.4$ immunoreactivity specifically in the subsarcolemmal compartment of the central region of intrafusal fibers in wildtype muscle spindles (Fig. 6C[25]), but a presence of this channel throughout the intrafusal fiber, including the equatorial region, in 8-month-old *Gaa*$^{-/-}$ mice (Fig. 6D). This demonstrates that in the central region of intrafusal fibers from 8-month-old *Gaa*$^{-/-}$ mice, $Na_v1.4$ and the myosin heavy chain 6 similarly redistribute.

To investigate the extracellular matrix and the integrity of the connective tissue capsule of muscle spindles from wildtype and mutant animals, we compared the distribution of the matrix protein versican in *Gaa*$^{-/-}$ mice and in age-matched 129/SvJ control mice. In skeletal muscle, anti-versican antibodies selectively label the muscle spindle extracellular matrix[26]. Versican immunoreactivity was restricted to the inner and outer capsule in muscle spindles from wildtype mice (Fig. 7A,C) and in 4-month-old *Gaa*$^{-/-}$ mice (Fig. 7B). In contrast, it appeared throughout the spindle in a punctate pattern in 8-month-old *Gaa*$^{-/-}$ mice (Fig. 7D). Moreover, 8-month-old muscle spindles showed signs of degeneration of the inner and outer capsule indicated by the fragmentation

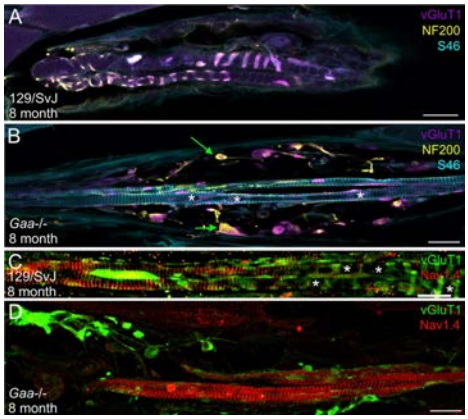

Figure 6. The varicosities formed by the sensory nerve terminal contain cytoskeletal elements and proteins of the polar region redistribute into the central region of intrafusal fiber's in 8-month-old *Gaa*$^{-/-}$ mice. Muscle spindles from 8-month-old wildtype (**A,C**) and *Gaa*$^{-/-}$ (**B,D**) mice were stained with antibodies against vGluT1 (purple channel in panels A and B and green channel in panels (**C,D**)), neurofilament 200 (NF 200; yellow channel in (**A,B**)), the myosin heavy chain 6 (S46 antibody; blue channel in (**A,B**)) and the voltage-gated sodium channel $Na_v1.4$ (red channel in (**C,D**)). In muscle spindles from wildtype 129/SvJ mice, neurofilament 200 immunoreactivity codistributed with the sensory nerve terminal (labeled by the anti-vGluT1 antibodies). The typical annulospiral morphology of the nerve terminal is detectable. In contrast, in muscle spindles from age-matched *Gaa*$^{-/-}$ mice (panels (**B,D**) show category 3 muscle spindles), the contact between the sensory nerve terminal and the intrafusal fibers was lost and the sensory nerve terminals had retracted to form numerous varicosities. The varicosities labeled by vGluT1 contained neurofilament 200 immunoreactivity (green arrows in panel (**B**)), demonstrating the accumulation of cytoskeletal elements in these structures. Note the absence of labeling with the S46 antibody in the central region of 8-month-old wildtype intrafusal fibers (**A**) and its presence in the central region of intrafusal fibers from age-matched *Gaa*$^{-/-}$ mice (**B**). Likewise, the voltage-gated sodium channel $Na_v1.4$ was concentrated underneath the subsarcolemmal plasma membrane in the central region of intrafusal fibers of wildtype animals (**C**) whereas it was present throughout the intrafusal fiber in 8-month-old *Gaa*$^{-/-}$ mice (**D**). Asterisks in panels (**B,C**) indicate the central region of intrafusal fibers. Scale bars: 20 µm.

of the capsule-associated anti-versican staining (Fig. 7D). These results demonstrate an altered distribution of the versican immunoreactivity in 8-month-old *Gaa*$^{-/-}$ mice, consistent with a degeneration of the extracellular matrix and the connective tissue capsule.

Lysosomal dysfunction in Pompe disease leads to incomplete autophagic flux and accumulation of autophagic debris, particularly in extrafusal fibers[23,27,28]. To investigate if autophagy is also initiated in muscle spindles from *Gaa*$^{-/-}$ mice, we used antibodies against the LC3A/B protein, a well-established marker for autophagosomes[29]. We observed no obvious autophagic vacuoles in muscle spindles from 4- and 8-month-old wildtype mice (Fig. 8A,C). In contrast, autophagosomes were detectable in muscle spindles from 4-month-old *Gaa*$^{-/-}$ mice as punctate immunoreactivity with anti-LC3A/B antibodies (white arrowheads in Fig. 8B). In 8-month-old muscle spindles from *Gaa*$^{-/-}$ mice, autophagosomes were enlarged, aggregated and often associated with the intrafusal fibers and with the large varicosities formed by the sensory nerve terminal (green arrows in Fig. 8D). Quantification of mice of both genotypes and age revealed a significant ($p = 0.0003$) increase of 202% of the total number of pixels above threshold in 4-month-old *Gaa*$^{-/-}$ mice. Likewise, the total number of LC3AB-positive pixels above background in 8-month-old *Gaa*$^{-/-}$ animals was significantly ($p = 0.0001$) increased by 160%. Moreover, the size of the pixel aggregates was significantly increased ($p = 0.0004$) by 227% in 4-month-old *Gaa*$^{-/-}$ mice. Likewise, in 8-month-old *Gaa*$^{-/-}$ mice, the size of the pixel aggregates was significantly ($p = 0.0010$) increased by 111.90%. These results demonstrate a buildup of autophagosomes in muscle spindles from *Gaa*$^{-/-}$ mice, and suggest that in these mice an abnormal autophagy might contribute to the severe degenerative processes of the muscle spindles.

Collectively, our immunohistochemical analyses demonstrate a severe and progressive degeneration of the sensory nerve terminal, the intrafusal fiber and the connective tissue capsule in muscle spindles from *Gaa*$^{-/-}$ mice.

Discussion

The *Gaa*$^{-/-}$ mouse line recapitulates many of the hallmarks of patients living with Pompe disease[20,30,31] and is therefore well suited to study the effect of a lack of GAA enzymatic activity on motor performance and muscle spindle structure and function. Using this mouse line, we provide three independent lines of evidence for a

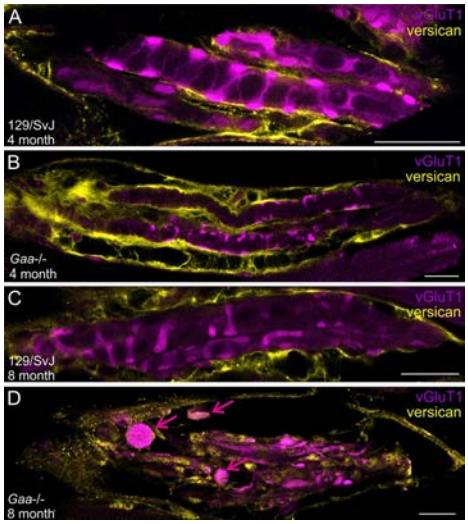

Figure 7. The muscle spindle connective tissue capsule deteriorates in 8-month-old *Gaa*$^{-/-}$ mice. Muscle spindles from 4- (**A,B**) and 8-month-old (**C,D**) wildtype (**A,C**) and *Gaa*$^{-/-}$ (**B,D**) mice were stained with antibodies against vGluT1 (purple channel) and the extracellular matrix protein versican (yellow channel). The antibodies labeled the inner and outer capsule of muscle spindles in wildtype and 4-month-old *Gaa*$^{-/-}$ mice. In 8-month-old *Gaa*$^{-/-}$ mice, the labeling was distributed throughout the muscle spindle and the inner- and outer capsule appeared fragmented. Note the vGluT1-positive varicosities (purple arrows in panel (**D**)) and the punctate versican immunoreactivity in the 8-month-old *Gaa*$^{-/-}$ mice. Scale bar: 20 µm.

progressively impaired muscle spindle structure and function: (1) the dynamic and static response of single unit proprioceptive afferents to stretch is severely compromised, (2) muscle spindles from 8-month-old *Gaa*$^{-/-}$ mice show severe signs of degeneration of intrafusal fibers, sensory nerve terminals and of the spindle capsule and, finally, (3) the locomotor behavior of these mice revealed an abnormal limb- and paw coordination as well as gait problems. Our results therefore suggest that degenerating muscle spindles could contribute to the gait instability, the frequent falls and the movement coordination deficits of patients living with Pompe disease.

The loss of contact of the sensory nerve terminals to the intrafusal fibers as well as the formation of varicosities and the accumulation of cytoskeletal elements in the varicosities of *Gaa*$^{-/-}$ mice is typical for an axonal "dying back mechanism"[24]. Similar events have been described in muscle spindles from the gracile axonal dystrophy mouse line[32]. This structural disorganization together with the presence of autophagosomes suggest a preponderance of degenerative events occurring in muscle spindles but the underlying mechanism for the degeneration is unclear. One possibility is that the degeneration of the intrafusal fibers causes the degeneration of the sensory nerve terminal. It has been previously shown that sensory nerve terminals require the secretion of neurotrophin-3, which activates the tropomyosin receptor kinase C (TrkC) receptor on proprioceptive sensory neurons and by this secures the survival of the sensory neuron[33–35]. Thus, the degeneration of intrafusal fibers could secondarily cause the degeneration and retraction of the proprioceptive sensory axon. On the other hand, glycogen deposits have also been observed in the peripheral nervous system and in dorsal root ganglia neurons of patients with Pompe disease[18,20,36–38]. Accordingly, these patients develop a polyneuropathy[38] and a loss of peripheral nerves, leading among others to peripheral areflexia[9,39]. Since the continuous secretion of neuregulin-1 by the sensory neuron is required for intrafusal fiber survival[40], the degeneration of the intrafusal fibers might be secondary to the degeneration of the sensory terminal. Finally, it is also possible that the degeneration of the sensory neuron and of the intrafusal fibers are independent processes occurring in parallel. In any case, the result would be a degeneration of the entire muscle spindle. If this degeneration is causal to the proprioceptive deficits, including uncoordinated movements and an abnormal gait, however, remains to be shown by a more detailed study.

Degenerating muscle spindles are not well characterized on the molecular level. We therefore used the *Gaa*$^{-/-}$ mice to investigate the subcellular distribution of a number of molecules during the degeneration process. Among others, we observed that several proteins usually almost exclusively present in both polar regions of intrafusal fibers redistributed into the central (equatorial) region of intrafusal fibers in 8-month-old *Gaa*$^{-/-}$ mice. For example, the voltage-gated sodium channel $Na_v1.4$ was present in the central region of wildtype muscle spindles only as a thin layer underneath the plasma membrane[25]. In contrast, it appeared throughout the intrafusal

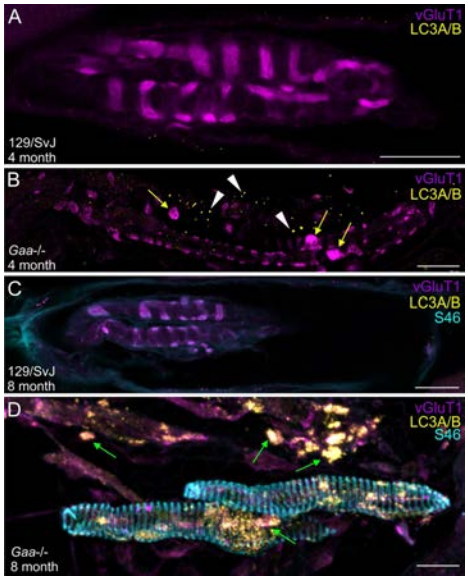

Figure 8. Autophagosomes accumulate in muscle spindles from *Gaa*$^{-/-}$ mice. Muscle spindles from 4- (**A,B**) and 8-month-old (**C,D**) wildtype (**A,C**) and *Gaa*$^{-/-}$ (**B,D**) mice were stained with antibodies against vGluT1 (purple channel) and the autophagosome marker LC3A/B (yellow channel). Muscle spindles from 8-month-old wildtype and *Gaa*$^{-/-}$ mice were additionally stained with antibodies against myosin heavy chain 6 (S46 antibody; blue channel in panels (**C,D**)). While autophagosomes were mostly absent in muscle spindles from 4- and 8-month-old wildtype mice, they appeared in 4-month-old *Gaa*$^{-/-}$ mice (white arrowheads in panel (**B**); category 2 muscle spindle). In 8-month-old *Gaa*$^{-/-}$ mice autophagosomes were abundant (arrows in panel (**D**); category 3 muscle spindle) and the LC3A/B immunoreactivity was associated with intrafusal fibers (arrows in panel (**D**)) and with the varicosities formed by the sensory nerve terminal (green arrows in panel (**D**)). Note the formation of small varicosities by the sensory nerve terminal in muscle spindles from 4-month-old *Gaa*$^{-/-}$ mice (yellow arrows in panel (**B**)). S46 immunoreactivity was absent in the central region of intrafusal fibers of 8-month-old 129/SvJ mice (**C**), but present in age-matched *Gaa*$^{-/-}$ mice (**D**), confirming the reorganization of the intrafusal contractile filaments. Scale bars: 20 µm.

fiber in degenerating muscle spindles from 8-month old *Gaa*$^{-/-}$ mice. Similarly, the nuclear bag fiber-specific myosin heavy chain 6 (stained by the S46 antibody) labeled only the subsarcolemmal sarcomeres in the central region of wildtype intrafusal fibers[25] but was present throughout the central part of intrafusal fibers in 8-month-old *Gaa*$^{-/-}$ mice. This suggests that intrafusal fibers change the subcellular distribution of their cytoskeleton and of associated molecules in degenerating muscle spindles. The altered distribution of the contractile apparatus was observed in the predominantly fast twitch EDL muscle and in the predominantly slow twitch soleus muscle. Therefore, the degeneration and the changes in the distribution of the contractile apparatus did not apparently depend on the muscle's fiber composition. It will be interesting to investigate if the innervation by the sensory nerve regulates the sarcomere distribution in intrafusal fibers.

Electrophysiological analyses of the muscle spindle response to ramp-and-hold stretches revealed severe defects in *Gaa*$^{-/-}$ mice, i.e. the dynamic as well as the static components of the stretch response were significantly reduced. These deficits were present already in 4-month-old mice and we therefore consider them the first functional signs of the muscle spindle degeneration. In contrast, ~ 30% of the recordings from 8-month-old *Gaa*$^{-/-}$ mice did not show a constant resting discharge but instead fired in bursts and did not respond to stretch. Since we only observed bursting behavior in 8-month-old *Gaa*$^{-/-}$ mice, it is likely that it represents a later stage of the degeneration process. One possibility to explain these bursts is that the generation of high frequency action potentials requires a continuous availability of glucose, which in the absence of GAA enzymatic activity might not be abound. Increasing the glucose content in the ACSF bathing solution, however, did not affect the bursting behavior. Moreover, the bursts could be recorded for several hours with only little changes in their duration and in their interburst interval, suggesting that they might reflect long-term axonal changes and are not the result of an acute glucose deficiency or damage. Since a similar spontaneous bursting behavior has been observed previously

in human muscle spindle afferents during postischemic or mechanically-induced paresthesiae[41,42], these bursts might reflect the degeneration of the axon and of its myelin sheath. The consequences of the reduced static and dynamic sensitivity and of the failed response to stretch would be a severely compromised proprioception, consistent with the abnormal motor coordination observed in 8-month-old *Gaa*$^{-/-}$ mice.

The muscle spindles with a bursting behavior did not respond to stretch. Since stretch sensitivity together with the spindle pause after the stretch are essential criteria for the identification of proprioceptive afferents, we do not have proof that the neurons with the bursting behavior are proprioceptive sensory afferents. However, since they appeared only in 8-month-old *Gaa*$^{-/-}$ mice and since their action potential frequencies were in the same range as that of proprioceptive afferents, and since similar bursting behavior has been described previously in sensory afferents from damaged muscle spindles, we consider it likely that they represent proprioceptive afferents, which had degenerated to an extend not allowing them to respond to stretch.

While the majority of muscle spindles from 8-month-old *Gaa*$^{-/-}$ mice displayed severe signs of structural degeneration with, for example, an absence of normal annulospiral structure of the sensory terminal, approximately 70% were still able to respond to stretch, albeit at reduced instantaneous frequencies. The reason for this discrepancy is unclear, but it should be noted that in our electrophysiological experiments, we are strongly biased towards muscle spindles with a stretch response and completely non-functional spindles would not have been detected. It is therefore possible that in our electrophysiological analyses, the few remaining functional muscle spindles are overrepresented. It should also be considered, that proprioceptive sensory neurons from damaged muscle spindles might still be able to rudimentarily respond to stretch even without direct contact to intrafusal fibers. A more detailed study directly relating structural degeneration of muscle spindles with altered responses to stretch is required to causally link both processes.

Previous studies have shown several motor symptoms in *Gaa*$^{-/-}$ mice including a reduced activity in an open field environment, symptoms of skeletal muscle deterioration, including an abnormal waddling gait, muscle weakness, poor performance in the rotarod test and remarkably different footprints[16]. Most of these deficits were detected in aged (> 12 month old) animals and directly or indirectly reflect the progressive skeletal muscle weakness of these animals. Our study, analyzing 4- and 8-month-old mice (presumably with less severe symptoms and representing an early symptomatic stage), represents the first systematic analysis of the limb- and paw coordination in this model organism for Pompe disease. We observed significant deficits particularly in inter-limb and inter-paw coordination. It is tempting to speculate that these deficits are caused by the degeneration of muscle spindle structure and function. However, interpreting the gait analysis requires caution, since some differences in the motor behavior are likely to be explained by the progressive degeneration of skeletal muscle tissue in *Gaa*$^{-/-}$ mice. Moreover, we compared *Gaa*$^{-/-}$ mice, which have a mixed C57BL/6 and 129/J background, with inbred 129/SvJ mice and, therefore, some of the differences could be due to the strain differences. However, transection of the dorsal column in rat (selectively eliminating the proprioceptive input to the CNS without affecting weight), resulted in similar motor coordination and gait changes as observed in *Gaa*$^{-/-}$ mice[43], demonstrating that these parameters can reflect proprioceptive deficits. Additionally, the print area was significantly increased across all paws in the *Gaa*$^{-/-}$ mice, even though their body weight is less compared to the 129/SvJ control mice. A more detailed study is required to demonstrate that the functional and structural degeneration of the muscle spindles causes the gait impairment and that the altered gait is caused by an altered proprioception.

Late-onset Pompe disease patients exhibit a number of motor coordination deficits, including for example decreased velocity and cadence, increased stance phase, increased time of double limb support, shorter step and stride length as well as a wider base of support[7]. The lateral displacement results, increased stance time and increase in hind base of support in *Gaa*$^{-/-}$ mice are similar to the motor symptoms in patients. Differences in the mutant mice between the front- and hindlimbs (including for example the wider base of support) are likely explained by the fact that the hindlimbs are outside of the visual field preventing a visual compensation of the motor coordination deficits[44]. The fundamental differences between biped humans and quadruped mice, however, make a direct translation of *Gaa*$^{-/-}$ mouse gait abnormalities to humans difficult[7–9].

We were not able to directly analyze the accumulation of glycogen in muscle spindles from *Gaa*$^{-/-}$ mice due to the incompatibility of the histochemical staining for glycogen and the immunohistochemical staining required to identify muscle spindles. However, in an autopsy study of a single Pompe disease patient, glycogen accumulation in intrafusal fibers from several different muscles has been reported[45]. Consistent with a glycogen accumulation-based degeneration of muscle spindles, Pompe disease patients present with reduced gait velocity, cadence, time in single stand and other abnormalities during posturographic analysis[9]. These symptoms together with the loss in muscle strength lead to an increased risk of falls, hospitalization and as a result in muscular atrophy due to immobilization[46,47]. Our study suggests that muscle spindle deficits might contribute to the posturographic symptoms and the frequent falls of Pompe patients. Proprioceptive training[48,49], including whole body vibration training with an oscillating platform[50,51], should therefore be incorporated into the Pompe disease therapy to improve proprioception and reduce the risk of injury and hospitalization.

Methods

Animals and muscle preparation. Experiments were performed on muscles from *Gaa*$^{-/-}$ mice (B6;129-*Gaa*^{tm1Rabn}/J; The Jackson Laboratories, strain 004154), originally generated by Raben et al.[15]. In these mice, exon 6 of the *GAA* gene was targeted with a termination codon and a neomycin cassette leading to a complete absence of the GAA enzyme in these mice. Mice of both sexes were tested at an age of 16 to 18 weeks (4-month-old) or between 34 and 36 weeks (8-month-old), respectively. Age- and sex-matched 129/SvJ mice (129X1/SvJ; The Jackson Laboratories; strain 000691) were used as controls in all experiments. At 16 to 18 weeks of age, the *Gaa*$^{-/-}$ mice have a reduced mobility and strength particularly in vertical motion and an accumulation of lysosomes in extrafusal fibers[15,16,52]. At 8 months of age, the *Gaa*$^{-/-}$ mice develop obvious muscle wasting, a weak

waddling gait and a decline in motor performance and coordination[15,16,20]. In agreement with the literature, we observed no difference between male and female mice in our experiments and no change in the body weight between *Gaa*$^{-/-}$ and wildtype control mice at 8 month of age[22,53]. A total of 52 animals (8 wildtype and 9 *Gaa*$^{-/-}$ mice were used for immunocytochemistry and 10 wildtype and 25 *Gaa*$^{-/-}$ mice for electrophysiology) were used in this study. All animal procedures used in this study were performed according to the guidelines from Directive 2010/63/EU of the European Parliament on the protection of animals used for scientific purposes. The study is reported in accordance with ARRIVE (Animal Research: Reporting of In Vivo Experiments) guidelines (https://arriveguidelines.org). Experimental protocols were designed to minimize the number of experimental animals. All experiments were approved by the local authorities of the State of Bavaria, Germany (Az.: ROB-55.2-2532.Vet 02-17-82).

Locomotor behavior. The gait of twelve 4-month-old and nine 8-month old *Gaa*$^{-/-}$ mice was compared with 17 and 8, respectively, age-matched 129/SvJ control mice using the CatWalk XT system (Noldus Information Technology, Wageningen, Netherlands[21,54]). This system allows the observer-independent quantitative analysis of several movement parameters, including speed of locomotion, symmetry of leg use as well as paw and digit position[54–56]. Animals were brought to the testing room 7 days before the commencement of the experiments. Before each experiment, mice were acclimatized to the walkway and the dark testing room for 5 min per day for 1 week. The experiments were conducted according to the manufacturer's suggestions and always at the same time of the day (between 10am and 1 pm). Each traverse of the walkway is termed a "run". All runs for a given animal are termed a "trial". Three consecutive compliant runs per trial were averaged and three trials for every mouse were performed. Each animal was tested individually, and food was placed in a goal-orientated box. Incomplete or non-compliant runs (below or above the set run duration of 0.5 to 5 s) were not scored. The same detection settings were used for all mice (Camera Gain: 9.64, Green Intensity Threshold: 0.11, Red Ceiling Light: 17.8, and Green Walkway Light: 19.00). After all test animals were analyzed, the raw data were exported as an Excel file for further analysis by the CatWalk XT software (version 10.6, Noldus Information Technology).

For the analysis of the ~ 200 parameters, we categorized them according to Ref.[21] into 4 major groups: (1) run characteristics and kinetic parameters, (2) temporal parameters, (3) spatial parameters, and (4) interlimb coordination parameters. The first three categories are more sensitive to muscle strength, locomotion speed and body weight[21,57], whereas the last category is considered proprioception-related and therefore the parameters of this group were analyzed in more detail. These included base of support, print position and regularity index.

Electrophysiology. Afferent sensory neuron responses to stretch were assayed using an isolated muscle–nerve preparation previously described[58–61]. Ten muscle spindles from four 4-month-old and 16 muscle spindles from six 8-month-old 129/SvJ mice were investigated and compared to 21 muscle spindles from eight 4-month-old and 22 muscle spindles from fourteen 8-month-old *Gaa*$^{-/-}$ mice, respectively. In brief, mice were sacrificed by cervical dislocation to avoid an interference of the anesthetic with the sensory afferent recordings. The extensor digitorum longus (EDL) muscle together with the deep peroneal branch of the sciatic nerve were then dissected and placed in a 25 ml in vitro tissue bath (809B-IV, Aurora Scientific, Dublin) containing oxygenated artificial cerebrospinal fluid (ACSF[58]). The tendons at one end were sutured to a fixed post and at the other end to a lever arm, connected to a dual force and length controller (300C-LR; Aurora Scientific, Dublin, Ireland) allowing the simultaneous recording of muscle tension and muscle length. Sensory activity was sampled using a suction electrode (tip diameter 50–70 µm) connected to an extracellular amplifier (Model 1800, A&M Systems, Elkhart, USA). A signal was classified as being from a putative muscle spindle afferent if it displayed a characteristic instantaneous frequency response to stretch as well as a pause during twitch contraction[58–60]. Baseline muscle length (L_0) was defined as the minimal length at which maximal twitch contractile force was generated. For every muscle spindle afferent recording, triplicates of 10 s resting discharge followed by ramp-and-hold stretches (L_0 plus 2.5, 5 or 7.5% of L_0; ramp speed 40% L_0 s^{-1}; ramp phase duration: 0.1 s; hold phase: 3.8 s; stretch duration: 4 s with 45 s intervals between each stretch[61]) were recorded and averaged. From these recordings the dynamic peak (DP; highest firing rate during ramp), the dynamic index (DI; firing rate of dynamic peak – initial static time), the initial static time (IST; firing rate 0.45–0.55 s into stretch) and the final static time (FST; firing rate 3.25–3.75 s into stretch) were determined[25,60,62] and compared to the same values from age-matched 129/SvJ control mice.

At the end of each recording, general muscle health was ensured by determining the maximal contractile force during a direct tetanic stimulation (500 ms train at 120 Hz frequency and 0.5 ms pulse length, supramaximal voltage; Grass SD9 stimulator; Natus, Pleasanton, USA[58,60]). This value was normalize for differences in muscle size and mass by determining the diameter of the EDL muscle at L_0. With this information, the specific force (force/cross-sectional area) was determined in wildtype and *Gaa*$^{-/-}$ mice and compared to the previously reported peak force of the EDL of 23,466 N/cm[263,64]. We observed no statistically significant difference in the specific force between wildtype and *Gaa*$^{-/-}$ mice at both ages analyzed.

For data analysis, action potentials from individual sensory neurons were identified by spike shape and the discriminator view using the Spike Histogram feature of LabChart (v8.1.5; ADInstruments, Sydney, Australia). Action potentials from additional potential muscle spindles that appeared during the stretch (detectable by a different frequencies and amplitudes) were not scored. No attempt was made to discriminate group Ia from group II afferents (see Wilkinson et al.[58] for a detailed discussion).

Statistical analysis. Differences between the means of the action potential frequencies and the gait parameters were compared statistically using student's unpaired t-test. All statistical analyses were performed using

GraphPad Prism (version 9.3.1). The level of significance (p-value) for all statistical tests was set at * < 0.05, ** < 0.01, *** < 0.001 and **** < 0.0001.

Immunocytochemistry. Immunofluorescence labelling was performed as described previously[25,60,61,65]. To obtain muscle tissue for immunohistochemistry, mice were deeply anaesthetized via an I.P. injection of ketamine (100 mg kg^{-1}; Pfizer, Berlin, Germany) and xylazine (10 mg kg^{-1}; Bayer AG, Leverkusen, Germany). After transcardial perfusion with PBS followed by 4% paraformaldehyde, the soleus, the gastrocnemius, the tibialis anterior and EDL muscles were dissected. Fixed muscles were embedded in Tissue-Tek O.C.T. Compound (Sakura Finetek Europe, AJ Alphen an den Rijn, Netherlands), rapidly frozen and cryo-sectioned along the longitudinal axis at 20–30 µm thickness.

Dried frozen sections were rehydrated for 10 min in PBS. Sections were then blocked in PBS containing 0.2% Triton X-100 (Sigma-Aldrich Chemie GmbH, Taufkirchen, Germany) and 1% bovine serum albumin (Carl Roth GmbH, Karlsruhe, Germany; blocking solution) for 60 min at room temperature and incubated with the primary antibody in blocking solution at 4 °C overnight.

Sensory nerve terminals were identified using antibodies from guinea pig against the vesicular glutamate transporter 1 (vGluT1; AB5905, Millipore, Darmstadt, Germany; 1:1000)[60,65]. The S46 monoclonal antibody (diluted 1:50) against the slow tonic myosin heavy chain 6 developed by F. Stockdale[66] was obtained from the Developmental Studies Hybridoma Bank, created by the NICHD of the NIH and maintained at The University of Iowa (Department of Biology, Iowa City, IA 52242)[25,67–69]. Neurofilament was detected using antibodies against NF200 (N4142, Sigma-Aldrich, Darmstadt, Germany; 1:500). To investigate autophagosomes, an antibody against LC3A/B was used (PAI-16931; Thermo Fisher Scientific-Invitrogen, Waltham, USA; 1:500)[29]. Antibodies against the lysosomal membrane glycoprotein LAMP1 (L1418, Sigma-Aldrich, Darmstadt, Germany; 1:500), which plays an important role in lysosome biogenesis and autophagy, were used to investigate lysosomal buildup. Versican was detected using a rabbit anti-versican antibody (Ab19345; Abcam, Cambridge, UK; 1:500[26]). The distribution of the voltage-gated sodium channel was analyzed using a polyclonal rabbit antibody (SCN4A; #ASC-020; Alomone labs, Jerusalem, Israel; 1:500[25]).

Primary antibodies were detected using the appropriate Alexa488-, Alexa594- and Alexa647-conjugated goat anti-rabbit (A11034; Thermo Fisher Scientific-Invitrogen, Waltham, USA; 1:1000), goat anti-guinea pig (A11076; Thermo Fischer Scientific-Invitrogen; 1:1000) or goat anti-mouse (A32723; Thermo Fischer Scientific-Invitrogen 1:1000) secondary antibody. To detect false positive results due to unspecific binding of antibodies, negative controls (without primary antibodies or with normal goat serum as primary antibodies) were stained in parallel. No specific labelling was observed under these conditions.

After immunofluorescence labelling, the sections were embedded in Aqua Polymount (18606; Polymount, Hirschberg, Germany) and analyzed using a Zeiss LSM 710 laser scanning confocal microscope (Carl Zeiss AG, Oberkochen, Germany) as previously described[25,59–61]. We observed no obvious morphological difference between muscle spindles of the EDL, the soleus, the tibialis anterior or the gastrocnemius muscle in mice of the same age and genotype. Therefore, the structural data of muscle spindles from all muscles of the same age and genotype were pooled and compared to pooled data from age-matched mice with a different genotype. Quantification of the number of muscle spindles per soleus muscle was performed as described previously[61]. The soleus muscle was chosen since it is a small muscle and since the number of muscle spindles has been analyzed previously[61,70,71]. Three soleus muscles each from a different wildtype or 8-month-old *Gaa*$^{-/-}$ mouse, respectively, were reconstructed.

Digital processing of entire images, including adjustment of brightness and contrast, was performed using Photoshop CS6 (Adobe Inc., San Jose, USA). Compound images were assembled using CorelDraw (vs 19.1.0.419; Corel Corporation, Ottawa, Canada).

To quantify the progression of the degenerative processes in muscle spindles from different ages, four different categories were defined, which can be distinguished in cryostat sections using brightfield microscopy (see Fig. 4A for representative examples of the categories):

Category 1 (no degeneration): normal structure of the muscle spindle, complete circumferential elements of the annulospiral endings, intrafusal fibers in close proximity to each other and normal distribution of nuclei typical for nuclear bag and nuclear chain fibers, few sarcomeric structures in the central region of intrafusal fibers, no varicosities formed by sensory terminal.
Category 2 (mild degeneration) Sensory terminals have formed few varicosities, circumferential elements present but often not continuous, sections with more than 8 nuclei in a row in typical nuclear bag and nuclear chain fiber arrangement detectable, intrafusal fibers partially detached from each other.
Category 3 (severe degeneration) several large varicosities formed by sensory terminal, severe degradation of circumferential parts of the annulospiral endings, circumferential elements are mostly disrupted, sarcomeric structures abundant in central region of intrafusal fiber, nuclei evenly distributed within capsule and no nuclear arrangement typical for nuclear bag and chain fibers detectable, intrafusal fibers are separated by a large space.
Category 4 (completely deteriorated) Sensory nerve terminal completely absent or only detectable as a large varicosity with no circumferential elements, no intrafusal fiber present, no sarcomeric structures detectable, capsule filled with cellular debris, outer capsule swollen, nuclei pycnotic.

To quantify the immunofluorescence signal detected in muscle spindles with antibodies against LAMP1 and LC3AB, muscle spindles from the EDL, the soleus and the tibialis anterior were analyzed. Since we did not observe obvious differences between muscle spindles form different muscles with respect to the categories

described above, results from all muscles of the same age and genotype were pooled. Sections were stained as detailed above and images were acquired as z-stacks using the same scanning speed and averaging. Using the ZEN software (vs. 3.5 blue edition, Carl Zeiss Microscopy GmbH, Göttingen, Germany) z-stacks were orthogonally projected using maximum intensity of the frontal plane (XY) and the background was subtracted from all images. The channels were split and pixels above threshold in the appropriate channel were counted unbiased using ImageJ (version 1.53q[72]). Thresholding was kept consistent across all images. The "Analyze Particles" function was used to calculate the total number of pixels above threshold in a defined area and the sum of the pixels above threshold in an identified particle ("size of particle"). Results were expressed as percent of control. The following number of animals (N) and number of spindles (n) were analysed: Four-month-old 129/SvJ animals: N = 4, n = 8; 8-month-old control animals: N = 3, n = 5; 4-month-old *Gaa*$^{-/-}$ animals: N = 3, n = 6; 8-month-old *Gaa*$^{-/-}$ animals: N = 3, n = 6. Statistical significance was calculated using the unpaired student's T-test in Excel (Microsoft Corporation, Redmond, USA).

Data availability

The datasets generated during and/or analyzed during the current study are available from the corresponding author on reasonable request.

Received: 11 October 2022; Accepted: 14 April 2023
Published online: 21 April 2023

References

1. van der Ploeg, A. T. & Reuser, A. J. Pompe's disease. *Lancet* **372**, 1342–1353 (2008).
2. Lim, J. A., Li, L. & Raben, N. Pompe disease: From pathophysiology to therapy and back again. *Front. Aging Neurosci.* **6**, 177. https://doi.org/10.3389/fnagi.2014.00177 (2014).
3. Kohler, L., Puertollano, R. & Raben, N. Pompe disease: From basic science to therapy. *Neurotherapeutics* **15**, 928–942 (2018).
4. Peruzzo, P., Pavan, E. & Dardis, A. Molecular genetics of Pompe disease: A comprehensive overview. *Ann. Transl. Med.* **7**, 278 (2019).
5. Martiniuk, F., Bodkin, M., Tzall, S. & Hirschhorn, R. Isolation and partial characterization of the structural gene for human acid alpha glucosidase. *DNA Cell Biol.* **10**, 283–292 (1991).
6. De Filippi, P. *et al.* Genotype-phenotype correlation in Pompe disease, a step forward. *Orphanet J. Rare Dis.* **9**, 102. https://doi.org/10.1186/s13023-014-0102-z (2014).
7. McIntosh, P. T., Case, L. E., Chan, J. M., Austin, S. L. & Kishnani, P. Characterization of gait in late onset Pompe disease. *Mol. Genet. Metab.* **116**, 152–156 (2015).
8. Valle, M. S. *et al.* Quantitative analysis of upright standing in adults with late-onset Pompe disease. *Sci. Rep.* **6**, 37040. https://doi.org/10.1038/srep37040 (2016).
9. Schneider, I. *et al.* Characterization of gait and postural regulation in late-onset Pompe disease. *Appl. Sci.* **10**, 197001. https://doi.org/10.3390/app10197001 (2020).
10. Proske, U. & Gandevia, S. C. The proprioceptive senses: Their roles in signaling body shape, body position and movement, and muscle force. *Physiol. Rev.* **92**, 1651–1697 (2012).
11. Kröger, S. Proprioception 2.0: Novel functions for muscle spindles. *Curr. Opin. Neurol.* **31**, 592–598 (2018).
12. Kröger, S. & Watkins, B. Muscle spindle function in healthy and diseased muscle. *Skelet. Muscle* **11**, 3. https://doi.org/10.1186/s13395-020-00258-x (2021).
13. De-Doncker, L., Picquet, F., Petit, J. & Falempin, M. Characterization of spindle afferents in rat soleus muscle using ramp-and-hold and sinusoidal stretches. *J. Neurophysiol.* **89**, 442–449 (2003).
14. Banks, R. W. The motor innervation of mammalian muscle-spindles. *Prog. Neurobiol.* **43**, 323–362 (1994).
15. Raben, N. *et al.* Targeted disruption of the acid alpha-glucosidase gene in mice causes an illness with critical features of both infantile and adult human glycogen storage disease type II. *J. Biol. Chem.* **273**, 19086–19092 (1998).
16. Raben, N., Nagaraju, K., Lee, E. & Plotz, P. Modulation of disease severity in mice with targeted disruption of the acid alpha-glucosidase gene. *Neuromuscul. Disord.* **10**, 283–291 (2000).
17. Yi, H. *et al.* Antibody-mediated enzyme replacement therapy targeting both lysosomal and cytoplasmic glycogen in Pompe disease. *J. Mol. Med.* **95**, 513–521 (2017).
18. Lee, N. C. *et al.* Ultrastructural and diffusion tensor imaging studies reveal axon abnormalities in Pompe disease mice. *Sci. Rep.* **10**, 20239. https://doi.org/10.1038/s41598-020-77193-w (2020).
19. Almodovar-Paya, A. *et al.* Preclinical research in glycogen storage diseases: A comprehensive review of current animal models. *Int. J. Mol. Sci.* **21**, 249621. https://doi.org/10.3390/ijms21249621 (2020).
20. Sidman, R. L. *et al.* Temporal neuropathologic and behavioral phenotype of 6neo/6neo Pompe disease mice. *J. Neuropathol. Exp. Neurol.* **67**, 803–818 (2008).
21. Pitzer, C., Kurpiers, B. & Eltokhi, A. Gait performance of adolescent mice assessed by the CatWalk XT depends on age, strain and sex and correlates with speed and body weight. *Sci. Rep.* **11**, 21372. https://doi.org/10.1038/s41598-021-00625-8 (2021).
22. Falk, D. J. *et al.* Peripheral nerve and neuromuscular junction pathology in Pompe disease. *Hum. Mol. Genet.* **24**, 625–636 (2015).
23. Fukuda, T. *et al.* Autophagy and lysosomes in Pompe disease. *Autophagy* **2**, 318–320 (2006).
24. Yong, Y., Hunter-Chang, S., Stepanova, E. & Deppmann, C. Axonal spheroids in neurodegeneration. *Mol. Cell. Neurosci.* **117**, 103679. https://doi.org/10.1016/j.mcn.2021.103679 (2021).
25. Watkins, B., Schuster, H. M., Gerwin, L., Schoser, B. & Kröger, S. The effect of methocarbamol and mexiletine on murine muscle spindle function. *Muscle Nerve* **66**, 96–105 (2022).
26. Bornstein, B. *et al.* Molecular characterization of the intact mouse muscle spindle using a multi-omics approach. *eLife* **12**, 81843. https://doi.org/10.7554/eLife.81843 (2023).
27. Raben, N. *et al.* Enzyme replacement therapy in the mouse model of Pompe disease. *Mol. Genet. Metab.* **80**, 159–169 (2003).
28. Fukuda, T. *et al.* Dysfunction of endocytic and autophagic pathways in a lysosomal storage disease. *Ann. Neurol.* **59**, 700–708 (2006).
29. Kabeya, Y. *et al.* LC3, a mammalian homologue of yeast Apg8p, is localized in autophagosome membranes after processing. *EMBO J.* **19**, 5720–5728 (2000).
30. Raben, N. *et al.* Conditional tissue-specific expression of the acid alpha-glucosidase (GAA) gene in the GAA knockout mice: Implications for therapy. *Hum. Mol. Genet.* **10**, 2039–2047 (2001).
31. Byrne, B. J. *et al.* Pompe disease: Design, methodology, and early findings from the Pompe registry. *Mol. Genet. Metab.* **103**, 1–11 (2011).

32. Oda, K., Yamazaki, K., Miura, H., Shibasaki, H. & Kikuchi, T. Dying back type axonal degeneration of sensory nerve terminals in muscle spindles of the gracile axonal dystrophy (GAD) mutant mouse. *Neuropathol. Appl. Neurobiol.* **18**, 265–281 (1992).
33. Smeyne, R. J. *et al.* Severe sensory and sympathetic neuropathies in mice carrying a disrupted Trk/NGF receptor gene. *Nature* **368**, 246–249 (1994).
34. Ernfors, P., Lee, K. F., Kucera, J. & Jaenisch, R. Lack of neurotrophin-3 leads to deficiencies in the peripheral nervous system and loss of limb proprioceptive afferents. *Cell* **77**, 503–512 (1994).
35. Klein, R. *et al.* Disruption of the neurotrophin-3 receptor gene trkC eliminates la muscle afferents and results in abnormal movements. *Nature* **368**, 249–251 (1994).
36. Gambetti, P., DiMauro, S. & Baker, L. Nervous system in Pompe's disease. Ultrastructure and biochemistry. *J. Neuropathol. Exp. Neurol.* **30**, 412–430 (1971).
37. Martin, J. J., de Barsy, T., van Hoof, F. & Palladini, G. Pompe's disease: an inborn lysosomal disorder with storage of glycogen. A study of brain and striated muscle. *Acta Neuropathol.* **23**, 229–244 (1973).
38. Lamartine, S. M. M. & Remiche, G. Late-onset Pompe disease associated with polyneuropathy. *Neuromuscul. Disord.* **29**, 968–972 (2019).
39. Tsai, L. K., Hwu, W. L., Lee, N. C., Huang, P. H. & Chien, Y. H. Clinical features of Pompe disease with motor neuronopathy. *Neuromuscul. Disord.* **29**, 903–906 (2019).
40. Cheret, C. *et al.* Bace1 and Neuregulin-1 cooperate to control formation and maintenance of muscle spindles. *EMBO J.* **32**, 2015–2028 (2013).
41. Ochoa, J., Torebjork, H. E., Culp, W. J. & Schady, W. Abnormal spontaneous activity in single sensory nerve fibers in humans. *Muscle Nerve* **5**, S74-77 (1982).
42. Nordin, M., Nystrom, B., Wallin, U. & Hagbarth, K. E. Ectopic sensory discharges and paresthesiae in patients with disorders of peripheral nerves, dorsal roots and dorsal columns. *Pain* **20**, 231–245 (1984).
43. Fagoe, N. D. *et al.* Evaluation of five tests for sensitivity to functional deficits following cervical or thoracic dorsal column transection in the rat. *PLoS ONE* **11**, e0150141. https://doi.org/10.1371/journal.pone.0150141 (2016).
44. Mayer, W. P. & Akay, T. The role of muscle spindle feedback in the guidance of hindlimb movement by the ipsilateral forelimb during locomotion in mice. *eNeuro* **8**, 1. https://doi.org/10.1523/ENEURO.0432-21.2021 (2021).
45. van der Walt, J. D., Swash, M., Leake, J. & Cox, E. L. The pattern of involvement of adult-onset acid maltase deficiency at autopsy. *Muscle Nerve* **10**, 272–281 (1987).
46. Horlings, C. G., van Engelen, B. G., Allum, J. H. & Bloem, B. R. A weak balance: The contribution of muscle weakness to postural instability and falls. *Nat. Clin. Pract. Neurol.* **4**, 504–515 (2008).
47. Horlings, C. G. *et al.* Balance control in patients with distal versus proximal muscle weakness. *Neuroscience* **164**, 1876–1886 (2009).
48. Aman, J. E., Elangovan, N., Yeh, I. L. & Konczak, J. The effectiveness of proprioceptive training for improving motor function: A systematic review. *Front. Hum. Neurosci.* **8**, 1075. https://doi.org/10.3389/fnhum.2014.01075 (2014).
49. Yong, M. S. & Lee, Y. S. Effect of ankle proprioceptive exercise on static and dynamic balance in normal adults. *J. Phys. Ther. Sci.* **29**, 242–244 (2017).
50. Iolascon, G. *et al.* Adapted physical activity and therapeutic exercise in late-onset Pompe disease (LOPD): A two-step rehabilitative approach. *Neurol. Sci.* **41**, 859–868 (2020).
51. Montagnese, F., Thiele, S., Wenninger, S. & Schoser, B. Long-term whole-body vibration training in two late-onset Pompe disease patients. *Neurol. Sci.* **37**, 1357–1360 (2016).
52. Schaaf, G. J. *et al.* Lack of robust satellite cell activation and muscle regeneration during the progression of Pompe disease. *Acta Neuropathol. Commun.* **3**, 65. https://doi.org/10.1186/s40478-015-0243-x (2015).
53. Hintze, S. *et al.* Uptake of moss-derived human recombinant GAA in Gaa (−/−) mice. *JIMD Rep.* **59**, 81–89 (2021).
54. Garrick, J. M., Costa, L. G., Cole, T. B. & Marsillach, J. Evaluating gait and locomotion in rodents with the CatWalk. *Curr. Protoc.* **1**, e220. https://doi.org/10.1002/cpz1.220 (2021).
55. Mock, J. T. *et al.* Gait analyses in mice: Effects of age and glutathione deficiency. *Aging Dis.* **9**, 634–646 (2018).
56. Brooks, S. P. & Dunnett, S. B. Tests to assess motor phenotype in mice: A user's guide. *Nature Rev. Neurosci.* **10**, 519–529 (2009).
57. Batka, R. J. *et al.* The need for speed in rodent locomotion analyses. *Anat. Rec.* **297**, 1839–1864 (2014).
58. Wilkinson, K. A., Kloefkorn, H. E. & Hochman, S. Characterization of muscle spindle afferents in the adult mouse using an in vitro muscle-nerve preparation. *PLoS ONE* **7**, e39140. https://doi.org/10.1371/journal.pone.0039140 (2012).
59. Franco, J. A., Kloefkorn, H. E., Hochman, S. & Wilkinson, K. A. An in vitro adult mouse muscle-nerve preparation for studying the firing properties of muscle afferents. *J. Vis. Exp.* https://doi.org/10.3791/51948 (2014).
60. Gerwin, L., Haupt, C., Wilkinson, K. A. & Kröger, S. Acetylcholine receptors in the equatorial region of intrafusal muscle fibres modulate mouse muscle spindle sensitivity. *J. Physiol.* **597**, 1993–2006 (2019).
61. Gerwin, L. *et al.* Impaired muscle spindle function in murine models of muscular dystrophy. *J. Physiol.* **598**, 1591–1609 (2020).
62. Than, K. *et al.* Vesicle-released glutamate is necessary to maintain muscle spindle afferent excitability but not dynamic sensitivity in adult mice. *J. Physiol.* **599**, 2953–2967 (2021).
63. Larsson, L. & Edstrom, L. Effects of age on enzyme-histochemical fibre spectra and contractile properties of fast- and slow-twitch skeletal muscles in the rat. *J. Neurol. Sci.* **76**, 69–89 (1986).
64. Brooks, S. V. & Faulkner, J. A. Contractile properties of skeletal muscles from young, adult and aged mice. *J. Physiol.* **404**, 71–82 (1988).
65. Zhang, Y., Wesolowski, M., Karakatsani, A., Witzemann, V. & Kröger, S. Formation of cholinergic synapse-like specializations at developing murine muscle spindles. *Dev. Biol.* **393**, 227–235 (2014).
66. Miller, J. B., Crow, M. T. & Stockdale, F. E. Slow and fast myosin heavy chain content defines three types of myotubes in early muscle cell cultures. *J. Cell Biol.* **101**, 1643–1650 (1985).
67. Pedrosa, F., Soukup, T. & Thornell, L. E. Expression of an alpha cardiac-like myosin heavy chain in muscle spindle fibres. *Histochemistry* **95**, 105–113 (1990).
68. Kucera, J., Walro, J. M. & Gorza, L. Expression of type-specific MHC isoforms in rat intrafusal muscle fibers. *J. Histochem. Cytochem.* **40**, 293–307 (1992).
69. Walro, J. M. & Kucera, J. Why adult mammalian intrafusal and extrafusal fibers contain different myosin heavy-chain isoforms. *Trends Neurosci.* **22**, 180–184 (1999).
70. Lionikas, A. *et al.* Analyses of muscle spindles in the soleus of six inbred mouse strains. *J. Anat.* **223**, 289–296 (2013).
71. Sonner, M. J., Walters, M. C. & Ladle, D. R. Analysis of proprioceptive sensory innervation of the mouse soleus: A whole-mount muscle approach. *PLoS ONE* **12**, e0170751. https://doi.org/10.1371/journal.pone.0170751 (2017).
72. Schneider, C. A., Rasband, W. S. & Eliceiri, K. W. NIH Image to ImageJ: 25 years of image analysis. *Nat. Method* **9**, 671–675 (2012).

Acknowledgements

The authors would like to thank Florence Bareyre and Julie Fourneau for invaluable help with the CatWalk XT system and Corinna Haupt for help with the confocal microscopy. They are thankful to Eli Zelzer and Bavat Bornstein for sharing their unpublished results on the distribution of versican in muscle spindles. The critical reading and improving of the manuscript by Katherine Wilkinson is gratefully acknowledged. This study was supported

by the Deutsche Forschungsgemeinschaft (DFG; KR1039/16-2), the German Society for Muscle Disease (DGM), the German Academic Exchange Program (DAAD) and the Munich Center for Neurosciences—Brain and Mind, Ludwig-Maximilians-Universität München.

Author contributions

B.W., J.S., A.R., S.H., P.M., B.S. and S.K. designed the study; B.W., J.S., A.R., performed the experiments; B.W., J.S., A.R., B.S., and S.K. analyzed the data; and B.W., J.S., A.F., S.H., P.M., B.S. and S.K. wrote and revised the manuscript. All authors read and approved the final manuscript.

Funding

Open Access funding enabled and organized by Projekt DEAL.

Competing interests

The authors declare no competing interests.

Additional information

Supplementary Information The online version contains supplementary material available at https://doi.org/10.1038/s41598-023-33543-y.

Correspondence and requests for materials should be addressed to S.K.

Reprints and permissions information is available at www.nature.com/reprints.

Publisher's note Springer Nature remains neutral with regard to jurisdictional claims in published maps and institutional affiliations.

5. References

Abbruzzese, G., & Berardelli, A. (2003). Sensorimotor integration in movement disorders. *Mov Disord*, *18*(3), 231-240. https://doi.org/10.1002/mds.10327

Abdel Shaheed, C., Maher, C. G., Williams, K. A., & McLachlan, A. J. (2017). Efficacy and tolerability of muscle relaxants for low back pain: Systematic review and meta-analysis. *Eur J Pain*, *21*(2), 228-237. https://doi.org/10.1002/ejp.907

Adrian, E. D., & Zotterman, Y. (1926). The impulses produced by sensory nerve-endings: Part II. The response of a Single End-Organ. *J Physiol*, *61*(2), 151-171. https://doi.org/10.1113/jphysiol.1926.sp002281

Aimonetti, J. M., Ribot-Ciscar, E., Rossi-Durand, C., Attarian, S., Pouget, J., & Roll, J. P. (2005). Functional sparing of intrafusal muscle fibers in muscular dystrophies. *Muscle Nerve*, *32*(1), 88-94. https://doi.org/10.1002/mus.20335

Aljuhani, O., Kopp, B. J., & Patanwala, A. E. (2017). Effect of Methocarbamol on Acute Pain After Traumatic Injury. *Am J Ther*, *24*(2), e202-e206. https://doi.org/10.1097/MJT.0000000000000364

Aman, J. E., Elangovan, N., Yeh, I. L., & Konczak, J. (2014). The effectiveness of proprioceptive training for improving motor function: a systematic review. *Front Hum Neurosci*, *8*, 1075. https://doi.org/10.3389/fnhum.2014.01075

Angelini, C., & Engel, A. G. (1972). Comparative study of acid maltase deficiency. Biochemical differences between infantile, childhood, and adult types. *Arch Neurol*, *26*(4), 344-349. https://doi.org/10.1001/archneur.1972.00490100074007

Angelini, C., & Semplicini, C. (2012). Enzyme replacement therapy for Pompe disease. *Curr Neurol Neurosci Rep*, *12*(1), 70-75. https://doi.org/10.1007/s11910-011-0236-5

Assaraf, E., Blecher, R., Heinemann-Yerushalmi, L., Krief, S., Carmel Vinestock, R., Biton, I. E., Brumfeld, V., Rotkopf, R., Avisar, E., Agar, G., & Zelzer, E. (2020). Piezo2 expressed in proprioceptive neurons is essential for skeletal integrity. *Nat Commun*, *11*(1), 3168. https://doi.org/10.1038/s41467-020-16971-6

Ausems, M. G., Verbiest, J., Hermans, M. P., Kroos, M. A., Beemer, F. A., Wokke, J. H., Sandkuijl, L. A., Reuser, A. J., & van der Ploeg, A. T. (1999). Frequency of glycogen storage disease type II in The Netherlands: implications for diagnosis and genetic counselling. *Eur J Hum Genet*, *7*(6), 713-716. https://doi.org/10.1038/sj.ejhg.5200367

Banks, R. W. (1986). Observations on the primary sensory ending of tenuissimus muscle spindles in the cat. *Cell Tissue Res*, *246*(2), 309-319. https://doi.org/10.1007/BF00215893

Banks, R. W. (1994a). Intrafusal motor innervation: a quantitative histological analysis of tenuissimus muscle spindles in the cat. *J Anat*, *185*(Pt 1), 151-172.

Banks, R. W. (1994b). The motor innervation of mammalian muscle spindles. *Prog Neurobiol*, *43*(4-5), 323-362. https://doi.org/10.1016/0301-0082(94)90059-0

Banks, R. W. (2015). The innervation of the muscle spindle: a personal history. *J Anat*, *227*(2), 115-135. https://doi.org/10.1111/joa.12297

Banks, R. W., & Barker, D. (2004). The Muscle Spindle. In Engel, A.G. & Franzini-Armstrong, C. (Eds.), *Myology* (3 ed., pp. 489-509). McGraw-Hill Co.

Banks, R. W., Barker, D., & Stacey, M. J. (1982). Form and distribution of sensory terminals in cat hindlimb muscle spindles. *Philos Trans R Soc Lond B Biol Sci*, *299*(1096), 329-364. https://doi.org/10.1098/rstb.1982.0136

Banks, R. W., Harker, D. W., & Stacey, M. J. (1977). A study of mammalian intrafusal muscle fibres using a combined histochemical and ultrastructural technique. *J Anat*, *123*(Pt 3), 783-796.

Barker, D. (1974). The Morphology of Muscle Receptors. In Hunt, C. C. (Ed.), *Muscle Receptors* (Vol. 3, pp. 1-190). Springer. https://doi.org/10.1007/978-3-642-65945-4_1

Beebe, F. A., Barkin, R. L., & Barkin, S. (2005). A clinical and pharmacologic review of skeletal muscle relaxants for musculoskeletal conditions. *Am J Ther*, *12*(2), 151-171. https://doi.org/10.1097/01.mjt.0000134786.50087.d8

Bell, C. (1833a). *The Hand: Its mechanism and vital endowments as evincing design* (Vol. 1). W. Pickering.

Bell, C. (1833b). On the nervous circle which connects the voluntary muscles with the brain. *Philos Trans Royal Society 2*(116), 163-173. https://doi.org/10.1098/rspl.1815.0284

Bewick, G. S., & Banks, R. W. (2015). Mechanotransduction in the muscle spindle. *Pflugers Arch*, *467*(1), 175-190. https://doi.org/10.1007/s00424-014-1536-9

Bewick, G. S., Reid, B., Richardson, C., & Banks, R. W. (2005). Autogenic modulation of mechanoreceptor excitability by glutamate release from synaptic-like vesicles: evidence from the rat muscle spindle primary sensory ending. *J Physiol*, *562*(Pt 2), 381-394. https://doi.org/10.1113/jphysiol.2004.074799

Bewick, Guy S., & Banks, Robert W. (2021). Mechanotransduction channels in proprioceptive sensory nerve terminals: still an open question? *Curr Opin Physiol*, *20*, 90-104. https://doi.org/10.1016/j.cophys.2020.11.007

Billups, S. J., Delate, T., & Hoover, B. (2011). Injury in an elderly population before and after initiating a skeletal muscle relaxant. *Ann Pharmacother*, *45*(4), 485-491. https://doi.org/10.1345/aph.1P628

Bischoff, G. (1932). Zum klinischen Bild der Glykogen-Speicherungskrankheit (Glykogenose). *Zeitschrift für Kinderheilkunde*, *52*(6), 722-726. https://doi.org/10.1007/bf02248461

Blecher, R., Heinemann-Yerushalmi, L., Assaraf, E., Konstantin, N., Chapman, J. R., Cope, T. C., Bewick, G. S., Banks, R. W., & Zelzer, E. (2018). New functions for the proprioceptive system in skeletal biology. *Philos Trans R Soc Lond B Biol Sci*, *373*(1759), 20170327. https://doi.org/10.1098/rstb.2017.0327

Blecher, R., Krief, S., Galili, T., Assaraf, E., Stern, T., Anekstein, Y., Agar, G., & Zelzer, E. (2017a). The proprioceptive system regulates morphologic restoration of fractured bones. *Cell Rep*, *20*(8), 1775-1783. https://doi.org/10.1016/j.celrep.2017.07.073

Blecher, R., Krief, S., Galili, T., Biton, I. E., Stern, T., Assaraf, E., Levanon, D., Appel, E., Anekstein, Y., Agar, G., Groner, Y., & Zelzer, E. (2017b). The proprioceptive system masterminds spinal alignment: Insight into the mechanism of scoliosis. *Dev Cell*, *42*(4), 388-399 e383. https://doi.org/10.1016/j.devcel.2017.07.022

Boon, M., Martini, C., & Dahan, A. (2018). Recent advances in neuromuscular block during anesthesia. *F1000Res*, *7*, 167. https://doi.org/10.12688/f1000research.13169.1

Bornstein, B., Heinemann-Yerushalmi, L., Krief, S., Adler, R., Dassa, B., Leshkowitz, D., Kim, M., Bewick, G., Banks, R. W., & Zelzer, E. (2023a). Molecular characterization of the intact mouse muscle spindle using a multi-omics approach. *elife*, *12*, e81843. https://doi.org/10.7554/eLife.81843

Bornstein, B., Konstantin, N., Alessandro, C., Tresch, M.C., & Zelzer, E. (2021). More than movement: the proprioceptive system as a new regulator of musculoskeletal biology. *Curr Opin Physiol*, *20*, 77-89. https://doi.org/10.1016/j.cophys.2021.01.004

Bornstein, B., Watkins, B., Passini, F. S., Blecher, R., Assaraf, E., Sui, X. M., Brumfeld, V., Tsoory, M., Kröger, S., & Zelzer, E. (2023b). The mechanosensitive ion channel ASIC2 mediates both proprioceptive sensing and spinal alignment. *Exp Physiol*, *Epub ahead of print*, 1-13. https://doi.org/10.1113/EP090776

Boyd, I. A. (1962). The structure and innervation of the nuclear bag muscle fibre system and the nuclear chain muscle fibre system in mammalian muscle spindles. *Phil Trans Royal Soc Series B, Biol Sci.*, *245*(720), 81-136. https://doi.org/10.1098/rstb.1962.0007

Boyd, I. A., Gladden, M. H., McWilliam, P. N., & Ward, J. (1977). Control of dynamic and static nuclear bag fibres and nuclear chain fibres by gamma and beta axons in isolated cat muscle spindels. *J Physiol*, *265*(1), 133-162. https://doi.org/10.1113/jphysiol.1977.sp011709

Brooks, S. P., & Dunnett, S. B. (2009). Tests to assess motor phenotype in mice: a user's guide. *Nat Rev Neurosci*, *10*(7), 519-529. https://doi.org/10.1038/nrn2652

Brown, M. C., & Butler, R. G. (1973). Studies on the site of termination of static and dynamic fusimotor fibres within muscle spindles of the tenuissimus muscle of the cat. *J Physiol*, *233*(3), 553-573. https://doi.org/10.1113/jphysiol.1973.sp010323

Cabello, J., & Marsden, D. (2016). Pompe disease: clinical perspectives. *Orphan Drugs: Res Rev*, *7*, 1-10. https://doi.org/10.2147/odrr.S69109

Calderon, J. C., Bolanos, P., & Caputo, C. (2014). The excitation-contraction coupling mechanism in skeletal muscle. *Biophys Rev*, *6*(1), 133-160. https://doi.org/10.1007/s12551-013-0135-x

Caldwell, J. H. (1986). Distribution of sodium channels in muscle. *Ann N Y Acad Sci*, *479*, 364-376. https://doi.org/10.1111/j.1749-6632.1986.tb15582.x

Caldwell, J. H., Campbell, D. T., & Beam, K. G. (1986). Na channel distribution in vertebrate skeletal muscle. *J Gen Physiol*, *87*(6), 907-932. https://doi.org/10.1085/jgp.87.6.907

Cameron, M. H., Horak, F. B., Herndon, R. R., & Bourdette, D. (2008). Imbalance in multiple sclerosis: a result of slowed spinal somatosensory conduction. *Somatosens Mot Res*, *25*(2), 113-122. https://doi.org/10.1080/08990220802131127

Campbell, R. W. (1987). Mexiletine. *N Engl J Med*, *316*(1), 29-34. https://doi.org/10.1056/NEJM198701013160106

Carr, R. W., Morgan, D. L., & Proske, U. (1996). Impulse initiation in the mammalian muscle spindle during combined fusimotor stimulation and succinyl choline infusion. *J Neurophysiol*, *75*(4), 1703-1713. https://doi.org/10.1152/jn.1996.75.4.1703

Carr, R. W., & Proske, U. (1996). Action of cholinesters on sensory nerve endings in skin and muscle. *Clin Exp Pharmacol Physiol*, *23*(5), 355-362. https://doi.org/10.1111/j.1440-1681.1996.tb02741.x

Cazzato, G., & Walton, J. N. (1968). The pathology of the muscle spindle. A study of biopsy material in various muscular and neuromuscular diseases. *J Neurol Sci*, *7*(1), 15-70. https://doi.org/10.1016/0022-510x(68)90003-8

Chan, J., Desai, A. K., Kazi, Z. B., Corey, K., Austin, S., Hobson-Webb, L. D., Case, L. E., Jones, H. N., & Kishnani, P. S. (2017). The emerging phenotype of late-onset Pompe disease: A systematic literature review. *Mol Genet Metab*, *120*(3), 163-172. https://doi.org/10.1016/j.ymgme.2016.12.004

Chen, H. H., Hippenmeyer, S., Arber, S., & Frank, E. (2003). Development of the monosynaptic stretch reflex circuit. *Curr Opin Neurobiol*, *13*(1), 96-102. https://doi.org/10.1016/s0959-4388(03)00006-0

Chen, Y. J., Cheng, F. C., Sheu, M. L., Su, H. L., Chen, C. J., Sheehan, J., & Pan, H. C. (2014). Detection of subtle neurological alterations by the Catwalk XT gait analysis system. *J Neuroeng Rehabil*, *11*, 62. https://doi.org/10.1186/1743-0003-11-62

Chesler, A. T., Szczot, M., Bharucha-Goebel, D., Ceko, M., Donkervoort, S., Laubacher, C., Hayes, L. H., Alter, K., Zampieri, C., Stanley, C., Innes, A. M., Mah, J. K., Grosmann, C. M., Bradley, N., Nguyen, D., Foley, A. R., Le Pichon, C. E., & Bonnemann, C. G. (2016). The role of PIEZO2 in human mechanosensation. *N Engl J Med*, *375*(14), 1355-1364. https://doi.org/10.1056/NEJMoa1602812

Chou, R., Peterson, K., & Helfand, M. (2004). Comparative efficacy and safety of skeletal muscle relaxants for spasticity and musculoskeletal conditions: a systematic review. *J Pain Symptom Manage*, *28*(2), 140-175. https://doi.org/10.1016/j.jpainsymman.2004.05.002

Cohen, L. A. (1958). Analysis of position sense in human shoulder. *J Neurophysiol*, *21*(6), 550-562. https://doi.org/10.1152/jn.1958.21.6.550

Colon, A., Guo, X., Akanda, N., Cai, Y., & Hickman, J. J. (2017). Functional analysis of human intrafusal fiber innervation by human gamma-motoneurons. *Sci Rep*, *7*(1), 17202. https://doi.org/10.1038/s41598-017-17382-2

Conte, A., Khan, N., Defazio, G., Rothwell, J. C., & Berardelli, A. (2013). Pathophysiology of somatosensory abnormalities in Parkinson disease. *Nat Rev Neurol*, *9*(12), 687-697. https://doi.org/10.1038/nrneurol.2013.224

Crankshaw, D. P., & Raper, C. (1968). Some studies on peripheral actions of mephenesin, methocarbamol and diazepam. *Br J Pharmacol*, *34*(3), 579-590. https://doi.org/10.1111/j.1476-5381.1968.tb08486.x

Crankshaw, D. P., & Raper, C. (1970). Mephenesin, methocarbamol, chlordiazepoxide and diazepam: actions on spinal reflexes and ventral root potentials. *Br J Pharmacol*, *38*(1), 148-156. https://doi.org/10.1111/j.1476-5381.1970.tb10343.x

D'Mello, S., & Shum, L. (2016). A review of the use of mexiletine in patients with myotonic dystrophy and non-dystrophic myotonia. *Eur J Hosp Pharm*, *23*(6), 359-363. https://doi.org/10.1136/ejhpharm-2015-000839

Davidoff, R. A. (1985). Antispasticity drugs: mechanisms of action. *Ann Neurol*, *17*(2), 107-116. https://doi.org/10.1002/ana.410170202

De-Doncker, L., Picquet, F., Petit, J., & Falempin, M. (2003). Characterization of spindle afferents in rat soleus muscle using ramp-and-hold and sinusoidal stretches. *J Neurophysiol*, *89*(1), 442-449. https://doi.org/10.1152/jn.00153.2002

De Bellis, M., Sanarica, F., Carocci, A., Lentini, G., Pierno, S., Rolland, J. F., Conte Camerino, D., & De Luca, A. (2017). Dual Action of Mexiletine and Its Pyrroline Derivatives as Skeletal Muscle Sodium Channel Blockers and Anti-oxidant Compounds: Toward Novel Therapeutic Potential. *Front Pharmacol*, *8*, 907. https://doi.org/10.3389/fphar.2017.00907

de Faria, D. O. S., In't Groen, S. L. M., Hoogeveen-Westerveld, M., Niño, M. Y., van der Ploeg, A. T., Bergsma, A. J., & Pijnappel, W. W. M. P. (2021). Update of the Pompe variant database for the prediction of clinical phenotypes: Novel disease-associated variants, common sequence variants, and results from newborn screening. *Hum Mutat*, *42*(2), 119-134. https://doi.org/10.1002/humu.24148

De Filippi, P., Saeidi, K., Ravaglia, S., Dardis, A., Angelini, C., Mongini, T., Morandi, L., Moggio, M., Di Muzio, A., Filosto, M., Bembi, B., Giannini, F., Marrosu, G., Rigoldi, M., Tonin, P., Servidei, S., Siciliano, G., Carlucci, A., Scotti, C., Comelli, M., Toscano, A., & Danesino, C. (2014). Genotype-phenotype correlation in Pompe disease, a step forward. *Orphanet J Rare Dis*, *9*, 102. https://doi.org/10.1186/s13023-014-0102-z

Delle Vedove, A., Storbeck, M., Heller, R., Holker, I., Hebbar, M., Shukla, A., Magnusson, O., Cirak, S., Girisha, K. M., O'Driscoll, M., Loeys, B., & Wirth, B. (2016). Biallelic loss of proprioception-related PIEZO2 causes muscular atrophy with perinatal respiratory distress, arthrogryposis, and scoliosis. *Am J Hum Genet*, *99*(6), 1406-1408. https://doi.org/10.1016/j.ajhg.2016.11.009

Durbaba, R., Taylor, A., Ellaway, P. H., & Rawlinson, S. (2006). Classification of longissimus lumborum muscle spindle afferents in the anaesthetized cat. *J Physiol*, *571*(Pt 2), 489-498. https://doi.org/10.1113/jphysiol.2005.102731

Dutia, M. B. (1980). Activation of cat muscle spindle primary, secondary and intermediate sensory endings by suxamethonium. *J Physiol*, *304*, 315-330. https://doi.org/10.1113/jphysiol.1980.sp013326

Ebashi, S., & Lipmann, F. (1962). Adenosine triphosphate-linked concentration of calcium ions in a particulate fraction of rabbit muscle. *J Cell Biol*, *14*(3), 389-400. https://doi.org/10.1083/jcb.14.3.389

Ellis, K. O., & Carpenter, J. F. (1972). Studies on the mechanism of action of dantrolene sodium. A skeletal muscle relaxant. *Naunyn Schmiedebergs Arch Pharmacol*, *275*(1), 83-94. https://doi.org/10.1007/BF00505069

Engel, A. G. (1970). Acid maltase deficiency in adults: studies in four cases of a syndrome which may mimic muscular dystrophy or other myopathies. *Brain*, *93*(3), 599-616. https://doi.org/10.1093/brain/93.3.599

Florez-Paz, D., Bali, K. K., Kuner, R., & Gomis, A. (2016). A critical role for Piezo2 channels in the mechanotransduction of mouse proprioceptive neurons. *Sci Rep*, *6*, 25923. https://doi.org/10.1038/srep25923

Foldes, F. F., Wnuck, A. L., Hodges, R. J., Thesleff, S., & Debeer, E. J. (1957). The mode of action of depolarizing relaxants. *Anesth Analg*, *36*(5), 23-37.

Franco, J. A., Kloefkorn, H. E., Hochman, S., & Wilkinson, K. A. (2014). An in vitro adult mouse muscle-nerve preparation for studying the firing properties of muscle afferents. *J Vis Exp*, *91*(91), e51948. https://doi.org/10.3791/51948

Gandevia, S.C., Burke, D.C., & Anthony, M. (1993). *Science and Practice in Clinical Neurology* (1 ed., Vol. 1). Cambridge University Press.

Garrick, J. M., Costa, L. G., Cole, T. B., & Marsillach, J. (2021). Evaluating gait and locomotion in rodents with the CatWalk. *Curr Protoc*, *1*(8), e220. https://doi.org/10.1002/cpz1.220

Geel, T. M., McLaughlin, P. M., de Leij, L. F., Ruiters, M. H., & Niezen-Koning, K. E. (2007). Pompe disease: current state of treatment modalities and animal models. *Mol Genet Metab*, *92*(4), 299-307. https://doi.org/10.1016/j.ymgme.2007.07.009

Gerwin, L., Haupt, C., Wilkinson, K. A., & Kröger, S. (2019). Acetylcholine receptors in the equatorial region of intrafusal muscle fibres modulate mouse muscle spindle sensitivity. *J Physiol*, *597*(7), 1993-2006. https://doi.org/10.1113/JP277139

Gerwin, L., Rossmanith, S., Haupt, C., Schultheiss, J., Brinkmeier, H., Bittner, R. E., & Kröger, S. (2020). Impaired muscle spindle function in murine models of muscular dystrophy. *J Physiol*, *598*(8), 1591-1609. https://doi.org/10.1113/JP278563

Ginanneschi, F., Mignarri, A., Lucchiari, S., Ulzi, G., Comi, G. P., Rossi, A., & Dotti, M. T. (2017). Neuromuscular excitability changes produced by sustained voluntary contraction and response to mexiletine in myotonia congenita. *Neurophysiol Clin*, *47*(3), 247-252. https://doi.org/10.1016/j.neucli.2017.01.003

Gregory, J. E., & Proske, U. (1987). Responses of muscle receptors in the kitten to succinyl choline. *Exp Brain Res*, *66*(1), 167-174. https://doi.org/10.1007/BF00236212

Griffin, J. L. (1984). Infantile acid maltase deficiency. I. Muscle fiber destruction after lysosomal rupture. *Virchows Arch B Cell Pathol Incl Mol Pathol*, *45*(1), 23-36. https://doi.org/10.1007/BF02889849

Hers, H. G. (1963). alpha-Glucosidase deficiency in generalized glycogenstorage disease (Pompe's disease). *Biochem J*, *86*(1), 11-16. https://doi.org/10.1042/bj0860011

Hirschhorn, R., & Reuser, A. J.J. (2001). Glycogen storage disease Type II: acid α-glucosidase (acid maltase) deficiency. In Scriver C, Beaudet A, Sly W, Valle D (Ed.), *The metabolic and molecular bases of inherited disease* (pp. 3389–3420). McGraw-Hill.

Holzwarth, J., Minopoli, N., Pfrimmer, C., Smitka, M., Borrel, S., Kirschner, J., Muschol, N., Hartmann, H., Hennermann, J. B., Neubauer, B. A., Hobbiebrunken, E., Husain, R. A., & Hahn, A. (2022). Clinical and genetic aspects of juvenile onset Pompe disease. *Neuropediatrics*, *53*(1), 39-45. https://doi.org/10.1055/s-0041-1735250

Horlings, C. G., van Engelen, B. G., Allum, J. H., & Bloem, B. R. (2008). A weak balance: the contribution of muscle weakness to postural instability and falls. *Nat Clin Pract Neurol*, *4*(9), 504-515. https://doi.org/10.1038/ncpneuro0886

Hulliger, M. (1984). The mammalian muscle spindle and its central control. *Rev Physiol Biochem Pharmacol*, *101*, 1-110. https://doi.org/10.1007/BFb0027694

Hunt, C. C. (1952). Drug effects on mammalian muscle spindles. *Fed Proc*, *11*(1), 75-75.

Hunt, C. C. (1990). Mammalian muscle spindle: peripheral mechanisms. *Physiol Rev*, *70*(3), 643-663. https://doi.org/10.1152/physrev.1990.70.3.643

Hunt, C. C., & Kuffler, S. W. (1951a). Further study of efferent small-nerve fibers to mammalian muscle spindles; multiple spindle innervation and activity during contraction. *J Physiol*, *113*(2-3), 283-297. https://doi.org/10.1113/jphysiol.1951.sp004572

Hunt, C. C., & Kuffler, S. W. (1951b). Stretch receptor discharges during muscle contraction. *J Physiol*, *113*(2-3), 298-315. https://doi.org/10.1113/jphysiol.1951.sp004573

Hunter, J. M. (1995). New neuromuscular blocking drugs. *N Engl J Med*, *332*(25), 1691-1699. https://doi.org/10.1056/NEJM199506223322507

Kaya, D., Yertutanol, F.D.K, & Calik, M. (2018). Neurophysiology and Assessment of the Proprioception. In Kaya, D., Yosmaoglu, B., & Doral, M.N. (Eds.), *Proprioception in Orthopaedics, Sports Medicine and Rehabilitation* (pp. 3-11). Springer International Publishing. https://doi.org/10.1007/978-3-319-66640-2_1

Kheder, A., & Nair, K. P. (2012). Spasticity: pathophysiology, evaluation and management. *Pract Neurol*, *12*(5), 289-298. https://doi.org/10.1136/practneurol-2011-000155

Kim, M., Franke, V., Brandt, B., Lowenstein, E. D., Schowel, V., Spuler, S., Akalin, A., & Birchmeier, C. (2020). Single-nucleus transcriptomics reveals functional compartmentalization in syncytial skeletal muscle cells. *Nat Commun*, *11*(1), 6375. https://doi.org/10.1038/s41467-020-20064-9

Kishnani, P. S., & Beckemeyer, A. A. (2014). New therapeutic approaches for Pompe disease: enzyme replacement therapy and beyond. *Pediatr Endocrinol Rev*, *12 Suppl 1*, 114-124.

Kishnani, P. S., & Howell, R. R. (2004). Pompe disease in infants and children. *J Pediatr*, *144*(5 Suppl), S35-43. https://doi.org/10.1016/j.jpeds.2004.01.053

Kishnani, P. S., Steiner, R. D., Bali, D., Berger, K., Byrne, B. J., Case, L. E., Crowley, J. F., Downs, S., Howell, R. R., Kravitz, R. M., Mackey, J., Marsden, D., Martins, A. M., Millington, D. S., Nicolino, M., O'Grady, G., Patterson, M. C., Rapoport, D. M., Slonim, A., Spencer, C. T., Tifft, C. J., & Watson, M. S. (2006). Pompe disease diagnosis and management guideline. *Genet Med*, *8*(5), 267-288. https://doi.org/10.1097/01.gim.0000218152.87434.f3

Kissane, R. W. P., Charles, J. P., Banks, R. W., & Bates, K. T. (2022). Skeletal muscle function underpins muscle spindle abundance. *Proc Biol Sci*, *289*(1976), 20220622. https://doi.org/10.1098/rspb.2022.0622

Koeberl, D. D., Luo, X., Sun, B., McVie-Wylie, A., Dai, J., Li, S., Banugaria, S. G., Chen, Y. T., & Bali, D. S. (2011). Enhanced efficacy of enzyme replacement therapy in Pompe disease through mannose-6-phosphate receptor expression in skeletal muscle. *Mol Genet Metab*, *103*(2), 107-112. https://doi.org/10.1016/j.ymgme.2011.02.006

Kohler, L., Puertollano, R., & Raben, N. (2018). Pompe disease: From basic science to therapy. *Neurotherapeutics*, *15*(4), 928-942. https://doi.org/10.1007/s13311-018-0655-y

Kölliker, A. (1862). *Untersuchungen ueber die letzten Endigungen der Nerven: Ueber die Endigungen der Nerven in den Muskeln des Frosches. Erste Abhandlung*. Wilhelm Engelmann.

Krause, T., Gerbershagen, M. U., Fiege, M., Weisshorn, R., & Wappler, F. (2004). Dantrolene - a review of its pharmacology, therapeutic use and new developments. *Anaesthesia*, *59*(4), 364-373. https://doi.org/10.1111/j.1365-2044.2004.03658.x

Kröger, S. (2018). Proprioception 2.0: novel functions for muscle spindles. *Curr Opin Neurol*, *31*(5), 592-598. https://doi.org/10.1097/WCO.0000000000000590

Kröger, S., & Watkins, B. (2021). Muscle spindle function in healthy and diseased muscle. *Skelet Muscle*, *11*(1), 3. https://doi.org/10.1186/s13395-020-00258-x

Kroos, M., Hoogeveen-Westerveld, M., van der Ploeg, A., & Reuser, A. J. (2012). The genotype-phenotype correlation in Pompe disease. *Am J Med Genet C Semin Med Genet*, *160C*(1), 59-68. https://doi.org/10.1002/ajmg.c.31318

Kruidering-Hall, M., & Campbell, L. (2017). Skeletal muscle relaxants. In Katzung BG, Masters SB, Trevor AJ (Ed.), *Basic and Clinical Pharmacology* (Vol. 14e). McGraw Hill.

Kühne, W. (1863). Die Muskelspindeln. *Archiv f. pathol. Anat*, *28*(5-6), 528-538. https://doi.org/10.1007/bf01942820

Lamartine, S. Monteiro M., & Remiche, G. (2019). Late-onset Pompe disease associated with polyneuropathy. *Neuromuscul Disord*, *29*(12), 968-972. https://doi.org/10.1016/j.nmd.2019.08.016

Lim, J. A., Li, L., & Raben, N. (2014). Pompe disease: from pathophysiology to therapy and back again. *Front Aging Neurosci*, *6*, 177. https://doi.org/10.3389/fnagi.2014.00177

Lin, S. H., Cheng, Y. R., Banks, R. W., Min, M. Y., Bewick, G. S., & Chen, C. C. (2016). Evidence for the involvement of ASIC3 in sensory mechanotransduction in proprioceptors. *Nat Commun*, *7*, 11460. https://doi.org/10.1038/ncomms11460

Lionikas, A., Smith, C. J., Smith, T. L., Bunger, L., Banks, R. W., & Bewick, G. S. (2013). Analyses of muscle spindles in the soleus of six inbred mouse strains. *J Anat*, *223*(3), 289-296. https://doi.org/10.1111/joa.12076

Logigian, E. L., Martens, W. B., Moxley, R. T. th, McDermott, M. P., Dilek, N., Wiegner, A. W., Pearson, A. T., Barbieri, C. A., Annis, C. L., Thornton, C. A., & Moxley, R. T., 3rd. (2010). Mexiletine is an effective antimyotonia treatment in myotonic dystrophy type 1. *Neurology*, *74*(18), 1441-1448. https://doi.org/10.1212/WNL.0b013e3181dc1a3a

Looke, T. D., & Kluth, C. T. (2013). Effect of preoperative intravenous methocarbamol and intravenous acetaminophen on opioid use after primary total hip and knee replacement. *Orthopedics*, *36*(2 Suppl), 25-32. https://doi.org/10.3928/01477447-20130122-54

Macefield, V. G., & Knellwolf, T. P. (2018). Functional properties of human muscle spindles. *J Neurophysiol*, *120*(2), 452-467. https://doi.org/10.1152/jn.00071.2018

Manuel, M., & Zytnicki, D. (2019). Molecular and electrophysiological properties of mouse motoneuron and motor unit subtypes. *Curr Opin Physiol*, *8*, 23-29. https://doi.org/10.1016/j.cophys.2018.11.008

Marasco, P. D., & de Nooij, J. C. (2023). Proprioception: A new era set in motion by emerging genetic and bionic strategies? *Annu Rev Physiol*, *85*, 1-24. https://doi.org/10.1146/annurev-physiol-040122-081302

Martinac, B. (2022). 2021 Nobel Prize for mechanosensory transduction. *Biophys Rev*, *14*(1), 15-20. https://doi.org/10.1007/s12551-022-00935-9

Martiniuk, F., Bodkin, M., Tzall, S., & Hirschhorn, R. (1991). Isolation and partial characterization of the structural gene for human acid alpha glucosidase. *DNA Cell Biol*, *10*(4), 283-292. https://doi.org/10.1089/dna.1991.10.283

Martyn, J. A., Fagerlund, M. J., & Eriksson, L. I. (2009). Basic principles of neuromuscular transmission. *Anaesthesia*, *64 Suppl 1*, 1-9. https://doi.org/10.1111/j.1365-2044.2008.05865.x

Matthews, B. H. (1933). Nerve endings in mammalian muscle. *J Physiol*, *78*(1), 1-53. https://doi.org/10.1113/jphysiol.1933.sp002984

Matthews, P. B. (2015). Where Anatomy led, Physiology followed: a survey of our developing understanding of the muscle spindle, what it does and how it works. *J Anat*, *227*(2), 104-114. https://doi.org/10.1111/joa.12345

Matthews, Peter B. C. (1972). *Mammalian muscle receptors and their central actions*. Edward Arnold.

McCarthy, M. L., & Baum, C. R. (2017). Centrally Acting Muscle Relaxants. In Brent, J., Burkhart, K., Dargan, P., Hatten, B., Megarbane, B., Palmer, R., & White, J. (Eds.),

Critical Care Toxicology (pp. 1133-1141). Springer International Publishing. https://doi.org/10.1007/978-3-319-17900-1_72

McIntosh, P. T., Case, L. E., Chan, J. M., Austin, S. L., & Kishnani, P. (2015). Characterization of gait in late onset Pompe disease. *Mol Genet Metab*, *116*(3), 152-156. https://doi.org/10.1016/j.ymgme.2015.09.001

Meleger, A. L. (2006). Muscle relaxants and antispasticity agents. *Phys Med Rehabil Clin N Am*, *17*(2), 401-413. https://doi.org/10.1016/j.pmr.2005.12.005

Mense, S., & Masi, Alfonse T. (2010). Increased muscle tone as a cause of muscle pain. In Mense, S. & Gerwin, R.D. (Eds.), *Muscle Pain: Understanding the Mechanisms* (pp. 207-249). Springer https://doi.org/10.1007/978-3-540-85021-2_6

Mock, J. T., Knight, S. G., Vann, P. H., Wong, J. M., Davis, D. L., Forster, M. J., & Sumien, N. (2018). Gait analyses in mice: Effects of age and glutathione deficiency. *Aging Dis*, *9*(4), 634-646. https://doi.org/10.14336/AD.2017.0925

Monk, J. P., & Brogden, R. N. (1990). Mexiletine. A review of its pharmacodynamic and pharmacokinetic properties, and therapeutic use in the treatment of arrhythmias. *Drugs*, *40*(3), 374-411. https://doi.org/10.2165/00003495-199040030-00005

Nakagawa, H., Munakata, T., & Sunami, A. (2019). Mexiletine block of voltage-gated sodium channels: Isoform- and state-dependent drug-pore interactions. *Mol Pharmacol*, *95*(3), 236-244. https://doi.org/10.1124/mol.118.114025

Niemi, S. (2019). Muscle Relaxants and Antispasticity Drugs. In Abd-Elsayed, A. (Ed.), *Pain* (pp. 279-283). Springer International Publishing. https://doi.org/10.1007/978-3-319-99124-5_61

Niño, M. Y., In't Groen, S. L. M., de Faria, D. O. S., Hoogeveen-Westerveld, M., van den Hout, Hjmp, van der Ploeg, A. T., Bergsma, A. J., & Pijnappel, W. W. M. P. (2021). Broad variation in phenotypes for common GAA genotypes in Pompe disease. *Hum Mutat*, *42*(11), 1461-1472. https://doi.org/10.1002/humu.24272

Nyberg-Hansen, R. (1965). Anatomical demonstration of gamma motoneurons in the cat's spinal cord. *Exp Neurol*, *13*(1), 71-81. https://doi.org/10.1016/0014-4886(65)90006-3

Oliver, K. M., Florez-Paz, D. M., Badea, T. C., Mentis, G. Z., Menon, V., & de Nooij, J. C. (2021). Molecular correlates of muscle spindle and Golgi tendon organ afferents. *Nat Commun*, *12*(1), 1451. https://doi.org/10.1038/s41467-021-21880-3

Oskarsson, B., Moore, D., Mozaffar, T., Ravits, J., Wiedau-Pazos, M., Parziale, N., Joyce, N. C., Mandeville, R., Goyal, N., Cudkowicz, M. E., Weiss, M., Miller, R. G., & McDonald, C. M. (2018). Mexiletine for muscle cramps in amyotrophic lateral sclerosis: A randomized, double-blind crossover trial. *Muscle Nerve*, *58*(1), 42-48. https://doi.org/10.1002/mus.26117

Ovalle, W. K., & Dow, P. R. (1985). Morphological aspects of the muscle spindle capsule and its functional significance. In Boyd, I. A. & Gladden, M. H. (Eds.), *The Muscle Spindle* (1 ed., pp. 23-28). Palgrave Macmillan UK. https://doi.org/10.1007/978-1-349-07695-6_1

Ovalle, W. K., Jr. (1971). Fine structure of rat intrafusal muscle fibers. The polar region. *J Cell Biol*, *51*(1), 83-103. https://doi.org/10.1083/jcb.51.1.83

Ovalle, W. K., & Smith, R. S. (1972). Histochemical identification of three types of intrafusal muscle fibers in the cat and monkey based on the myosin ATPase reaction. *Can J Physiol Pharmacol*, *50*(3), 195-202. https://doi.org/10.1139/y72-030

Pandyan, A. D., Gregoric, M., Barnes, M. P., Wood, D., Van Wijck, F., Burridge, J., Hermens, H., & Johnson, G. R. (2005). Spasticity: clinical perceptions, neurological realities and meaningful measurement. *Disabil Rehabil*, *27*(1-2), 2-6. https://doi.org/10.1080/09638280400014576

Papaioannou, S., & Dimitriou, M. (2020). Muscle spindle function in muscular dystrophy: A potential target for therapeutic intervention. *J Physiol*, *598*(8), 1433-1434. https://doi.org/10.1113/JP279611

Park, H. W. (1958). Clinical results with methocarbamol, a new interneuronal blocking agent. *J Am Med Assoc*, *167*(2), 168-172. https://doi.org/10.1001/jama.1958.02990190022005

Pau, C. (2023). Muscle Relaxants. In Li, J., Jiang, W., & Vadivelu, N. (Eds.), *First Aid Perioperative Ultrasound* (1 ed., pp. 147-157). Springer International Publishing. https://doi.org/10.1007/978-3-031-21291-8_10

Peruzzo, P., Pavan, E., & Dardis, A. (2019). Molecular genetics of Pompe disease: a comprehensive overview. *Ann Transl Med*, *7*(13), 278. https://doi.org/10.21037/atm.2019.04.13

Pierrot-Deseilligny, E., & Mazevet, D. (2000). The monosynaptic reflex: a tool to investigate motor control in humans. Interest and limits. *Neurophysiol Clin*, *30*(2), 67-80. https://doi.org/10.1016/s0987-7053(00)00062-9

Pitzer, C., Kurpiers, B., & Eltokhi, A. (2021). Gait performance of adolescent mice assessed by the CatWalk XT depends on age, strain and sex and correlates with speed and body weight. *Sci Rep*, *11*(1), 21372. https://doi.org/10.1038/s41598-021-00625-8

Pompe, JC. (1932). Over idiopathische hypertrophie van het hart. *Ned Tijdschr Geneeskd*, *76*, 304-312.

Proske, U. (1997). The mammalian muscle spindle. *News Physiol Sci.*, *12*(1), 37-42. https://doi.org/10.1152/physiologyonline.1997.12.1.37

Proske, U., & Gandevia, S. C. (2012). The proprioceptive senses: their roles in signaling body shape, body position and movement, and muscle force. *Physiol Rev*, *92*(4), 1651-1697. https://doi.org/10.1152/physrev.00048.2011

Proske, U., Gregory, J. E., & Morgan, D. L. (1991). Where in the muscle spindle is the resting discharge generated? *Exp Physiol*, *76*(5), 777-785. https://doi.org/10.1113/expphysiol.1991.sp003543

Puthucheary, Z., Harridge, S., & Hart, N. (2010). Skeletal muscle dysfunction in critical care: wasting, weakness, and rehabilitation strategies. *Crit Care Med*, *38*(10 Suppl), S676-682. https://doi.org/10.1097/CCM.0b013e3181f2458d

Putschar, M. (1932). Uber angeborene Glykogenspeicher-Krankheit des herzens. *Beitr. Pathol. Anat. Allg. Pathol*, *90*, 222.

Raben, N., Nagaraju, K., Lee, E., Kessler, P., Byrne, B., Lee, L., LaMarca, M., King, C., Ward, J., Sauer, B., & Plotz, P. (1998). Targeted disruption of the acid alpha-glucosidase gene in mice causes an illness with critical features of both infantile and adult human glycogen storage disease type II. *J Biol Chem*, *273*(30), 19086-19092. https://doi.org/10.1074/jbc.273.30.19086

Raben, N., Nagaraju, K., Lee, E., & Plotz, P. (2000). Modulation of disease severity in mice with targeted disruption of the acid alpha-glucosidase gene. *Neuromuscul Disord*, *10*(4-5), 283-291. https://doi.org/10.1016/s0960-8966(99)00117-0

Raghavendra, T. (2002). Neuromuscular blocking drugs: discovery and development. *J R Soc Med*, *95*(7), 363-367. https://doi.org/10.1177/014107680209500713

Ravaglia, S., Danesino, C., Moglia, A., Costa, A., Cena, H., Maccarini, L., Carlucci, A., Pichiecchio, A., Bini, P., De Filippi, P., & Rossi, M. (2010). Changes in nutritional status and body composition during enzyme replacement therapy in adult-onset type II glycogenosis. *Eur J Neurol*, *17*(7), 957-962. https://doi.org/10.1111/j.1468-1331.2010.02959.x

Reuser, A. J. J., van der Ploeg, A. T., Chien, Y. H., Llerena, J., Jr., Abbott, M. A., Clemens, P. R., Kimonis, V. E., Leslie, N., Maruti, S. S., Sanson, B. J., Araujo, R., Periquet, M., Toscano, A., Kishnani, P. S., & On Behalf Of The Pompe Registry, Sites. (2019). GAA variants and phenotypes among 1,079 patients with Pompe disease: Data from the Pompe Registry. *Hum Mutat*, *40*(11), 2146-2164. https://doi.org/10.1002/humu.23878

Reuser, A.J.J., & Schoser, B. (2022). *Pompe Disease* (3 ed.). UNI-MED Verlag AG; ISBN: 978-3-8374-2433-1.

Richards, B. L., Whittle, S. L., van der Heijde, D. M., & Buchbinder, R. (2012). The efficacy and safety of muscle relaxants in inflammatory arthritis: a Cochrane systematic review. *J Rheumatol Suppl*, *90*, 34-39. https://doi.org/10.3899/jrheum.120340

Rodriguez Cruz, P. M., Cossins, J., Beeson, D., & Vincent, A. (2020). The neuromuscular junction in health and disease: Molecular mechanisms governing synaptic formation and homeostasis. *Front Mol Neurosci*, *13*, 610964. https://doi.org/10.3389/fnmol.2020.610964

Roszkowski, A. P. (1960). A pharmacological comparison of therapeutically useful centrally acting skeletal muscle relaxants. *J Pharmacol Exp Ther*, *129*, 75-81.

Ruffini, A. (1898). On the minute anatomy of the neuromuscular spindles of the cat, and on their physiological significance. *J Physiol*, *23*(3), 190-208 193. https://doi.org/10.1113/jphysiol.1898.sp000723

Sandow, A. (1952). Excitation-contraction coupling in muscular response. *Yale J Biol Med*, *25*(3), 176-201.

Sangari, S., Iglesias, C., El Mendili, M. M., Benali, H., Pradat, P. F., & Marchand-Pauvert, V. (2016). Impairment of sensory-motor integration at spinal level in amyotrophic lateral sclerosis. *Clin Neurophysiol*, *127*(4), 1968-1977. https://doi.org/10.1016/j.clinph.2016.01.014

Schaaf, G. J., van Gestel, T. J., Brusse, E., Verdijk, R. M., de Coo, I. F., van Doorn, P. A., van der Ploeg, A. T., & Pijnappel, W. W. M. P. . (2015). Lack of robust satellite cell activation and muscle regeneration during the progression of Pompe disease. *Acta Neuropathol Commun*, *3*(1), 65. https://doi.org/10.1186/s40478-015-0243-x

Schneider, I., Zierz, S., Schulze, S., Delank, K.S., Laudner, K.G., Brill, R., & Schwesig, R. (2020). Characterization of gait and postural regulation in late-onset Pompe disease. *Appl Sci*, *10*(19), 7001. https://doi.org/10.3390/app10197001

Schoser, B., & Laforet, P. (2022). Therapeutic thoroughfares for adults living with Pompe disease. *Curr Opin Neurol*, *35*(5), 645-650. https://doi.org/10.1097/WCO.0000000000001092

Schüller, A., Wenninger, S., Strigl-Pill, N., & Schoser, B. (2012). Toward deconstructing the phenotype of late-onset Pompe disease. *Am J Med Genet C Semin Med Genet*, *160C*(1), 80-88. https://doi.org/10.1002/ajmg.c.31322

See, S., & Ginzburg, R. (2008a). Choosing a skeletal muscle relaxant. *Am Fam Physician*, *78*(3), 365-370.

See, S., & Ginzburg, R. (2008b). Skeletal muscle relaxants. *Pharmacotherapy*, *28*(2), 207-213. https://doi.org/10.1592/phco.28.2.207

Sherrington, C. S. (1894). On the anatomical constitution of nerves of skeletal muscles; with remarks on recurrent fibres in the ventral spinal nerve-root. *J Physiol*, *17*(3-4), 210 212-258. https://doi.org/10.1113/jphysiol.1894.sp000528

Sherrington, C. S. (1907). On the proprio-ceptive System, especially in Its reflex aspect. *Brain*, *29*(4), 467-482. https://doi.org/10.1093/brain/29.4.467

Simon, A., Shenton, F., Hunter, I., Banks, R. W., & Bewick, G. S. (2010). Amiloride-sensitive channels are a major contributor to mechanotransduction in mammalian muscle spindles. *J Physiol*, *588*(Pt 1), 171-185. https://doi.org/10.1113/jphysiol.2009.182683

Simons, G. D., & Mense, S. (1998). Understanding and measurement of muscle tone as related to clinical muscle pain. *Pain*, *75*(1), 1-17. https://doi.org/10.1016/S0304-3959(97)00102-4

Smith, C. M. (1963). Neuromuscular pharmacology: Drugs and muscle spindles. *Annu Rev Pharmacol*, *3*(1), 223-242. https://doi.org/10.1146/annurev.pa.03.040163.001255

Soliman, O. I., van der Beek, N. A., van Doorn, P. A., Vletter, W. B., Nemes, A., Van Dalen, B. M., ten Cate, F. J., van der Ploeg, A. T., & Geleijnse, M. L. (2008). Cardiac involvement

in adults with Pompe disease. *J Intern Med*, *264*(4), 333-339. https://doi.org/10.1111/j.1365-2796.2008.01966.x

Sonner, M. J., Walters, M. C., & Ladle, D. R. (2017). Analysis of proprioceptive sensory innervation of the mouse soleus: A whole-mount muscle approach. *PLoS One*, *12*(1), e0170751. https://doi.org/10.1371/journal.pone.0170751

Soreq, H., & Seidman, S. (2001). Acetylcholinesterase--new roles for an old actor. *Nat Rev Neurosci*, *2*(4), 294-302. https://doi.org/10.1038/35067589

Statland, J. M., Bundy, B. N., Wang, Y., Rayan, D. R., Trivedi, J. R., Sansone, V. A., Salajegheh, M. K., Venance, S. L., Ciafaloni, E., Matthews, E., Meola, G., Herbelin, L., Griggs, R. C., Barohn, R. J., Hanna, M. G., & Consortium, for the Consortium for Clinical Investigation of Neurologic Channelopathies. (2012). Mexiletine for symptoms and signs of myotonia in nondystrophic myotonia: a randomized controlled trial. *JAMA*, *308*(13), 1357-1365. https://doi.org/10.1001/jama.2012.12607

Strothotte, S., Strigl-Pill, N., Grunert, B., Kornblum, C., Eger, K., Wessig, C., Deschauer, M., Breunig, F., Glocker, F. X., Vielhaber, S., Brejova, A., Hilz, M., Reiners, K., Muller-Felber, W., Mengel, E., Spranger, M., & Schoser, B. (2010). Enzyme replacement therapy with alglucosidase alfa in 44 patients with late-onset glycogen storage disease type 2: 12-month results of an observational clinical trial. *J Neurol*, *257*(1), 91-97. https://doi.org/10.1007/s00415-009-5275-3

Stunnenberg, B. C., Raaphorst, J., Groenewoud, H. M., Statland, J. M., Griggs, R. C., Woertman, W., Stegeman, D. F., Timmermans, J., Trivedi, J., Matthews, E., Saris, C. G. J., Schouwenberg, B. J., Drost, G., van Engelen, B. G. M., & van der Wilt, G. J. (2018). Effect of mexiletine on muscle stiffness in patients with nondystrophic myotonia evaluated using aggregated N-of-1 trials. *JAMA*, *320*(22), 2344-2353. https://doi.org/10.1001/jama.2018.18020

Suetterlin, K. J., Bugiardini, E., Kaski, J. P., Morrow, J. M., Matthews, E., Hanna, M. G., & Fialho, D. (2015). Long-term safety and efficacy of mexiletine for patients with skeletal muscle channelopathies. *JAMA Neurol*, *72*(12), 1531-1533. https://doi.org/10.1001/jamaneurol.2015.2338

Suslak, T. J., Watson, S., Thompson, K. J., Shenton, F. C., Bewick, G. S., Armstrong, J. D., & Jarman, A. P. (2015). Piezo is essential for amiloride-sensitive stretch-activated mechanotransduction in larval drosophila dorsal bipolar dendritic sensory neurons. *PLoS One*, *10*(7), e0130969. https://doi.org/10.1371/journal.pone.0130969

Swash, M., & Fox, K. P. (1975). The pathology of the muscle spindle in myasthenia gravis. *J Neurol Sci*, *26*(1), 39-47. https://doi.org/10.1016/0022-510x(75)90112-4

Swash, M., & Fox, K. P. (1976). The pathology of the muscle spindle in Duchenne muscular dystrophy. *J Neurol Sci*, *29*(1), 17-32. https://doi.org/10.1016/0022-510x(76)90077-0

Takeoka, A., & Arber, S. (2019). Functional local proprioceptive feedback circuits initiate and maintain locomotor recovery after spinal cord injury. *Cell Rep*, *27*(1), 71-85 e73. https://doi.org/10.1016/j.celrep.2019.03.010

Takeoka, A., Vollenweider, I., Courtine, G., & Arber, S. (2014). Muscle spindle feedback directs locomotor recovery and circuit reorganization after spinal cord injury. *Cell*, *159*(7), 1626-1639. https://doi.org/10.1016/j.cell.2014.11.019

Tanabe, T., Beam, K. G., Adams, B. A., Niidome, T., & Numa, S. (1990). Regions of the skeletal muscle dihydropyridine receptor critical for excitation-contraction coupling. *Nature*, *346*(6284), 567-569. https://doi.org/10.1038/346567a0

Taylor, A., Rodgers, J. F., Fowle, A. J., & Durbaba, R. (1992). The effect of succinylcholine on cat gastrocnemius muscle spindle afferents of different types. *J Physiol*, *456*, 629-644. https://doi.org/10.1113/jphysiol.1992.sp019357

Than, K., Kim, E., Navarro, C., Chu, S., Klier, N., Occiano, A., Ortiz, S., Salazar, A., Valdespino, S. R., Villegas, N. K., & Wilkinson, K. A. (2021). Vesicle-released glutamate is

necessary to maintain muscle spindle afferent excitability but not dynamic sensitivity in adult mice. *J Physiol*, *599*(11), 2953-2967. https://doi.org/10.1113/JP281182

Tintignac, L. A., Brenner, H. R., & Ruegg, M. A. (2015). Mechanisms regulating neuromuscular junction development and function and causes of muscle wasting. *Physiol Rev*, *95*(3), 809-852. https://doi.org/10.1152/physrev.00033.2014

Toscano, A., Rodolico, C., & Musumeci, O. (2019). Multisystem late onset Pompe disease (LOPD): an update on clinical aspects. *Ann Transl Med*, *7*(13), 284. https://doi.org/10.21037/atm.2019.07.24

Toscano, A., & Schoser, B. (2013). Enzyme replacement therapy in late-onset Pompe disease: a systematic literature review. *J Neurol*, *260*(4), 951-959. https://doi.org/10.1007/s00415-012-6636-x

Truitt, E. B., Jr., & Little, J. M. (1958). A pharmacologic comparison of methocarbamol (AHR-85), the monocarbamate of 3-(o-methoxyphenoxy)-1,2-propanediol with chemically related interneuronal depressant drugs. *J Pharmacol Exp Ther*, *122*(2), 239-246.

Tuthill, J. C., & Azim, E. (2018). Proprioception. *Curr Biol*, *28*(5), R194-R203. https://doi.org/10.1016/j.cub.2018.01.064

Umapathysivam, K., Hopwood, J. J., & Meikle, P. J. (2005). Correlation of acid alpha-glucosidase and glycogen content in skin fibroblasts with age of onset in Pompe disease. *Clin Chim Acta*, *361*(1-2), 191-198. https://doi.org/10.1016/j.cccn.2005.05.025

Valle, M. S., Casabona, A., Fiumara, A., Castiglione, D., Sorge, G., & Cioni, M. (2016). Quantitative analysis of upright standing in adults with late-onset Pompe disease. *Sci Rep*, *6*, 37040. https://doi.org/10.1038/srep37040

van Capelle, C. I., van der Beek, N. A., Hagemans, M. L., Arts, W. F., Hop, W. C., Lee, P., Jaeken, J., Frohn-Mulder, I. M., Merkus, P. J., Corzo, D., Puga, A. C., Reuser, A. J., & van der Ploeg, A. T. (2010). Effect of enzyme therapy in juvenile patients with Pompe disease: a three-year open-label study. *Neuromuscul Disord*, *20*(12), 775-782. https://doi.org/10.1016/j.nmd.2010.07.277

van Capelle, C. I., van der Meijden, J. C., van den Hout, J. M., Jaeken, J., Baethmann, M., Voit, T., Kroos, M. A., Derks, T. G., Rubio-Gozalbo, M. E., Willemsen, M. A., Lachmann, R. H., Mengel, E., Michelakakis, H., de Jongste, J. C., Reuser, A. J., & van der Ploeg, A. T. (2016). Childhood Pompe disease: clinical spectrum and genotype in 31 patients. *Orphanet J Rare Dis*, *11*(1), 65. https://doi.org/10.1186/s13023-016-0442-y

Van der Beek, N. A., Hagemans, M. L., Reuser, A. J., Hop, W. C., Van der Ploeg, A. T., Van Doorn, P. A., & Wokke, J. H. (2009). Rate of disease progression during long-term follow-up of patients with late-onset Pompe disease. *Neuromuscul Disord*, *19*(2), 113-117. https://doi.org/10.1016/j.nmd.2008.11.007

van der Ploeg, A. T., & Reuser, A. J. (2008). Pompe's disease. *Lancet*, *372*(9646), 1342-1353. https://doi.org/10.1016/S0140-6736(08)61555-X

Vaughan, S. K., Kemp, Z., Hatzipetros, T., Vieira, F., & Valdez, G. (2015). Degeneration of proprioceptive sensory nerve endings in mice harboring amyotrophic lateral sclerosis-causing mutations. *J Comp Neurol*, *523*(17), 2477-2494. https://doi.org/10.1002/cne.23848

Watkins, B., Schultheiss, J., Rafuna, A., Hintze, S., Meinke, P., Schoser, B., & Kröger, S. (2023). Degeneration of muscle spindles in a murine model of Pompe disease. *Sci Rep*, *13*(1), 6555. https://doi.org/10.1038/s41598-023-33543-y

Watkins, B., Schuster, H. M., Gerwin, L., Schoser, B., & Kröger, S. (2022). The effect of methocarbamol and mexiletine on murine muscle spindle function. *Muscle Nerve*, *66*(1), 96-105. https://doi.org/10.1002/mus.27546

Weiss, M., & Weiss, S. (1962). Methocarbamol in low-back pain: clinical study. *J Am Osteopath Assoc*, *62*, 142-144.

Wilkinson, K. A. (2022). Molecular determinants of mechanosensation in the muscle spindle. *Curr Opin Neurobiol*, *74*, 102542. https://doi.org/10.1016/j.conb.2022.102542

Witenko, C., Moorman-Li, R., Motycka, C., Duane, K., Hincapie-Castillo, J., Leonard, P., & Valaer, C. (2014). Considerations for the appropriate use of skeletal muscle relaxants for the management of acute low back pain. *Pharm Ther*, *39*(6), 427-435.

Woo, S. H., Lukacs, V., de Nooij, J. C., Zaytseva, D., Criddle, C. R., Francisco, A., Jessell, T. M., Wilkinson, K. A., & Patapoutian, A. (2015). Piezo2 is the principal mechanotransduction channel for proprioception. *Nat Neurosci*, *18*(12), 1756-1762. https://doi.org/10.1038/nn.4162

Wu, H., Petitpre, C., Fontanet, P., Sharma, A., Bellardita, C., Quadros, R. M., Jannig, P. R., Wang, Y., Heimel, J. A., Cheung, K. K. Y., Wanderoy, S., Xuan, Y., Meletis, K., Ruas, J., Gurumurthy, C. B., Kiehn, O., Hadjab, S., & Lallemend, F. (2021). Distinct subtypes of proprioceptive dorsal root ganglion neurons regulate adaptive proprioception in mice. *Nat Commun*, *12*(1), 1026. https://doi.org/10.1038/s41467-021-21173-9

Wu, S. X., Koshimizu, Y., Feng, Y. P., Okamoto, K., Fujiyama, F., Hioki, H., Li, Y. Q., Kaneko, T., & Mizuno, N. (2004). Vesicular glutamate transporter immunoreactivity in the central and peripheral endings of muscle-spindle afferents. *Brain Res*, *1011*(2), 247-251. https://doi.org/10.1016/j.brainres.2004.03.047

Yamamoto, T., Morgan, D. L., Gregory, J. E., & Proske, U. (1994). Blockade of intrafusal neuromuscular junctions of cat muscle spindles with gallamine. *Exp Physiol*, *79*(3), 365-376. https://doi.org/10.1113/expphysiol.1994.sp003771

Yong, M. S., & Lee, Y. S. (2017). Effect of ankle proprioceptive exercise on static and dynamic balance in normal adults. *J Phys Ther Sci*, *29*(2), 242-244. https://doi.org/10.1589/jpts.29.242

Yong, Y., Hunter-Chang, S., Stepanova, E., & Deppmann, C. (2021). Axonal spheroids in neurodegeneration. *Mol Cell Neurosci*, *117*, 103679. https://doi.org/10.1016/j.mcn.2021.103679

Zhang, Y., Otto, P., Qin, L., Eiber, N., Hashemolhosseini, S., Kröger, S., & Brinkmeier, H. (2021). Methocarbamol blocks muscular Na(v) 1.4 channels and decreases isometric force of mouse muscles. *Muscle Nerve*, *63*(1), 141-150. https://doi.org/10.1002/mus.27087

Zhang, Y., Wesolowski, M., Karakatsani, A., Witzemann, V., & Kröger, S. (2014). Formation of cholinergic synapse-like specializations at developing murine muscle spindles. *Dev Biol*, *393*(2), 227-235. https://doi.org/10.1016/j.ydbio.2014.07.011

Appendix A: Paper III

Bornstein, B., **Watkins, B**., Passini, F. S., Blecher, R., Assaraf, E., Sui, X. M., Brumfeld, V., Tsoory, M., Kröger, S., & Zelzer, E. (2023). The mechanosensitive ion channel ASIC2 mediates both proprioceptive sensing and spinal alignment. *Exp Physiol*, *Epub ahead of print*, 1-13. https://doi.org/10.1113/EP090776

Received: 22 November 2022 | Accepted: 20 February 2023

DOI: 10.1113/EP090776

Experimental Physiology WILEY

RESEARCH ARTICLE

The mechanosensitive ion channel ASIC2 mediates both proprioceptive sensing and spinal alignment

Bavat Bornstein[1] | **Bridgette Watkins**[2] | **Fabian S. Passini**[1] | **Ronen Blecher**[3] | **Eran Assaraf**[4] | **Xiao Meng Sui**[5] | **Vlad Brumfeld**[5] | **Michael Tsoory**[6] | **Stephan Kröger**[2] | **Elazar Zelzer**[1]

[1]Department of Molecular Genetics, Weizmann Institute of Science, Rehovot, Israel

[2]Department of Physiological Genomics, Biomedical Center, Ludwig-Maximilians-University, Planegg-Martinsried, Germany

[3]Orthopedic Department, Assuta Ashdod University Hospital, Ashdod, Israel, affiliated to Ben Gurion University of the Negev, Beer Sheba, Israel

[4]Department of Orthopedic Surgery, Shamir Medical Center, Assaf HaRofeh Campus, Zeffifin, Israel, affiliated to Sackler Faculty of Medicine, Tel Aviv University, Tel Aviv, Israel

[5]Department of Chemical Research Support, Weizmann Institute of Science, Rehovot, Israel

[6]Department of Veterinary Resources, Weizmann Institute of Science, Rehovot, Israel

Correspondence
Bavat Bornstein and Elazar Zelzer, Department of Molecular Genetics, Weizmann Institute of Science, PO Box 26, Rehovot 7610001, Israel.
Email: bavat.bornstein@weizmann.ac.il; eli.zelzer@weizmann.ac.il

Funding information
The David and Fella Shapell Family center for Genetic Disorders Research, Grant/Award Number: Elazar Zelzer; Julie and Eric Borman Family Research Funds; Nella and Leon Benoziyo Center for Neurological Diseases, Weizmann Institute of Science; The Yves Cotrel Foundation

This article was presented at the 'Mechanotransduction, Muscle Spindles and Proprioception', which took place at Ludwig-Maximilians Universitat, Munich, 25–28 July 2022.

Handling Editor: Ronan Berg

Abstract

By translating mechanical forces into molecular signals, proprioceptive neurons provide the CNS with information on muscle length and tension, which is necessary to control posture and movement. However, the identities of the molecular players that mediate proprioceptive sensing are largely unknown. Here, we confirm the expression of the mechanosensitive ion channel ASIC2 in proprioceptive sensory neurons. By combining in vivo proprioception-related functional tests with ex vivo electrophysiological analyses of muscle spindles, we showed that mice lacking *Asic2* display impairments in muscle spindle responses to stretch and motor coordination tasks. Finally, analysis of skeletons of *Asic2* loss-of-function mice revealed a specific effect on spinal alignment. Overall, we identify ASIC2 as a key component in proprioceptive sensing and a regulator of spine alignment.

KEYWORDS
ASICs, ion channel, mechanosensitivity, muscle spindle, proprioception, scoliosis

1 | INTRODUCTION

Proprioception is the sense of self-movement and body position and, thus, it is essential for controlling coordinated movements and posture (Sherrington, 1907). In mammals, proprioception is initiated by mechanically sensitive sensory neurons whose cell bodies are located in the dorsal root ganglia (DRGs). These neurons project peripherally to muscles and tendons, ending in two types of sensory organs: muscle spindles (MSs), which lie in the muscle belly; and Golgi tendon organs (GTOs), which are located at the muscle–tendon interface.

Proprioceptive neurons terminate in different locations in the CNS. They project into the ventral horn of the spinal cord onto α-motor neurons or interneurons to influence premotor circuits (Chen et al., 2003; Delhaye et al., 2018). Additionally, they ascend via the dorsal column tract to synapse onto neurons in the dorsal column nuclei of the brainstem to relay information on the tensions and forces acting on the muscles (Delhaye et al., 2018; Kiehn, 2016; Marasco & de Nooij, 2022).

Recently, the proprioceptive system has also been shown to regulate skeletal development and function, specifically spinal alignment, bone fracture repair and joint morphogenesis (Assaraf et al., 2020; Blecher, Krief, Galili, Assaraf, et al., 2017; Blecher, Krief, Galili, Biton, et al., 2017; Bornstein et al., 2021). The importance of the proprioceptive system for controlling coordination and posture, in addition to its involvement in the aetiology of skeletal pathologies, emphasize the need to understand the molecular mechanisms underlying its function. However, the available information about these mechanisms is limited. Only in recent years have transcriptional analyses of DRG proprioceptive neurons (Oliver et al., 2021; Wu et al., 2021) and of MSs (Bornstein et al., 2023; Kim et al., 2020) provided the opportunity to find new molecules that mediate proprioceptive sensing and regulatory functions.

To date, two mechanosensitive ion channels have been implicated in mechanotransduction of proprioceptive sensory neurons (Wilkinson, 2022). *Piezo2*, which encodes a calcium-permeable ion channel, was shown to be expressed in sensory endings in MSs and GTOs (Woo et al., 2015). Its ablation resulted in loss of mechanotransduction in the proprioceptive neurons, in addition to scoliosis and hip dysplasia (Assaraf et al., 2020; Chesler AT et al., 2016; Woo et al., 2015). The other channel is acid-sensing ion channel 3 (ASIC3), a member of the ASIC family of proton-gated cation channels found in the central and peripheral nervous systems. *Asic3* loss of function in mice impaired mechanotransduction in proprioceptive neurons and led to deficits in motor tasks (Lin et al., 2016). Upon activation, the ASIC complex, composed of three homotrimeric and/or heterotrimeric subunits, induces neuronal depolarization via Na^+ ion influx. Although ASICs were originally shown to mediate acid sensing, they can also act as mechanically activated ion channels and, thereby, transform mechanical force into an electrical signal (Cheng et al., 2018). In mice, six ASIC isoforms are encoded by four genes. However, only ASIC1, ASIC2 and ASIC3 were shown to be expressed in DRG proprioceptive neurons (Lin et al., 2016; Wu et al., 2021), and only ASIC2 and ASIC3 were shown to be expressed in proprioceptive neuron terminals (Lin et al., 2016; Simon et al., 2010). Interestingly, amiloride, which antagonizes epithelial sodium channels such as ASICs, was shown to inhibit muscle spindle afferent discharge (Simon et al., 2010), raising the question of whether other ASICs besides ASIC3 contribute to proprioceptive mechanosensing.

To identify molecules that are important for proprioceptive sensing, we recently generated comprehensive transcriptomic and proteomic datasets of the entire MS (Bornstein et al., 2023). Here, we studied the involvement of *Asic2*, which was the most differentially expressed mechanosensitive ion channel in our transcriptomic data, in proprioceptive function and skeletal regulation. We detected ASIC2 protein expression in proprioceptive neuron endings of both MSs and GTOs. Moreover, *Asic2* knockout (KO) in mice showed that ASIC2 mediates proprioceptive sensing, coordinated movement and spinal alignment. These findings implicate ASIC2 in proprioceptive mechanotransduction and skeletal alignment and reinforce the importance of regulatory interactions between the proprioceptive system and the skeleton.

New Findings

- **What is the central question of this study?**
  Proprioception is initiated by mechanosensitive neurons. However, the identities of the molecular players that mediate proprioceptive sensing are largely unknown. Here, we aimed to identify potential mechanosensitive ion channels that mediate proprioceptive signalling.
- **What is the main finding and its importance?**
  We identify the mechanosensitive ion channel ASIC2 as a key component in proprioceptive sensing and a regulator of spine alignment.

2 | METHODS

2.1 | Ethical approval

All experiments involving mice were approved by the institutional animal care and use committee of the Weizmann Institute (protocol number #02190222-2). Electrophysiology experiments were performed according to Directive 2010/63/EU of the European Parliament on the protection of animals used for scientific purposes and were approved by the local authorities of the State of Bavaria, Germany (Az.: ROB-55.2-2532.Vet 02-17-82). In all cases, experimental protocols were designed to minimize the number of animals used.

2.2 | Mouse lines

Mice were housed in a temperature- and humidity-controlled vivarium on a 12 h–12 h light–dark cycle with free access to food and water.

The following strains were used: *Asic2* KO (*Asic2*^{tm1Wsh}/J; The Jackson Laboratory; #013126), *Thy1-YFP16* (The Jackson Laboratory; #003709), *Pvalb*^{Cre} (*Pvalb*$^{tm1(cre)Arbr}$/J; The Jackson Laboratory; #017320) and *Rosa26*^{tdTomato} (The Jackson Laboratory, #007909). In all experiments, *Asic2* KO mice are *Asic2*$^{-/-}$ and control mice are littermates that are either *Asic2*$^{+/+}$ or *Asic2*$^{-/+}$. Mice were genotyped by PCR of genomic DNA from ear clips. Primer sequences and amplicon sizes are listed in Table 1.

TABLE 1 Primer sequences and amplicon sizes used for PCR.

Reaction	Amplicon (bp)	Sequence
YFP (GFP)	300	Forward: GACGGCAACATCCTGGGGCACAAG Reverse: CGGCGGCGGTCACGAACTCC
Asic2 knockout	Wild-type: 365 Mutant: 300	Wild-type forward: GAAGAGGAAGGGAGCCATGATGAG Mutant forward: TGGATGTGGAATGTGTGCGA Common reverse: AGTCCTGCACGGTGGGAGCTTCTA
Cre	800	Forward: CCTGGAAAATGCTTCTGTCCGTTTGCC Reverse: GAGTTGATAGCTGGCTGGTGGCAGATG
tdTomato (wild-type)	297	Forward: AAGGGAGCTGCAGTGGAGTA Reverse: CCGAAAATCTGTGGGAAGTC
tdTomato (floxed allele)	196	Forward: GGCATTAAAGCAGCGTATCC Reverse: CTGTTCCTGTACGGCATGG

TABLE 2 Antibodies used for immunofluorescence.

Target	Species	Company	Catalogue number	Dilution
GFP	Goat	Abcam	Ab6658	1:100
ASIC2	Rabbit	LSBio	LS-B156	1:100
GLUT1	Rabbit	Abcam	ab195020	1:400
Rabbit	Cy5 conjugated donkey	Jackson Immunoresearch Laboratories	711-175-152	1:200
Biotin	Native streptavidin protein (DyLight 488)	Abcam	b134349	1:200

2.3 | Immunofluorescence

For whole-mount immunofluorescence, muscles were subjected to an optical tissue clearing protocol as described previously (Bornstein et al., 2023). Briefly, postfixed deep masseter muscle or extensor digitorum longus (EDL) muscle was dissected, washed in PBS and placed in A4P0 hydrogel {4% acrylamide and 0.25% 2′-azobis[2-(2-imidazolin-2-yl)propane]dihydrochloride in PBS}, shaking at 4°C overnight. Then the hydrogel was allowed to polymerize for 3 h at 37°C. Next, samples were washed in PBS, transferred to 5 mL of 10% SDS (pH 8.0) with 0.01% sodium azide, and shaken gently at 37°C for 3 days to remove lipid.

Cleared samples were washed with wash buffer (PBS containing 0.5% Tween-20) for 20 min, permeabilized with PBST (PBS containing 0.3% Triton X-100) for 20 min and washed again with wash buffer for 20 min, all at room temperature with shaking. Then the samples were blocked with 6% bovine serum albumin dissolved in PBS containing 0.3% Triton X-100 and 0.5% Tween-20 for 2 days at 37°C, with gentle shaking. Samples were subjected to primary antibodies (Table 2) for 5 days at 37°C, with gentle shaking, washed with wash buffer for 2 days at room temperature with frequent solution changes, incubated with secondary antibodies and 4′,6-diamidino-2-phenylindole (DAPI) for 5 days at 37°C, with shaking, and washed again with wash buffer for 2 days at room temperature, with frequent solution changes. For clearing and mounting, the samples were incubated in 500 μL of refractive index matching solution (RIMS; 74% w/v Histodenz in 0.02 M phosphate buffer) for 1 day at room temperature, with shaking. Samples were mounted in RIMS and imaged using a Zeiss LSM800 or LSM900 confocal microscope. Images were processed with ImageJ v.1.51 (US National Institutes of Health).

For DRG immunofluorescence, DRGs were isolated as described previously (Sleigh et al., 2016), fixed for 3 h in 4% paraformaldehyde (PFA)/PBS at 4°C, transferred to 30% sucrose overnight, then embedded in optimal cutting temperature (OCT) compound and sectioned by cryostat at a thickness of 10 μm. For ASIC2 staining, cryosections were dried and post-fixed for 10 min in 4% PFA, permeabilized with PBS with 0.3% Triton X-100, washed with PBS with 0.1% Tween-20 (PBST) for 5 min and blocked with 7% goat/horse serum and 1% bovine serum albumin dissolved in PBST. Then sections were incubated with primary antibody (Table 2) at 4°C overnight. The next day, sections were washed three times in PBST and incubated for 1 h with secondary antibody-conjugated fluorescent antibody, washed three times in PBST, counterstained with DAPI, mounted with Immu-Mount aqueous-based mounting medium (Thermo Fisher Scientific) and imaged using a Zeiss LSM800 or LSM900 confocal microscope. Images were processed with ImageJ v.1.51 (US National Institutes of Health).

2.4 | Behavioural procedures

Behavioural tests were performed on adult males (>90 days old) during the dark phase of the circadian cycle after ≥1 h of habituation to the test room, unless stated otherwise.

2.4.1 | Beam walking

Males were first trained to walk on a beam (50 cm long, 35 mm wide) suspended 30 cm above the working surface, in order to return to their home cage. Then the mice were tested by walking on a narrow beam

(6 mm wide) to return to their home cages. Five full-length walks with no stops were counted. Test sessions were video recorded using an overhead camera. The number of slips and travel time during the walks were measured for *Asic2* KO mice and their littermate controls.

2.4.2 | Home cage locomotion

Locomotion was assessed using the InfraMot system (TSE Systems). Mice were housed individually for 72 h, during which the first 24 h were considered habituation to the individual housing conditions. Measurements of locomotion was collected in 30 min intervals. General locomotion was measured as the mean of two light and two dark cycles during the last 48 h.

2.4.3 | Treadmill

The treadmill apparatus (Panlab; Harvard Apparatus; LE8710M) consisted of a rolling belt with adjustable speed and acceleration, with a grid situated at the end of the rolling belt to provide an electrical shock. Mice were tested on a 2-day protocol consisting of a habituation day, followed by a test day. During the habituation day, mice were placed on the treadmill for 10 min with the shocker operating at 0.2 mA while the treadmill belt was not moving. During the test day, mice were subjected to 15 min treadmill acceleration according to a crescendo protocol. Mice started with 10 min of gradual speed increments from 0.1 to 0.18 m/h, followed by 5 min of speed increment from 0.18 to 0.19 m/h. The total distance the mice travelled in 15 min was measured.

2.4.4 | CatWalk

Gait was assessed using the CatWalk XT 10.6 automated gait analysis system (Noldus Information Technology, Wageningen, The Netherlands). For each mouse, five runs were recorded. A successive run was determined by a duration range of 2–10 s and maximum variation of 60%. After the identification and labelling of each footprint, gait data were generated. The following parameters were analysed for each mouse: mean speed, phase dispersion, step sequence, stride length, print position and support.

2.5 | Electrophysiology

2.5.1 | Animals

Experiments were performed on muscles from nine C57BL/6J mice, including three heterozygous and four homozygous *Asic2* KO and two wild-type (WT) mice of both sexes. Age ranged between 10 and 15 weeks and weight between 22 and 28 g.

2.5.2 | Muscle preparation and electrophysiology

Afferent sensory neuron responses to stretch were assayed using an isolated muscle–nerve preparation previously described (Franco et al., 2014; Gerwin et al., 2019, 2020; Wilkinson et al., 2012). Twenty-four MSs from control animals (heterozygous and WT mice) and 21 muscle spindles from homozygous *Asic2* KO mice were recorded. Mice were killed by cervical dislocation to avoid interference of anaesthetic agent with the sensory afferent recordings. The EDL muscle together with the deep peroneal branch of the sciatic nerve were dissected and placed in a tissue bath containing oxygenated artificial cerebrospinal fluid (Wilkinson et al., 2012). The tendons were sutured at one end to a fixed post and at the other end to a lever arm connected to a dual force and length controller (300C-LR; Aurora Scientific, Dublin, Ireland), allowing the simultaneous recording of muscle tension and muscle length. Sensory activity was sampled using a suction electrode (tip diameter, 50–70 μm) connected to an extracellular amplifier (model 1800, A&M Systems, Elkhart, USA). The standard solution for muscle spindle afferent recordings was oxygenated artificial cerebrospinal fluid containing (mM): 128 NaCl, 1.9 KCl, 2.4 $CaCl_2$, 1.3 $MgSO_4$, 1.2 KH_2PO_4, 26 $NaHCO_3$ and 10 D-glucose.

A signal was classified as being from a putative muscle spindle afferent if it displayed a characteristic instantaneous frequency response to stretch, in addition to a pause during twitch contraction (Franco et al., 2014; Gerwin et al., 2019; Wilkinson et al., 2012). Baseline muscle length (L_0) was defined as the minimal length at which maximal twitch contractile force was generated. For each recording, triplicates of 10 s resting discharge followed by ramp-and-hold stretches (L_0 plus 2.5, 5.0 and 7.5% of L_0; ramp speed, 40% L_0/s; ramp phase duration, 0.1 s; hold phase, 3.8 s; stretch duration, 4 s with 45 s intervals between each stretch; Gerwin et al., 2020) were recorded and averaged.

From these recordings, the mean resting discharge (RD; mean baseline firing rate) and the dynamic peak (DP; highest firing rate during ramp minus baseline firing rate), the dynamic index (DI; dynamic peak minus firing rate 0.45–0.55 s into stretch minus baseline firing rate), the initial static time (IST; dynamic peak minus firing rate 0.45–0.55 s into stretch minus baseline firing rate) and the final static time (FST; firing rate 3.25–3.75 s into stretch minus baseline firing rate) were determined (Gerwin et al., 2019; Kröger & Watkins, 2021).

For data analysis, action potentials from individual sensory neurons were identified by spike shape and spike discriminator using the Spike Histogram feature of LabChart (v.8.1.5; AD Instruments, Sydney, NSW, Australia). Action potentials from additional potential muscle spindles that appeared during the stretch, detectable by different frequencies and amplitudes, were not scored. No attempt was made to discriminate group Ia afferents from group II (for a detailed discussion, see Wilkinson et al., 2012).

2.5.3 | Maximal tetanic force

At the end of each recording, the maximal contractile force during a direct tetanic stimulation of the muscle was determined as previously described (Gerwin et al., 2019, 2020; Wilkinson et al., 2012). Muscles were stimulated via paddle electrodes in the tissue bath (500 ms train at 120 Hz and ~1 ms pulse length, supramaximal voltage;

Grass SD9 stimulator; Natus, Pleasanton, CA, USA). The specific force (force/cross-sectional area) of the EDL muscle at L_0, which is a measure of the general health status of the muscle, was determined and compared with the previously reported peak force of a healthy EDL of 23.466 ± 6 N/cm^2 (Brooks & Faulkner, 1988; Larsson & Edström, 1986).

The instantaneous frequency [in impulses per second (imp/sec)] was compared between control and *Asic2* KO mice. Only single-unit spindle afferent responses that could be recorded without interruption throughout the entire experiment were included in the analysis. For the ramp-and-hold stretches, baseline values for all parameters (baseline firing rate, DP, IST and FST) were determined as a mean of three stretches, and the mean of all recordings was compared between WT and mutant mice. Values are reported as mean of the frequency (in impulses per second) in a dot plot, with each dot representing a different muscle spindle response.

2.6 | In vivo micro-computed tomography

In vivo micro-CT scans were performed on adult male and female mice (>90 days old) using the SkyScan 1276 system (Bruker). Before scanning, mice were anaesthetized by inhalation of isoflurane using inhalation chamber, with maintenance by inhalation mask during the scan. The entire spine was scanned in a continuous rotation mode, with a scanning speed of 40 s (360 rotations). Owing to the length limit, imaging was occasionally performed in three overlapping parts that were then merged into one dataset representing the entire region of interest. The total radiation dose was ~500 mGy. All micro-CT scans were reconstructed using N-recon software. Three-dimensional volume rendering images were produced using Amira software (Thermo Fisher Scientific).

2.7 | Measurements of spinal deformity

To measure the spinal curves of *Asic2* KO and control mice, we calculated the Cobb angle (Cobb, 1948) on three-dimensionally rendered images of the micro-CT scans, as described previously (Blecher, Krief, Galili, Assaraf et al., 2017). For scoliosis, the vertebrae that were the most side-tilted rostrally and caudally in the coronal plane were identified. Then, the angle between a line parallel to the superior endplate of the rostral end vertebra and a line parallel to the inferior endplate of the caudal end vertebra was measured. For kyphosis, the Cobb angle was measured between lines parallel to the superior and inferior end vertebrae in the sagittal plane.

2.8 | Ex vivo micro-computed tomography

Ex vivo micro-CT scans of the hip joint were performed on male and female mice (>180 days old) using an Xradia MicroXCT-400 scanner. Tissue was fixed overnight in 4% PFA–PBS and dehydrated to 100% ethanol. The source was set at 40 kV and 200 μA. A total of 1500 projections were taken over 180° with an exposure time of 1.5 s. The final voxel size was 10 μm.

2.9 | Measurements of hip deformity

Hip morphology was analysed on ex vivo hip joint CT scans using Amira software (Thermo Fisher Scientific). The acetabular index and congruency index were measured on a coronal slice of the hip joint, as described before (Assaraf et al., 2020). The acetabular index was measured between a horizontal line connecting both acetabular centres and a line extending from the acetabular centre to the sourcil. The congruency index was calculated for the upper acetabular roof as the mean distance along the joint line divided by the minimal value out of all measurements. A value of one indicates perfect congruence, whereas incongruence results in higher values.

2.10 | Statistical analysis

Statistical significance was determined using Student's unpaired two-tailed *t*-test when comparing two samples, whereas one-way or two-way ANOVA was used to compare multiple samples. All statistical analyses were performed using GraphPad Prism (v.9.3; Graphpad Software, La Jolla, CA, USA). For all statistical tests, significance was defined as a *P*-value <0.05. A summary of the statistical test used is provided in Supplementary File.

3 | RESULTS

3.1 | *Asic2* is expressed in proprioceptive neurons

To identify potential mechanosensitive ion channels that mediate proprioceptive signalling, we examined our MS transcriptomic data (Bornstein et al., 2023). We found six channels that were differentially upregulated in MS samples compared with extrafusal muscle fibres (Figure 1a). Of those, *Asic2* was the most highly upregulated ion channel in our analysis (log fold change of 3.92; Figure 1a). In accordance with previous reports (Lin et al., 2016; Wu et al., 2021), we also detected expression of *Asic1* and *Asic3* (Figure 1a), suggesting that all three ASIC genes are expressed in muscle spindles. However, only *Asic1* and *Asic2* were upregulated in spindles, and the latter was the most differentially expressed mechanosensitive ion channel. Therefore, we proceeded to investigate *Asic2* involvement in proprioceptive function and skeletal regulation.

ASIC2 was previously shown to be expressed in adult rat muscle spindles in the deep lumbrical muscles (Simon et al., 2010). We therefore verified ASIC2 protein expression in proprioceptive neurons of mice by performing immunofluorescence staining. We first analysed ASIC2 expression in DRG neurons and found it to be widely expressed in sensory neurons (Figure 1b). To recognize

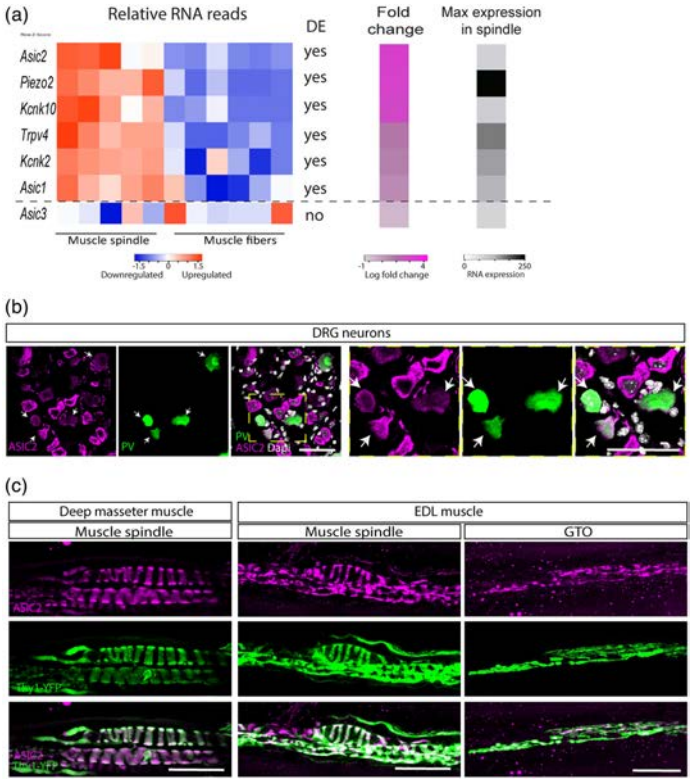

FIGURE 1 *Asic2* is expressed in proprioceptive sensory neuron terminals. (a) Left, heatmap showing the relative expression of mechanosensitive ion channels in muscle spindle samples compared with extrafusal fibres (Bornstein et al., 2023). The list to the right of the heatmap indicates whether the genes are differentially expressed (DE) between spindle and muscle samples. Right, colour bars showing the fold change in expression of each gene between the two samples (magenta) and the maximum expression of the gene in the muscle spindle samples (greyscale). (b) Confocal images of dorsal root ganglia (DRGs) from adult (>60 days old) *Pvalb*^{Cre}; *Rosa26*^{tdTomato} reporter mice (green) stained with antibody against ASIC2 (magenta). ASIC2 is expressed in *Pvalb*$^{+}$ DRG proprioceptive neurons ($n = 50$). Scale bars: 50 μm. (c) Confocal images of whole-mount deep masseter (left) and extensor digitorum longus (EDL) muscle (right) from adult (>60 days old) *Thy1-YFP* reporter mice (Feng et al., 2000) stained with antibodies against ASIC2 and GFP. ASIC2 is expressed in proprioceptive nerve endings innervating muscle spindles and Golgi tendon organs (GTOs) ($n = 3$ mice). Scale bars: 50 μm.

proprioceptive neurons, we marked them genetically by crossing *Pvalb*^{Cre} deleter mice with a *Rosa26*^{tdTomato} reporter line (Hippenmeyer et al., 2005; Madisen et al., 2010). We detected ASIC2 expression in all parvalbumin-positive neurons ($n = 50$; Figure 1b), confirming ASIC2 expression in proprioceptive neurons. Next, we performed whole-mount immunofluorescence staining of the deep masseter muscle. We detected ASIC2 protein expression in the annulospiral endings of proprioceptive neurons innervating the central region of muscle spindles (Figure 1c). We confirmed the co-localization of ASIC2 with the sensory nerve terminals by analysing the EDL muscle, where we detected ASIC2 expression in MSs and GTOs (Figure 1c).

3.2 | Impaired performance of proprioception-related tasks in *Asic2* KO mice

Previous studies of *Asic2* KO mice have implicated ASIC2 in the neurosensory mechanotransduction of touch (Price et al., 2000), the baroreceptive reflex (Lu et al., 2009), gastrointestinal sensing (Page et al., 2005) and pressure-induced constriction in the middle cerebral arteries (Gannon et al., 2008). To determine whether ASIC2 also plays a role in proprioceptive function, we first examined the morphology of proprioceptive sensory neurons in *Asic2* KO mice (Price et al., 2000). To visualize MSs and GTOs, we crossed these mice

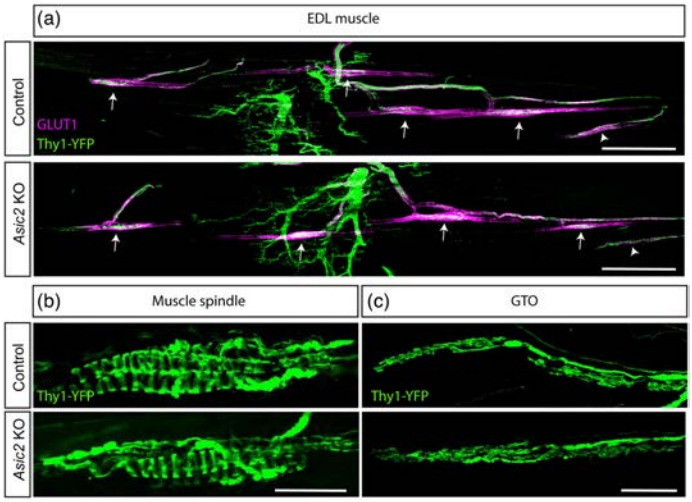

FIGURE 2 The morphology of muscle spindle and Golgi tendon organ (GTO) proprioceptive neurons is unchanged in *Asic2* knockout (KO) mice. (a–c) Confocal images of whole-mount extensor digitorum longus (EDL) muscle taken from control mice (top) and *Asic2* KO mice (bottom) expressing *Thy1-YFP*. The number of proprioceptors, marked by GLUT1 (a; magenta) and the morphology of muscle spindles (b) and GTOs (c) is similar in *Asic2* KO and control mice. Arrows indicate muscle spindles and arrowheads indicate GTOs. $n = 5$ in each group. Scale bars: 500 μm (a); 50 μm (b,c).

with *Thy1-YFP* reporter mice. Whole-mount imaging revealed similar numbers and morphologies of proprioceptors in control and *Asic2* KO mice (Figure 2).

We next examined the possible function of ASIC2 in the proprioceptive system by performing locomotion and coordination tasks. We first assessed coordination of *Asic2* KO and WT mice using the beam walking test (Brooks & Dunnett, 2009). *Asic2* KO mice needed significantly more time to cross the beam and displayed significantly more leg drops than their controls (Figure 3a,b), suggesting that ASIC2 is required for performance of proprioception-related tasks. To rule out the possibility of a general effect on locomotion, we preformed home cage locomotion (Figure 3c) and treadmill (Figure 3d) tests (Brooks & Dunnett, 2009). We found similar locomotor abilities in *Asic2* KO and control mice, supporting our hypothesis that ASIC2 is important specifically for motor coordination.

To characterize coordination deficits associated with loss of *Asic2* further, we used the CatWalk system to analyse gait parameters in *Asic2* KO and control mice. We focused on parameters that were shown to reflect coordination abilities accurately, including interlimb parameters such as phase dispersion, step sequence, stride length, print position and support (Pitzer et al., 2021; Figure 4a). *Asic2* KO mice displayed a significant increase in dispersion score in the diagonal phase (i.e., right forelimb vs. left hindlimb paws and vice versa; Figure 4b), but not in ipsilateral or interlimb scores, indicating that the interval between placement of two diagonal paws is longer. Additionally, step sequence analysis showed that *Asic2* KO mice use the Aa alternate pattern of walking (right fore–right hind–left fore–left hind) significantly more than control mice (Figure 4c). No difference was found between genotypes in the number of patterns used, regularity index, stride length, print position or support parameters (Figure 4d–h), indicating a restricted effect on interlimb coordination between diagonal paws. Additionally, *Asic2* KO mice moved at a similar speed to control mice (Figure 3i), supporting our observation that *Asic2* mutation does not affect general motor abilities, but rather movement coordination specifically.

3.3 | Muscle spindle response to stretch is different in *Asic2* KO mice

Given that *Asic2* KO mice displayed deficits in proprioception-related behavioural tasks, we next analysed the effect of *Asic2* deletion on MS function. Using an ex vivo electrophysiology preparation, we compared muscle spindle afferent firing during stretch between control and *Asic2* KO mice. We observed heterogeneous firing rates in all muscle spindles from mutant mice ($n = 4$) in comparison to heterozygous ($n = 3$) and WT animals ($n = 2$) (pooled as the control group). However, the abnormalities were very variable, even in MSs from the same muscle. The responses to stretch in *Asic2* KO mice could be categorized qualitatively into those that showed sustained firing in response to stretch (Figure 5b) or those that ceased firing for short moments during the hold phase of a ramp-and-hold stretch (Figure 5c).

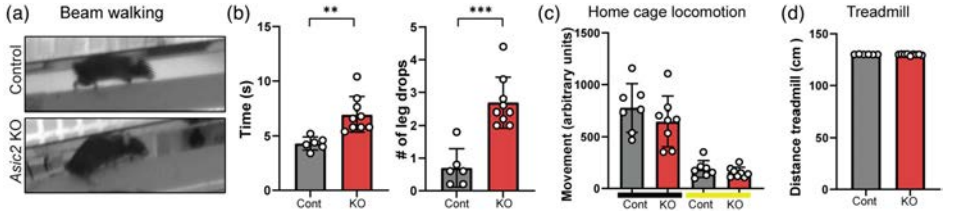

FIGURE 3 *Asic2* knockout (KO) mice display defects in performance of proprioception-related tasks. (a,b) Beam walking test. Mice were trained to walk on a beam 6 mm wide and 50 cm long. The number of slips and the duration of crossing were measured in *Asic2* KO and control (cont) mice ($n_{KO} = 9$, $n_{Control} = 8$; time, $P = 0.0022$; leg-drop, $P = 0.00014$; Student's two-tailed *t*-test), data are represented as the mean ± SD; each dot represents one mouse. (c) A home cage locomotion test was performed to measure locomotor abilities of *Asic2* KO and control mice in a single cage ($n_{KO} = 8$, $n_{Control} = 7$). No significant differences between the groups were found in either light (yellow line, $P = 0.31$) or dark (black line, $P = 0.35$) phases, as determined by Student's two-tailed *t*-test. Data are represented as the mean ± SD; each dot represents one mouse. (d) Treadmill test. Mice were trained to walk on a treadmill to avoid an electrical shock. The distance the mice travelled during the experiment was measured. *Asic2* KO mice travelled a similar distance to control mice ($n_{KO} = 9$, $n_{Control} = 6$; $P = 0.51$, Student's two-tailed *t*-test); data are represented as the mean ± SD; each dot represents one mouse.

To study the response to stretch in more detail, ramp-and-hold stretches of three different magnitudes (2.5, 5.0 and 7.5% of resting length, L_0) were applied, and the dynamic peak (DP), dynamic index (DI), initial static time (IST) and final static time (FST) (Kröger & Watkins, 2021) were compared between *Asic2* KO and control mice (Figure 5d–g; 5% L_0 ramps are shown). The muscle spindles that exhibited a sustained stretch response (Figure 5d–g, red dots) had a significantly increased instantaneous frequency over the dynamic peak (Figure 5d) and dynamic index (Figure 5e), while the muscle spindles that exhibited a non-sustained stretch response (Figure 5d–g, blue dots) had a significantly increased instantaneous frequency in all four parameter analysed (Figure 5d–g). In contrast, the maximum tetanic force (Figure 5h) was not significantly different between control and *Asic2* KO mice, indicating that the altered spindle responses were not attributable to impaired muscle health. Taken together, these results indicate that ASIC2 is required for modulation of proprioceptive afferents in response to stretch.

3.4 | *Asic2* loss of function results in skeletal malalignment

Previously, we have demonstrated that the proprioceptive system is necessary to maintain skeletal integrity (Assaraf et al., 2020; Blecher, Krief, Galili, Assaraf, et al., 2017; Blecher, Krief, Galili, Biton, et al., 2017). Having found that ASIC2 functions to mediate proprioceptive sensing, we proceeded to assess whether loss of *Asic2* would have an effect on the skeleton. For that, we compared spinal alignment between control and *Asic2* KO mice by using CT to determine the level of scoliosis and kyphosis in these mice. Scoliosis was defined as a lateral curve of the spine >10° in the coronal plane and kyphosis as excessive angulation of the spine in the sagittal plane compared with control animals. The results showed that 30% (5 or 17) of the *Asic2* KO mice exhibited mild scoliosis (Figure 6a,b), measured as a Cobb angle ranging from 10 to 15°. In comparison, none of the control mice had a curve of >10°. Interestingly, the scoliotic phenotype of the *Asic2* KO mice was not accompanied by kyphosis (Figure 6c,d), indicating that *Asic2* ablation affects only one plane of spine alignment.

Proprioception deficits also affected hip joint morphology, resulting in a shallow acetabulum and loss of joint congruency (Assaraf et al., 2020). Therefore, we analysed the hip joints of *Asic2* KO mice for features of hip dysplasia. However, micro-CT images of hip joints from *Asic2* KO mice and control littermates showed similar morphologies and no signs of hip dysplasia (Figure 6e), suggesting that loss of *Asic2* does not affect hip joint morphology.

Collectively, our results show that *Asic2* is expressed by proprioceptive neurons and plays important roles in mediating proprioceptive sensing, motor coordination and spine alignment.

4 | DISCUSSION

In this work, we showed that the mechanosensitive ion channel ASIC2 is expressed by proprioceptive neurons innervating MSs and GTOs. We then demonstrated its function in mediating proprioceptive sensing, motor coordination-related tasks and spine alignment, thus showing that ASIC2 is an important mediator of proprioceptive function.

ASIC2 was shown to be involved in mechanosensing of baroreceptive neurons (Lu et al., 2009) and of low-threshold cutaneous neurons (Price et al., 2000). Here, we have shown that ASIC2 contributes to proprioceptive sensing, as *Asic2* KO mice displayed an altered MS response to stretch and impaired performance of coordination-related tasks. These phenotypes are similar to proprioception defects observed in *Asic3* loss-of-function mice (Lin et al., 2016). Given that functional ASIC channels are homotrimers or heterotrimers assembled from three subunits (Kang et al., 2012), this phenotypic similarity might indicate redundancy between the different channels. However, given that ASICs can form heterotrimeric

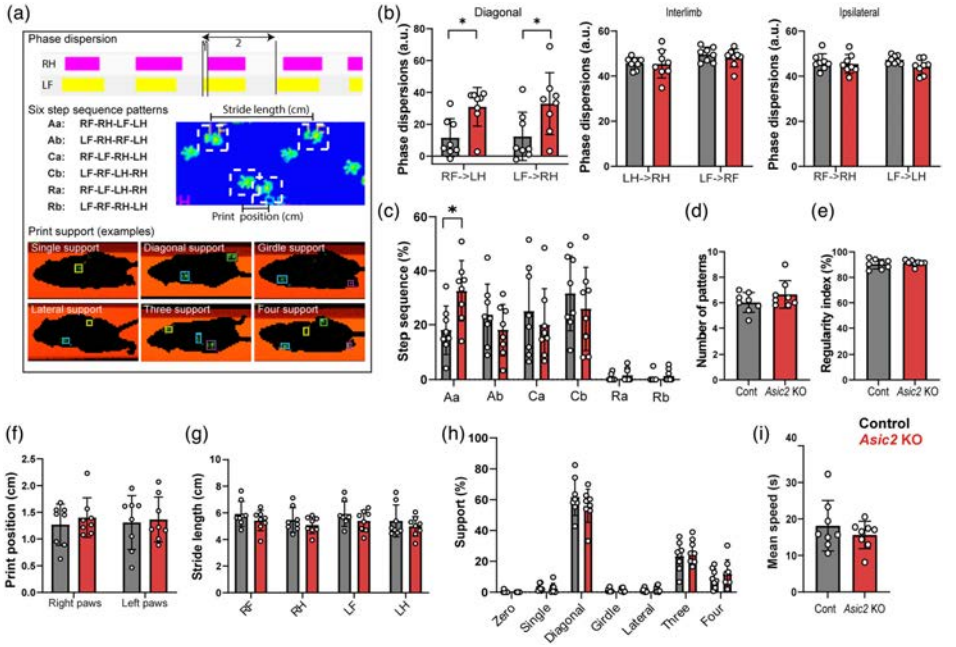

FIGURE 4 *Asic2* knockout (KO) mice display interlimb coordination defects. (a) Examples of CatWalk parameters indicating interlimb coordination. Phase dispersion describes the temporal relationship between placements of two paws. It measures the time interval (1) between the initial contact of an 'anchor' paw [here, left forelimb paw (LF)] and that of a 'target' paw [right hindlimb (RH)] as a percentage of the duration of a complete step cycle of the anchor paw (2). Step sequence pattern is the sequence of paw placement; the six most common patterns are presented. Step sequence categories: Aa, alternative a; Ab, alternative b; Ca, cruciate a; Cb cruciate b; Ra, rotary a; Rb, rotary b. Stride length is the distance between successive placements of the same paw, whereas print position is the distance between successive placements of different paws. Print support is the number and position of paws supporting the animal in each step. Key: LF, left forelimb (yellow); LH, left hindlimb (green); RF, right forelimb (blue); RH, right hindlimb (magenta). (b–i) Gait analysis using the CatWalk system. *Asic2* KO mice had a higher dispersion score in the diagonal phase (b; diagonal RF–LH, $P = 0.012$; diagonal LF–RH, $P = 0.034$; interlimb RF–RH, $P = 0.667$; interlimb LF–LH, $P = 0.0801$; ipsilateral LH–RH, $P = 0.930$; ipsilateral LF–RF, $P = 0.857$) and used the Aa step sequence pattern more frequently (c; Aa, $P = 0.040$; Ab, $P = 0.862$; Ca = 0.914; Cb = 0.866, Ra > 0.999, Rb > 0.999). No difference was found between *Asic2* KO mice and control mice in the number of patterns used (d; $P = 0.202$), regularity index (e; $P = 0.566$), print position (f; right paws, $P = 0.789$; left paws, $P = 0.956$), stride length (g; RF, $P = 0.684$; RH, $P = 0.857$; LF, $P = 0.653$; LH, $P = 0.836$), support (h; zero, $P = 0.999$; single, $P = 0.999$; diagonal, $P = 0.385$; girdle, $P = 0.999$; lateral, $P = 0.999$; three, $P = 0.953$; four, $P = 0.961$) or speed (i; $P = 0.379$) parameters [$P > 0.05$, ANOVA multiple comparison test in (b–h), Student's two-tailed *t*-test in (i)]. $n = 8$ in each group; data are represented as the mean ± SD; each dot represents one mouse.

complexes, we cannot rule out the possibility that ASIC2 and ASIC3 function together to regulate proprioception. Further investigation using *Asic2* and *Asic3* double-KO mice is needed to decide between these options.

Interestingly, we noticed heterogeneous afferent firing patterns in response to stretch in *Asic2* KO mice. A similar effect of opposite firing responses was also observed in stretch-evoked recordings of *Asic3* KO mice (Lin et al., 2016). These phenotypes could be explained by the fact that different combinations of ASIC subunits exhibit different electrophysiological properties (Cheng et al., 2018; Jasti et al., 2007). Thus, differences in ASIC composition between proprioceptive neurons would result in variation in sensitivities and ranges of firing responses to stretch. Indeed, single-cell RNA-seq analysis of proprioceptive neurons identified the expression of *Asic1* and *Asic2* in all subtypes of proprioceptive neurons, whereas *Asic3* was expressed in only a few subtypes (Wu et al., 2021), showing that different ASIC subunits are expressed by different individual neurons. Furthermore, the identification of different subtypes of proprioceptive neurons (Oliver et al., 2021; Wu et al., 2021) suggests that different proprioceptors have different functions. Thus, the combinatory expression of ASIC subunits suggests a mechanism for diversity in the sensing abilities of proprioceptive neurons. However, it is still unclear how knockout

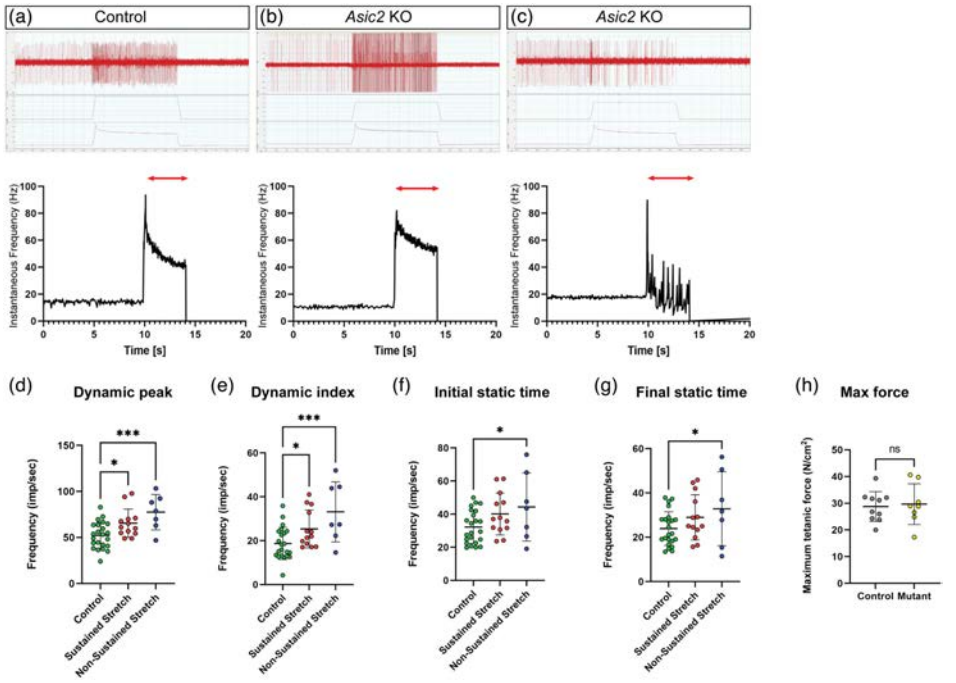

FIGURE 5 Muscle spindle afferent response to stretch is altered in *Asic2* knockout (KO) mice. (a–c) Top, the responses of muscle spindles to a 7.5% stretch from resting length (L_0) in control mice (a) and *Asic2* KO mice (b,c). Muscle spindle recordings from *Asic2* KO mice show sustained responses (b) and non-sustained responses (c). Bottom, the instantaneous frequency of the responses shown in the top panel. Red arrows indicate the duration of stretch. (d–g) Comparison of the instantaneous frequency of the dynamic peak (d; control vs. sustained stretch, $P = 0.0181$; control vs. non-sustained stretch, $P = 0.0005$), dynamic index (e; control vs. sustained stretch, $P = 0.0415$; control vs. non-sustained stretch, $P = 0.0007$), initial static time (f; control vs. sustained stretch, $P = 0.0852$; control vs. non-sustained stretch, $P = 0.0358$) and final static time (g; control vs. sustained stretch, $P = 0.1612$; control vs. non-sustained stretch, $P = 0.0493$) during 5% L_0 ramp-and-hold stretch between control mice (green dots) and *Asic2* KO mice with a sustained response to stretch (red dots) and *Asic2* KO mice with a non-sustained response to stretch (blue dots). $n_{Control} = 23$, $n_{KO} = 20$; ordinary one-way ANOVA with Fisher's LSD. (h) Comparison of the maximum tetanic force of the extensor digitorum longus (EDL) muscle between control mice (grey dots) and *Asic2* KO mice (yellow dots) shows no significant difference ($n_{KO} = 8$, $n_{Control} = 10$; $P = 0.77$, Student's two-tailed *t*-test).

of one ASIC gene affects the expression of different ASIC subunits in different neurons and how the ASIC subunit compositions translate into different proprioceptive signals.

The connection between the proprioceptive system and the skeleton was recently established (Bornstein et al., 2021), but most of the molecular components of this system that are involved in skeletal pathologies are unknown. Here, we have identified the ion channel ASIC2 as a regulator of skeletal integrity. Interestingly, we found that *Asic2* ablation affects only the lateral curve of the spine, causing scoliosis, without causing kyphosis or affecting hip joint morphology. To our knowledge, this is the first proprioception regulatory gene whose ablation selectively affects only one plane of skeletal alignment. This specific phenotype is consistent with previous observations that the severity of the skeletal phenotype is correlated with the severity of the proprioceptive defect. Specifically, *Runx3* KO mice, which lack functional proprioceptive neurons, display much stronger skeletal phenotypes than *Egr3* KO mice, which lack muscle spindles but not GTOs (Blecher, Krief, Galili, Biton et al., 2017). Thus, one explanation for the observed scoliosis is that the lateral curve of the spine is the most sensitive to proprioception defects. Alternatively, the specific effect of *Asic2* deletion might imply that proprioception regulates various aspects of skeletal integrity via different mechanisms. To decide between these two options, it will be necessary to evaluate the skeletal phenotypes caused by deletion of other genes that affect proprioception mildly. Thus, to gain a better understanding of the regulatory role of the proprioceptive system in skeletal biology, it is necessary to identify and study additional molecular players that mediate proprioception.

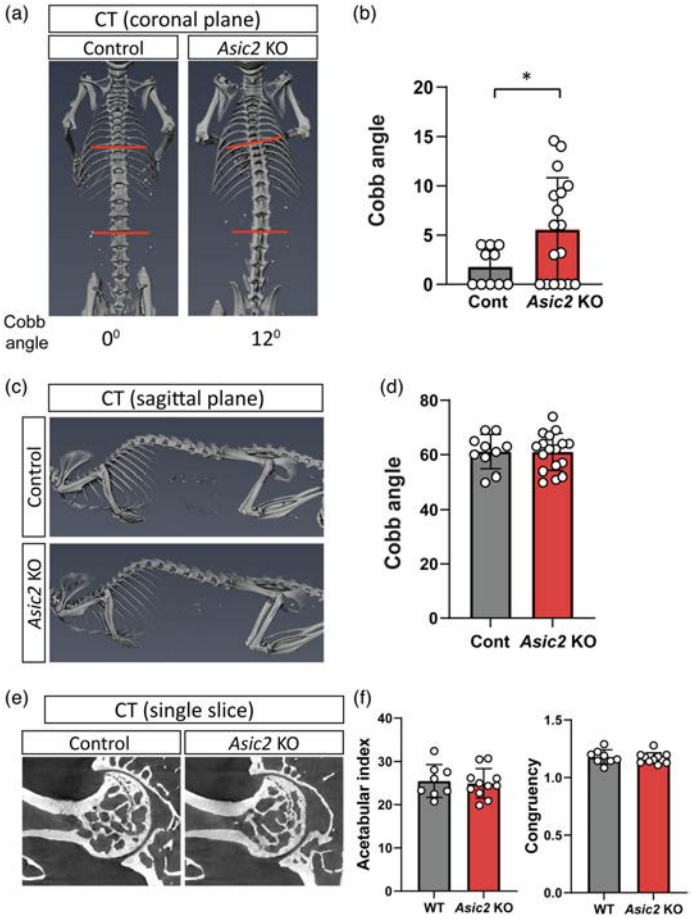

FIGURE 6 Loss of *Asic2* results in spine malalignment but not in altered hip morphology. (a) In vivo CT scans of spines of control and *Asic2* knockout (KO) mice aged >90 days, showing mild scoliosis (coronal plane) in the mutants. (b) Quantification of the Cobb angle measured in control ($n = 10$) and *Asic2* KO ($n = 17$) mice ($P = 0.039$, Student's two-tailed *t*-test). (c) In vivo CT scans of the spines of control and *Asic2* KO mice aged >90 days, showing no difference in kyphosis (sagittal plane) between mutants and control animals. (d) Quantification of the Cobb angle measured for control ($n = 10$) and *Asic2* KO ($n = 17$) mice ($P = 0.97$, Student's two-tailed *t*-test). (e) Ex vivo CT scans of hip joints of control and *Asic2* KO mice aged >90 days, showing no signs of dysplasia in mutants. (f) Graphs showing the acetabular index and congruency index (upper lips) in control ($n = 8$) and *Asic2* KO mice ($n = 10$). No significant differences were found in either measurement ($P = 0.75$ and $P = 0.65$, respectively, Student's two-tailed *t*-test). Data in (b,d,f) are represented as the mean ± SD; each dot represents one mouse.

One limitation of our study is that we used a conventional KO approach to delete *Asic2*. Given that ASIC2 expression in the DRG is not limited to proprioceptive neurons (Cheng et al., 2018; García-Añoveros et al., 2001; Price et al., 2000), we could not determine its cell-autonomous effects in different tissues. This question should be addressed in future studies by applying tissue-specific *Asic2* knockout.

Pervious works showed that *Piezo2* loss of function leads to a complete loss of proprioceptive neuron mechanotransduction and to severe abnormalities of the spine and hips (Assaraf et al., 2020; Woo et al., 2015). Interestingly, the *Asic2* loss-of-function mice displayed milder phenotypes in both mechanotransduction and skeletal alignment. This might suggest that PIEZO2 is necessary to

generate signals in proprioceptive neurons, whereas ASIC2 functions to modulate the signal.

Overall, here we have identified the mechanosensitive ion channel ASIC2 as another molecule that mediates proprioceptive sensing and skeletal alignment. The effect of ASIC2 on the skeleton also reveals the complexity of the regulatory interactions between the proprioceptive system and skeletal development.

AUTHOR CONTRIBUTIONS

Experiments were conducted in the laboratories of Stephan Kröger and Elazar Zelzer. Conception or design of the work: Bavat Bornstein and Elazar Zelzer. Acquisition, analysis or interpretation of data for the work: Bavat Bornstein, Bridgette Watkins, Fabian S. Passini, Ronen Blecher, Eran Assaraf, XiaoMeng Sui, Vlad Brumfeld, Michael Tsoory, Stephan Kröger and Elazar Zelzer. Drafting of the work or revising it critically for important intellectual content: Bavat Bornstein, Bridgette Watkins, Fabian S. Passini, Ronen Blecher, Eran Assaraf, XiaoMeng Sui, Vlad Brumfeld, Michael Tsoory, Stephan Kröger and Elazar Zelzer. All authors approved the final version of the manuscript and agree to be accountable for all aspects of the work in ensuring that questions related to the accuracy or integrity of any part of the work are appropriately investigated and resolved. All persons designated as authors qualify for authorship, and all those who qualify for authorship are listed.

ACKNOWLEDGEMENTS

We thank Nitzan Konstantin for expert editorial assistance and Dr. Inbal Biton from The Center for Comparative Medicine, Weizmann Institute of Science, for her help in in-vivo CT imaging. This study was supported by grants from The David and Fela Shapell Family Center for Genetic Disorders Research, the Julie and Eric Borman Family Research Funds, the Yves Cotrel Foundation, and by the Nella and Leon Benoziyo Center for Neurological Diseases at the Weizmann Institute of Science.

CONFLICT OF INTEREST

None declared.

DATA AVAILABILITY STATEMENT

All data that support the findings of this study are available from the corresponding authors upon request.

ORCID

Bavat Bornstein https://orcid.org/0000-0003-0838-4603
Elazar Zelzer https://orcid.org/0000-0002-1584-6602

REFERENCES

Assaraf, E., Blecher, R., Heinemann-Yerushalmi, L., Krief, S., Carmel Vinestock, R., Biton, I. E., Brumfeld, V., Rotkopf, R., Avisar, E., Agar, G., & Zelzer, E. (2020). Piezo2 expressed in proprioceptive neurons is essential for skeletal integrity. *Nature Communications*, *11*(1), 3168.

Blecher, R., Krief, S., Galili, T., Assaraf, E., Stern, T., Anekstein, Y., Agar, G., & Zelzer, E. (2017). The proprioceptive system regulates morphologic restoration of fractured bones. *Cell Reports*, *20*(8), 1775–1783.

Blecher, R., Krief, S., Galili, T., Biton, I. E., Stern, T., Assaraf, E., Levanon, D., Appel, E., Anekstein, Y., Agar, G., Groner, Y., & Zelzer, E. (2017). The proprioceptive system masterminds spinal alignment: Insight into the mechanism of scoliosis. *Developmental Cell*, *42*(4), 388–399.e3.

Bornstein, B., Heinemann-Yerushalmi, L., Krief, S., Adler, R., Dassa, B., Leshkowitz, D., Kim, M., Bewick, G., Banks, R. W., & Zelzer, E. (2023). Molecular characterization of the intact mouse muscle spindle using a multi-omics approach. *ELife*, *12*, e81843.

Bornstein, B., Konstantin, N., Alessandro, C., Tresch, M. C., & Zelzer, E. (2021). More than movement: the proprioceptive system as a new regulator of musculoskeletal biology. *Current Opinion in Physiology*, *20*(1), 77–89.

Brooks, S. P., & Dunnett, S. B. (2009). Tests to assess motor phenotype in mice: a user's guide. *Nature Reviews Neuroscience*, *10*(7), 519–529.

Brooks, S. V., & Faulkner, J. A. (1988). Contractile properties of skeletal muscles from young, adult and aged mice. *The Journal of Physiology*, *404*(1), 71–82.

Chen, H. H., Hippenmeyer, S., Arber, S., & Frank, E. (2003). Development of the monosynaptic stretch reflex circuit. *Current Opinion in Neurobiology*, *13*(1), 96–102.

Cheng, Y. R., Jiang, B. Y., & Chen, C. C. (2018). Acid-sensing ion channels: Dual function proteins for chemo-sensing and mechano-sensing. *Journal of Biomedical Science*, *25*(1), 1–14.

Chesler, A. T., Szczot, M., Bharucha-Goebel, D., Čeko, M., Donkervoort, S., Laubacher, C., Hayes, L. H., Alter, K., Zampieri, C., Stanley, C., Innes, A. M., Mah, J. K., Grosmann, C. M., Bradley, N., Nguyen, D., Foley, A. R., Le Pichon, C. E., & Bönnemann, C. G (2016). The ROLE of PIEZO2 in human mechanosensation. *N England Journal Medicine*, *375*(14), 1355–1364.

Cobb, J. R. (1948). Outline for the study of scoliosis. *Instr Course Lect AAOS*, *5*, 261–275.

Delhaye, B. P., Long, K. H., & Bensmaia, S. J. (2018). Neural basis of touch and proprioception in primate cortex. *Comprehensive Physiology*, *8*(4), 1575–1602.

Feng, G., Mellor, R. H., Bernstein, M., Keller-peck, C., Nguyen, Q. T., Wallace, M., Nerbonne, J. M., Lichtman, J. W., & Sanes, J. R. (2000). Imaging neuronal subsets in transgenic mice expressing multiple spectral variants of GFP. *Neuron*, *28*(1), 41–51.

Franco, J. A., Kloefkorn, H. E., Hochman, S., & Wilkinson, K. A. (2014). An in vitro adult mouse muscle-nerve preparation for studying the firing properties of muscle afferents. *Journal of Visualized Experiments*, *24*(91), e51948.

Gannon, K. P., Vanlandingham, L. G., Jernigan, N. L., Grifoni, S. C., Hamilton, G., & Drummond, H. A. (2008). Impaired pressure-induced constriction in mouse middle cerebral arteries of ASIC2 knockout mice. *American Journal of Physiology. Heart and Circulatory Physiology*, *294*(4), H1793–H1803.

García-Añoveros, J., Samad, T. A., Zuvela-Jelaska, L., Woolf, C. J., & Corey, D. P. (2001). Transport and localization of the DEG/ENaC ion channel BNaC1alpha to peripheral mechanosensory terminals of dorsal root ganglia neurons. *Journal of Neuroscience*, *21*(8), 2678–2686.

Gerwin, L., Haupt, C., Wilkinson, K. A., & Kröger, S. (2019). Acetylcholine receptors in the equatorial region of intrafusal muscle fibres modulate mouse muscle spindle sensitivity. *Journal of Physiology*, *597*(7), 1993–2006.

Gerwin, L., Rossmanith, S., Haupt, C., Schultheiß, J., Brinkmeier, H., Bittner, R. E., & Kröger, S. (2020). Impaired muscle spindle function in murine models of muscular dystrophy. *Journal of Physiology*, *598*(8), 1591–1609.

Hippenmeyer, S., Vrieseling, E., Sigrist, M., Portmann, T., Laengle, C., Ladle, D. R., & Arber, S. (2005). A developmental switch in the response of DRG neurons to ETS transcription factor signaling. *PLoS Biology*, *3*(5), 0878–0890.

Jasti, J., Furukawa, H., Gonzales, E. B., & Gouaux, E. (2007). Structure of acid-sensing ion channel 1 at 1.9 Å resolution and low pH. *Nature*, *449*(7160), 316–323.

Kang, S., Jang, J. H., Price, M. P., Gautam, M., Benson, C. J., Gong, H., Welsh, M. J., & Brennan, T. J. (2012). Simultaneous disruption of mouse ASIC1a, ASIC2 and ASIC3 genes enhances cutaneous mechanosensitivity. *PLoS ONE*, *7*(4), e35225.

Kiehn, O. (2016). Decoding the organization of spinal circuits that control locomotion. *Nature Reviews Neuroscience*, *17*(4), 224–238.

Kim, M., Franke, V., Brandt, B., Lowenstein, E. D., Schöwel, V., Spuler, S., Akalin, A., & Birchmeier, C. (2020). Single-nucleus transcriptomics reveals functional compartmentalization in syncytial skeletal muscle cells. *Nature Communications*, *11*(1), 1–14.

Kröger, S., & Watkins, B. (2021). Muscle spindle function in healthy and diseased muscle. *Skeletal Muscle*, *11*(1), 1–13.

Larsson, L., & Edström, L. (1986). Effects of age on enzyme-histochemical fibre spectra and contractile properties of fast- and slow-twitch skeletal muscles in the rat. *Journal of the Neurological Sciences*, *76*(1), 69–89.

Lin, S. H., Cheng, Y. R., Banks, R. W., Min, M. Y., Bewick, G. S., & Chen, C. C. (2016). Evidence for the involvement of ASIC3 in sensory mechanotransduction in proprioceptors. *Nature Communications*, *7*(1), 11460.

Lu, Y., Ma, X., Sabharwal, R., Snitsarev, V., Morgan, D., Rahmouni, K., Drummond, H. A., Whiteis, C. A., Costa, V., Price, M., Benson, C., Welsh, M. J., Chapleau, M. W., & Abboud, F. M. (2009). The ion channel ASIC2 is required for baroreceptor and autonomic control of the circulation. *Neuron*, *64*(6), 885–897.

Madisen, L., Zwingman, T. A., Sunkin, S. M., Oh, S. W., Zariwala, H. A., Gu, H., Ng, L. L., Palmiter, R. D., Hawrylycz, M. J., Jones, A. R., Lein, E. S., & Zeng, H. (2010). A robust and high-throughput Cre reporting and characterization system for the whole mouse brain. *Nature Neuroscience*, *13*(1), 133–140.

Marasco, P. D., & de Nooij, J. C. (2022). Proprioception: A new era set in motion by emerging genetic and bionic strategies? *Annual Review of Physiology*, *85*(1), 1–24.

Oliver, K. M., Florez-Paz, D. M., Badea, T. C., Mentis, G. Z., Menon, V., & de Nooij, J. C. (2021). Molecular correlates of muscle spindle and Golgi tendon organ afferents. *Nature Communications*, *12*(1), 1451.

Page, A. J., Brierley, S. M., Martin, C. M., Price, M. P., Symonds, E., Butler, R., Wemmie, J. A., & Blackshaw, L. A. (2005). Different contributions of ASIC channels 1a, 2, and 3 in gastrointestinal mechanosensory function. *Gut*, *54*(10), 1408–1415.

Pitzer, C., Kurpiers, B., & Eltokhi, A. (2021). Gait performance of adolescent mice assessed by the CatWalk XT depends on age, strain and sex and correlates with speed and body weight. *Scientific Reports*, *11*(1), 21372.

Price, M. P., Lewin, G. R., McIlwrath, S. L., Cheng, C., Xie, J., Heppenstall, P. A., Stucky, C. L., Mannsfeldt, A. G., Brennan, T. J., Drummond, H. A., Qiao, J., Benson, C. J., Tarr, D. E., Hrstka, R. F., Yang, B., Williamson, R. A., & Welsh, M. J. (2000). The mammalian sodium channel BNC1 is required for normal touch sensation. *Nature*, *407*(6807), 1007–1011.

Sherrington, C. S. (1907). On the Proprio-ceptive system, especially in its reflex aspect. *Brain*, *29*(4), 467–482.

Simon, A., Shenton, F., Hunter, I., Banks, R. W., & Bewick, G. S. (2010). Amiloride-sensitive channels are a major contributor to mechanotransduction in mammalian muscle spindles. *Journal of Physiology*, *588*(1), 171–185.

Sleigh, J. N., Weir, G. A., & Schiavo, G. (2016). A simple, step-by-step dissection protocol for the rapid isolation of mouse dorsal root ganglia. *BMC Research Notes*, *9*(1), 82.

Wilkinson, K. A. (2022). Molecular determinants of mechanosensation in the muscle spindle. *Current Opinion in Neurobiology*, *74*, 102542.

Wilkinson, K. A., Kloefkorn, H. E., & Hochman, S. (2012). Characterization of muscle spindle afferents in the adult mouse using an in vitro Muscle-nerve preparation. *PLoS ONE*, *7*(6), e39140.

Woo, S. H., Lukacs, V., De Nooij, J. C., Zaytseva, D., Criddle, C. R., Francisco, A., Jessell, T. M., Wilkinson, K. A., & Patapoutian, A. (2015). Piezo2 is the principal mechanotransduction channel for proprioception. *Nature Neuroscience*, *18*(12), 1756–1762.

Wu, H., Petitpré, C., Fontanet, P., Sharma, A., Bellardita, C., Quadros, R. M., Jannig, P. R., Wang, Y., Heimel, J. A., Cheung, K. K. Y., Wanderoy, S., Xuan, Y., Meletis, K., Ruas, J., Gurumurthy, C. B., Kiehn, O., Hadjab, S., & Lallemend, F. (2021). Distinct subtypes of proprioceptive dorsal root ganglion neurons regulate adaptive proprioception in mice. *Nature Communications*, *12*(1), 1–13.

SUPPORTING INFORMATION

Additional supporting information can be found online in the Supporting Information section at the end of this article.

How to cite this article: Bornstein, B., Watkins, B., Passini, F. S., Blecher, R., Assaraf, E., Sui, X. M., Brumfeld, V., Tsoory, M., Kröger, S., & Zelzer, E. (2023). The mechanosensitive ion channel ASIC2 mediates both proprioceptive sensing and spinal alignment. *Experimental Physiology*, 1–13. https://doi.org/10.1113/EP090776

Acknowledgements

I would like to express my gratitude to all of those who have helped me along the way to completing my Ph.D. thesis, without whom this journey would not have been possible.

First, I would like to thank my supervisor, Dr. Stephan Kröger. Thank you for challenging me. I had the privilege of benefitting from his support, guidance and mentorship. Under his supervision, I was able to develop my research skills, enhance my scientific understanding and advance my critical thinking.

I would also like to thank the members of my thesis advisory committee, Dr. Anja Horn-Bochtler and Dr. Benedikt Schoser for their insightful suggestions and reviews, which enhanced the scope and depth of my research. I would also like to thank Dr. Peter Meinke and Dr. Stefan Hintze for their assistance with the Pompe mice.

Thank you to Dr. Katherine Wilkinson and her lab, for the support and encouragement along the way. I very much enjoyed my time in San Jose, and at the conference in Munich. I would also like to thank the Zelzer group for the opportunity to visit their lab, I thoroughly enjoyed my visit at the Weizmann Institute.

To my lab mates – Arlind, Zoi and Jürgen: Thank you for making the long days in the lab endurable. The intellectual discussions, the many hours spent troubleshooting experiments and the coffee and cake breaks were an essential part of my time in the lab. Thank you to Jürgen, for his exceptional technical support throughout the duration of my time in the lab.

I would like to express my heartfelt thanks to my family and friends – I could not have completed this without your unwavering support. To all the new friends I have made along the way, thank you for reminding me of life outside the lab. A special thank you to Tori, for always being on the other end of the phone, even if it is the middle of the night.

Thank you to my parents, Michelle and Stephen for everything over the last 30 years, without your constant support, love and encouragement, none of this would have been possible. To Christoph, thank you for convincing me that everything would be ok. Your love and support over the last five years has made this PhD thesis possible.

Thank you all for everything.